

AD-A095 10\*

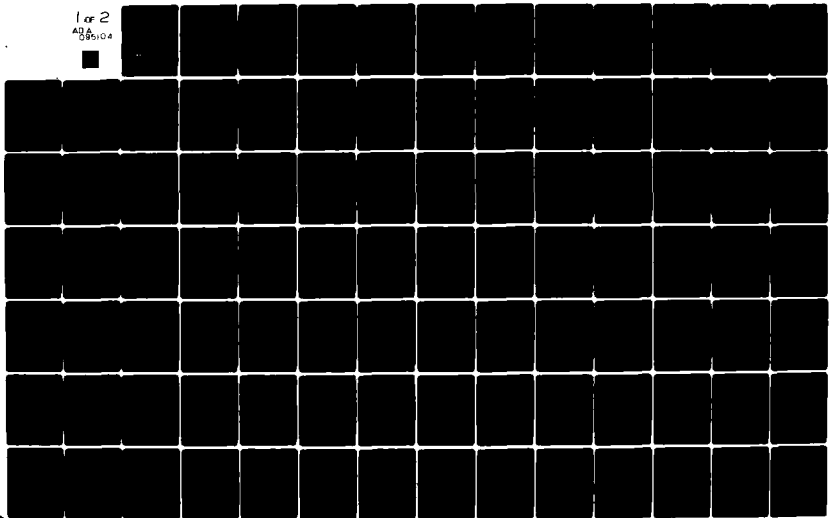
TEXAS UNIV AT AUSTIN INST FOR ADVANCED STUDY IN ORBIT--ETC F/6 17/1  
ESTIMATING THE MOTION OF A MANEUVERING TARGETS USING PASSIVE ME--ETC(U)  
AUG 80 B D TAPLEY, P A ABUSALI, B E SCHUTZ N00014-78-C-0563

UNCLASSIFIED

IASOM-TR-80-2

NL

1 of 2  
AD-A095 104





REPORT DOCUMENTATION PAGE		READ INSTRUCTIONS BEFORE COMPLETING FORM
1. REPORT NUMBER N00014-78-C-0663	2. GOVT ACCESSION NO. AD-A095104	3. RECIPIENT'S CATALOG NUMBER
4. TITLE (and Subtitle) Estimating the Motion of a Maneuvering Target Using Passive Measurements,		5. TYPE OF REPORT & PERIOD COVERED Final 9-1-78/12-31-80
		6. PERFORMING ORG. REPORT NUMBER IASOM-80-2
7. AUTHOR(s) B. D. Tapley, P.A.M./Abusali, B. E. Schutz		8. CONTRACT OR GRANT NUMBER(s) N00014-78-C-0663
9. PERFORMING ORGANIZATION NAME AND ADDRESS University of Texas at Austin Department of Aerospace Engineering and Engineering Mechanics		10. PROGRAM ELEMENT, PROJECT, TASK AREA & WORK UNIT NUMBERS 61153N R014-11-01 NR 277-278
11. CONTROLLING OFFICE NAME AND ADDRESS Naval Analysis Program (Code 431) Office of Naval Research Arlington, VA 22217		12. REPORT DATE Aug 1980
14. MONITORING AGENCY NAME & ADDRESS (if different from Controlling Office)		13. NUMBER OF PAGES 112
		15. SECURITY CLASS. (of this report) Unclassified
		15a. DECLASSIFICATION/DOWNGRADING SCHEDULE N.A.
16. DISTRIBUTION STATEMENT (of this Report) Approved for Public Release, Distribution Unlimited		
17. DISTRIBUTION STATEMENT (of the abstract entered in Block 20, if different from Report) NA		
18. SUPPLEMENTARY NOTES Prepared in cooperation with Tracor, Inc., Austin, Texas		
19. KEY WORDS (Continue on reverse side if necessary and identify by block number) Target Maneuver Acceleration; Dynamic Model; Bearing Angle, Doppler Frequency Shift; Passive Sensors; Extended Kalman Filter; Batch-Sequential Filter; Triangularization by Orthogonal Transformation.		
20. ABSTRACT (Continue on reverse side if necessary and identify by block number) The problem of estimating the trajectory of a maneuvering target using passive measurements obtained from an array of stationary sensors is investigated. The formulation is considered in a two-dimensional rectangular coordinate system. The unknown acceleration components are modelled as Brownian motion processes and consequently the dynamic model is linear. The types of measure- ments used in the estimation process are the frequency and the bearing angle of some sound signal emanating from the target. These measurements are non- linear functions of the state vector which consists of a reference frequency		

20. (continued)

and the components of position, velocity and acceleration. Computation algorithms for Extended Kalman Filter and "batch-sequential" filter are presented. Equations for including the effects of process noise on the batch solution are derived and the computation algorithm is also given. The performance of these filters is compared using noisy measurements simulated for two different scenarios with typical target maneuvers and sensor locations. Extended Kalman Filter is found to be the best in terms of computation time and accuracy of the estimated trajectory. Sensors located as far apart as feasible yield better results than those which are closer to each other.

Accession For	
NIIS OR&I	<input checked="" type="checkbox"/>
DTIC TAB	<input type="checkbox"/>
Unannounced	<input type="checkbox"/>
Justification	
By _____	
Distribution/ _____	
Availability Codes	
Dist	Avail and/or Special
A	

ESTIMATING THE MOTION OF MANEUVERING TARGETS  
USING PASSIVE MEASUREMENTS

by

B.D. Tapley, P.A.M. Abusali and B.E. Schutz

IASOM TR 80-2

August 1980

This report was prepared under  
Contract N00014-78-C-0663  
NR 277-278

for the  
Naval Analysis Program  
Office of Naval Research  
Arlington, Virginia

by the

Institute for the Advanced Study in Orbital Mechanics  
The University of Texas at Austin  
Austin, Texas 78712

Reproduction in whole or in part is permitted for any purpose  
of the United States Government

APPROVED FOR PUBLIC RELEASE: DISTRIBUTION UNLIMITED

Table of Contents

	Page
List of Figures . . . . .	iv
List of Tables . . . . .	vi
Abstract . . . . .	vii
1. Introduction . . . . .	1
2. Theoretical Background . . . . .	12
3. Dynamical Model for a Maneuvering Target . . . . .	22
4. Measurement Model. . . . .	27
5. Methods of Solution and Computation Algorithm . . . . .	33
6. Numerical Results. . . . .	50
7. Conclusions and Recommendations . . . . .	98
References . . . . .	101
Appendix A Batch Solution in the Presence of Process Noise . . . . .	103
Appendix B Process Noise Variance Computation for Adaptive Filtering . . . . .	110

List of Figures

	Page
1.1 Relative Polar Coordinate Geometry for a Single Observer . . . . .	6
1.2 Geometry for the Multi-Observer, Common Polar Coordinate System . . . . .	7
5.1 The Division of the Observation Set Into Several Batches . . . . .	37
6.1 Trajectory and Sensor Locations for Case A. . . . .	68
6.2 Frequency Measurement vs. Time for Case A.1 . . . . .	69
6.3 Bearing Angle Measurement vs. Time for Case A.1 . . . . .	70
6.4 Estimated and True Trajectories for the Observation Set Case A.1 by EKF . . . . .	71
6.5 Estimated Error in x-Component of position for Fig. 6.4 vs. Time (Case A.1) . . . . .	72
6.6 Estimated Error in y-Component of Position for Fig. 6.4 vs. Time (Case A.1) . . . . .	73
6.7 Estimated Error in x-Component of Velocity for Fig. 6.4 vs. Time (Case A.1) . . . . .	74
6.8 Estimated Error in y-Component of Velocity for Fig. 6.4 vs. Time (Case A.1) . . . . .	75
6.9 Estimated Error in x-Component of Acceleration for Fig. 6.4 vs. Time (Case A.1) . . . . .	76
6.10 Estimated Error in y-Component of Acceleration for Fig. 6.4 vs. Time (Case A.1) . . . . .	77
6.11 Estimated and True Trajectories for the Observation Set Case A.2 by EKF . . . . .	78
6.12 Estimated and True Trajectories for the Observation Set Case A.3 by EKF . . . . .	79
6.13 Estimated and True Trajectories for the Observation Set Case A.4 by EKF . . . . .	80
6.14 Estimated and True Trajectories for the Observation Set Case A.5 by EKF . . . . .	81
6.15 Estimated and True Trajectories for the Observation Set Case A.6 by EKF . . . . .	82

List of Figures (Continued)

	Page
6.16 Estimated and True Trajectories for the Observation Set Case A.1 by EKF with Perturbations in Initial State of the Target . . . . .	83
6.17 Estimated Error in x-Component of Position for Fig. 6.16 vs. Time (Case A.1). . . . .	84
6.18 Estimated Error in y-Component of Position for Fig. 6.16 vs. Time (Case A.1). . . . .	85
6.19 Trajectory and Sensor Locations for Case B. . . . .	86
6.20 Frequency Measurement vs. Time for Case B.1 . . . . .	87
6.21 Bearing Angle Measurement vs. Time for Case B.1 . . . . .	88
6.22 Estimated and True Trajectory for the Observation Set Case B.1 by EKF . . . . .	89
6.23 Estimated and True Trajectories for the Observation Set Case B.1 by 'Batch-Sequential' Method without Process Noise . . . . .	90
6.24 Estimated and True Trajectories for the Observation Set Case B.1 by 'Batch-Sequential' Method with Process Noise . . . . .	91
6.25 Estimated and True Trajectories for the Observation Set Case B.1 by EKF with Perturbations in Initial State of the Target . . . . .	92
6.26 Estimated Error in x-Component of Position for Fig. 6.25 vs. Time (Case B.1). . . . .	93
6.27 Estimated Error in y-Component of Position for Fig. 6.25 vs. Time (Case B.1). . . . .	94
6.28 Estimated and True Trajectories for Case B.2 by EKF with Perturbations in Initial State of the Target . . . . .	95
6.29 Estimated Error in x-Component of Position for Fig. 6.28 vs. Time (Case B.2). . . . .	96
6.30 Estimated Error in y-Component of Position for Fig. 6.28 vs. Time (Case B.2). . . . .	97

List of Tables

	Page
6.1 Sensor Location Coordinates for Case A.1 . . . . .	63
6.2 Values of $X_o$ , $P_o$ and Q for Processing Case A.1 through Case A.6 (Figures 6.4 through 6.15) . . . . .	63
6.3 Sensor Location Coordinates for Cases A.2 and A.3 . . . . .	64
6.4 Sensor Location Coordinates for Case A.4 . . . . .	64
6.5 Sensor Location Coordinates for Cases A.5 and A.6 . . . . .	64
6.6 Perturbed Values of $X_o$ , and Values of $P_o$ and Q for Case A.1 (Figures 6.16 through 6.18) <sup>o</sup> . . . . .	65
6.7 Sensor Location Coordinates for Case B.1 . . . . .	65
6.8 Values of $X_o$ , $P_o$ and Q Used for Case B.1 . . . . .	66
6.9 Perturbed Values of $X_o$ and Values of $P_o$ and Q for Cases B.1 and B.2 <sup>o</sup> (Figures 6.25 through 6.30) . . . . .	66
6.10 Sensor Location Coordinates for Case B.2 . . . . .	67

### Abstract

The problem of estimating the trajectory of a maneuvering target using passive sonar measurements obtained from an array of stationary sensors is investigated. The formulation is considered in a two-dimensional rectangular coordinate system. The unknown acceleration components are modelled as Brownian motion processes and consequently the dynamic model is linear. The types of measurements used in the estimation process are the frequency and the bearing angle of some sound signal emanating from the target. These measurements are nonlinear functions of the state vector which consists of a reference frequency and the components of position, velocity and acceleration. Computation algorithms for Extended Kalman Filter and "batch-sequential" filter are presented. Equations for including the effects of process noise on the batch solution are derived and the computation algorithm is also given. The performance of these filters is compared using noisy measurements simulated for two different scenarios with typical target maneuvers and sensor locations. Extended Kalman Filter is found to be the best in terms of computation time and accuracy of the estimated trajectory. Sensors located as far apart as feasible yield better results than those which are closer to each other.

## 1. Introduction

The problem of estimating the trajectory of a maneuvering target is one of the more difficult of the current estimation problems. For military applications the target may be an airborne vehicle, a surface ship or an underwater submarine. Though there are similarities in the problem formulation and in the methods of solution for these targets, the motion characteristics and the data required to track the motion are distinctly different. The airborne targets are usually fast moving and highly maneuverable, while the underwater targets are slower moving and have limitations on their ability to execute rapid maneuvers. The measurements made on the aircraft and missiles are of high quality, usually characterized by a high data rate active sensor signal, whereas those for underwater targets are obtained primarily from passive signals badly corrupted by the environment in which they travel. In this report, primary attention will be given to the problem of estimating the trajectory of a single unknown underwater target. As a consequence, attention is directed to the question of modeling the motion of the maneuvering target and to the questions of the structure of the estimation algorithm used to process the measurements.

Statistical estimation techniques, set in the framework of modern control theory, are applied to obtain a solution to this problem. With all the versatility of linear filtering theory, there are several unresolved aspects related to the tracking of maneuvering targets. The Extended Kalman Filter (EKF) [1], which is a local optimal nonlinear filter, represents the best contemporary approach. However this method encounters difficulties due to filter divergence; an effect

caused by modeling errors arising from incomplete a priori knowledge of the nature of the target maneuvers. Depending on the coordinate system, either the dynamics or the observation models or both will be nonlinear. The optimal solution to nonlinear estimation problems is extremely difficult to obtain. For example, finding the minimum variance estimate involves the computation of the mean of the conditional probability density function of the state for a given set of observations, and this in turn will require, in a general nonlinear problem, the solution of a partial differential equation which describes the evolution of the conditional probability density function [2]. Even assuming that the noise in the measurement, the noise influencing the system dynamics and the a priori state are all independent Gaussian random variables, the conditional probability density function will evolve as a non-Gaussian process due to the nonlinearities in the system model. Though some results are available for particular approximations of a few nonlinear models, no satisfactory theory has been developed for the general nonlinear problem. The contemporary approach to the solution to this class of problems is to linearize the problem by referencing the motion to a known solution. This known solution is selected to be "close" to the actual motion and the time-rate of change in the difference can be described by a set of linear differential equations. The estimation algorithm based on this approach is referred to as the Extended Kalman-Bucy Filter (EKF) [2] [3]. The EKF has been adopted as the best choice for solving the maneuvering target trajectory estimation problem in the majority of the previous investigations and this algorithm will be used as the basis for the investigations reported here. Having

selected the EKF algorithm, the next step is to find ways of overcoming the difficulties that may be encountered when the target executes a maneuver.

Several authors [4] have discussed the problem formulation for a single observer tracking a maneuvering target. They have considered two dimensional motion in a rectangular coordinate system. The acceleration is assumed to be zero and the state vector consists of position and velocity components. In the single-observer tracking problem using only bearing measurements, the observer must know his own motion and must execute a maneuver within the time period of the observation set if the target state to be observable. The Extended Kalman Filter is used in these investigations with different variations in the implementation. Alspach [5] discusses an approximate nonlinear estimation approach based on an optimal Bayesian filter implementation by the Gaussian sum approach. The results presented demonstrate the difference between this method and the EKF approach. Moose and McCabe [6] consider a two dimensional problem with passive time delay measurement and Doppler frequency measurement. Their approach is to model the target dynamics by assuming a time-correlated, randomly switching mean forcing function as a deterministic input command, and the single observer is assumed to be moving with constant velocity. The EKF is used to estimate the position and velocity in a relative polar coordinate system referenced to the moving observer.

The problem considered in this investigation is one of estimating the trajectory of a target moving into two dimensions, using measurements obtained from an array of stationary or drifting sensors. The

types of measurements are the 'Doppler frequency' of some sound signal emanating from the target and the direction from which this sound signal is coming. It should be noted that in an actual target motion analysis application these measurements must be considered in three dimensions due to the nature of signal propagation. Though the formulation is no more complicated (except for the algebra) than the two dimensional application, in order to demonstrate filtering approaches, we have used the two dimensional model.

#### Coordinate System

There are several choices for the coordinate systems used in the mathematical formulation of the maneuvering target problem, and a 'natural' coordinate system would be the polar coordinates from each sensor with each sensor in turn related to a common reference frame. Another convenient choice is a single polar coordinate system to which measurements from all the sensors are referred. However, selection of either of these co-ordinate systems will lead to a complicated nonlinear model for representing the dynamical motion. Hence a fixed rectangular coordinate system is chosen for the formulation. In this reference frame, the dynamics are linear (except for some advanced models), but the observation-state relation is nonlinear.

To illustrate the effect of the co-ordinate system selection, let the simplest estimation state vector for the polar coordinate system shown in Figure 1, be taken as,

$$\mathbf{x}^T = [f_0 \ \rho \ \theta \ \dot{\rho} \ \dot{\theta}] = [x_1 \ x_2 \ x_3 \ x_4 \ x_5] \quad (1.1)$$

so that

$$\dot{\mathbf{x}} = \mathbf{f}(\mathbf{x}, t) + \mathbf{w} \quad (1.2)$$

where

$$\begin{aligned} \dot{x}_1 &= f_1(\mathbf{x}, t) = 0 \\ \dot{x}_2 &= f_2(\mathbf{x}, t) = x_4 \\ \dot{x}_3 &= f_3(\mathbf{x}, t) = x_5 \\ \dot{x}_4 &= f_4(\mathbf{x}, t) = u_\rho + x_2 x_5^2 \\ \dot{x}_5 &= f_5(\mathbf{x}, t) = (u_\theta - 2x_4 x_5) / x_2 \end{aligned} \quad (1.3)$$

and

$$\mathbf{w}^T = [w_f \quad 0 \quad 0 \quad 0 \quad 0] \quad (1.4)$$

In the above,  $f_0$  is the reference frequency for Doppler frequency measurement,  $\rho$  is the range,  $\theta$  is the bearing angle,  $w_f$  is a zero-mean Gaussian white noise, and  $u_\rho$  and  $u_\theta$  are the input acceleration components in the radial and transverse directions respectively. The  $(\dot{\quad})$  indicates differentiation with respect to time. For the case with polar coordinates referenced to a single sensor, the components of  $\mathbf{x}$  refer to the relative motion of the target with respect to that sensor. As shown in Fig. 1.1, the observation-state relation for the bearing angle measurement is given by

$$G_\beta = 0(\mathbf{x}) + \varepsilon_\theta = x_3 + \varepsilon_\theta \quad (1.5)$$

For the formulation in a polar coordinate system common to all the sensors, the dynamics refers to the position and velocity of the target with respect to the origin of the coordinate system. To simplify the algebra, consider one of the sensors, located as shown in Fig. 1.2.

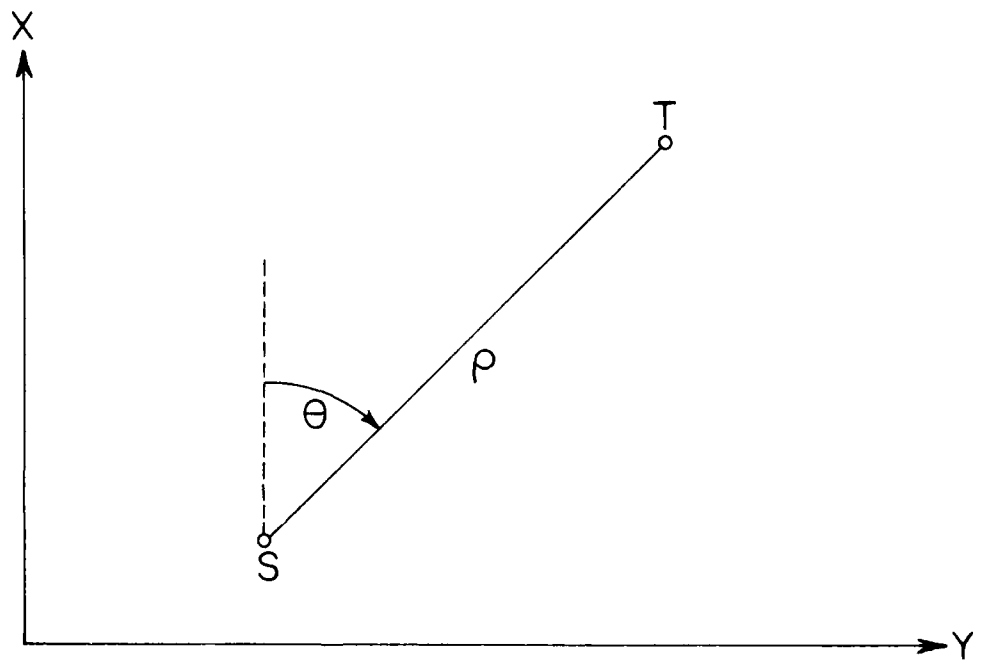


Fig. 1.1 Relative Polar Coordinate Geometry for a Single Observer

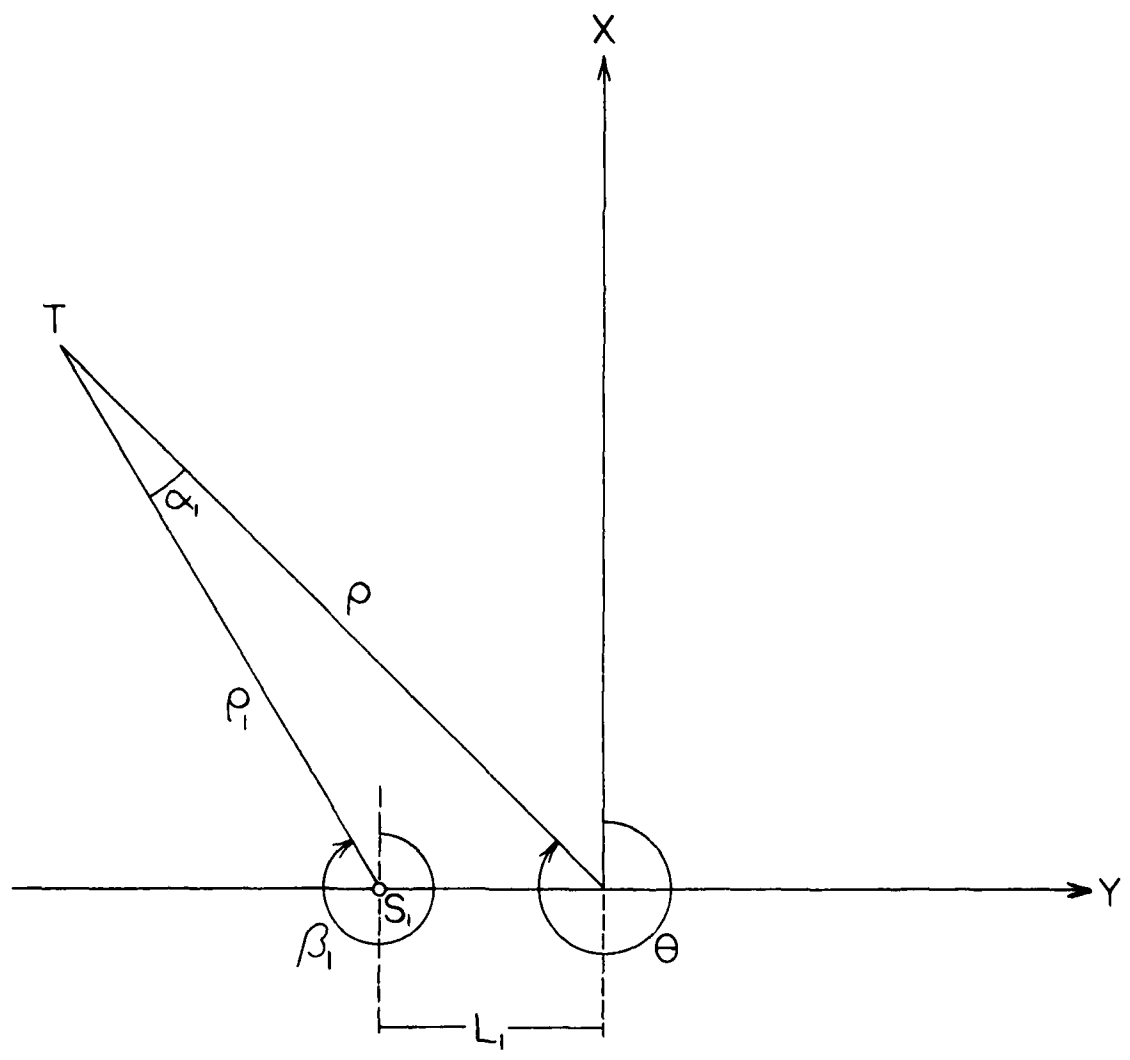


Fig. 1.2 Geometry for the Multi-Observer, Common Polar Coordinate System

Then the observation-state relation for the bearing angle measurement is obtained from the relation,

$$\beta_1 = \theta + \alpha_1 \quad (1.6)$$

To compute  $\alpha_1$ , note that

$$\rho_1 \cos \alpha_1 + L_1 \cos \theta' = \rho \quad (1.7)$$

with

$$\rho_1^2 = \rho^2 + L_1^2 - 2\rho L_1 \cos \theta' \quad \text{and} \quad \theta' = \theta - \frac{3\pi}{2} \quad (1.8)$$

It then follows that

$$\begin{aligned} G_\beta &= \beta_1 + \epsilon_\beta \\ &= x_3 + \cos^{-1} \frac{x_2 - L_1 \cos x_3'}{\sqrt{L_1^2 + x_2^2 - 2L_1 x_2 \cos x_3'}} + \epsilon_\beta \end{aligned} \quad (1.9)$$

$$\text{and} \quad x_3' = x_3 - \frac{3\pi}{2}$$

Thus, even if the bearing angle measurement is the only measurement type, in the latter system it is nonlinear. Furthermore, the second type of measurement to be considered, namely, the Doppler frequency has nonlinear forms, in both of the above two polar coordinates. In the former system, along with Equation 1.5, the Doppler measurement is given by

$$G_f = \frac{f_o}{(1 + \frac{\dot{\rho}}{c})} + \epsilon_f = \frac{x_1}{(1 + \frac{x_4}{c})} + \epsilon_f \quad (1.10)$$

In the latter system to obtain the relation between the state and frequency measurement, note that

$$\rho_1^2 = L_1^2 + \rho^2 - 2L_1\rho \cos \theta'$$

$$\dot{\rho}_1 = \frac{1}{\rho_1} (\rho\dot{\rho} - L_1\dot{\rho} \cos \theta' + L_1\rho\dot{\theta} \sin \theta')$$

Then

$$G_f = f_1 + \epsilon_f = \frac{f_o}{\rho_1 \left(1 + \frac{1}{c}\right)} + \epsilon_f \quad (1.11)$$

or

$$G_f = \frac{x_1}{\rho_1 \left(1 + \frac{1}{c}\right)} + \epsilon_f \quad (1.12)$$

where

$$\dot{\rho}_1 = \frac{x_2x_4 - L_1x_4 \cos x_3' + L_1x_2x_5 \sin x_3'}{\sqrt{L_1^2 + x_2^2 - 2L_1x_2 \cos x_3'}} \quad (1.13)$$

Hence in both the coordinate systems at least one type of measurement is nonlinear and the dynamics are always nonlinear. In a rectangular coordinate system, as will be shown in Chapter 3, the dynamic model is linear and although both the measurement types are nonlinear, the algebraic expressions are not as complicated as those given in Eqs. (1.9) through (1.13). Consequently, in the investigation described in the following chapters, the rectangular coordinate system is chosen to exploit the linearity in the dynamic model.

For this investigation, the estimation state vector will consist of the components of position, velocity and acceleration and also the reference frequency for the received signal. The reason for estimating

the acceleration components is as follows. The acceleration of the target cannot be known for the entire period of interest. While the target acceleration is zero for some periods of time, there will be other periods during target maneuvers when it will have a significant acceleration. Consequently, it is important to model the acceleration in such a way that the filter can detect any maneuver that the target might execute and track it as accurately as possible. One approach to satisfying this requirement is to model the acceleration components as Brownian motion processes. This model has been used to estimate the accelerations due to unmodeled forces in a number of previous investigations. See for example, References [7], [8] and [9]. By using this approach the time rate of change of the acceleration components can be included in the dynamic model as white noise. This representation is adopted for the model described in the following chapter.

An important requirement for the success of the Extended Kalman Filter throughout the estimation time period is that an acceptable initial estimate for the trajectory be available to satisfy the assumptions involved in linearizing the original nonlinear problem. One way of achieving this estimate is to process a limited set of measurements with a batch estimation algorithm to obtain a solution for the initial state and the error covariance matrix. This information can be used as the a priori state and the a priori covariance matrix to start the EKF. When the state error covariance and consequently the gain decays to some steady state values (small), at a later state, the filter may saturate and may not be able to detect a possible maneuver of the target and consequently may diverge. One

approach to avoid this situation would be to divide the period of interest into a number of smaller arcs and find the iterated least-square solution for each arc by propagating one arc solution (estimate and covariance) to the next. This method obviously will be time consuming and does not provide a real-time solution, although it does provide an on-line solution with some lag. The primary purpose of such an approach is to avoid the divergence associated with the Kalman (or sequential) filter. An alternate procedure for using the batch estimation algorithm is as a initializer for the EKF or sequential processing algorithm. Both approaches are considered in the subsequent investigation.

Finally, during this investigation, a sequential batch algorithm is developed by including the effects of process noise in the a priori batch estimation algorithm [3]. The development of this algorithm is described and in the numerical studies it is compared with the EKF algorithm to determine the relative accuracy of the methods in estimating the motion of a maneuvering target.

## 2. Theoretical Background

The linear state estimation problem is concerned with finding the best estimate of the state,  $x \in R^n$ , of a linear dynamical system whose time-evolution is characterized by the set of differential equations,

$$\dot{x}(t) = A(t)x(t) + B(t)w(t) \quad (2.1)$$

from a set of observations  $Y \in R^m$ , made on the system output  $x$ , where the linearized observations,  $y \in R^m$ , are related to the state at discrete epochs,  $t_1, t_2, \dots, t_\ell$ , through the following linear relation,

$$y_i = \tilde{H}_i x_i + \varepsilon_i, \quad i = 1, 2, \dots, \ell \quad (2.2)$$

The subscript,  $i$ , represents the discrete observation epochs. In the above equations,  $A(t)$  and  $B(t)$  are called the system matrices,  $w(t) \in R^q$  is a zero mean Gaussian random disturbance vector and  $\varepsilon_i$  is the noise in the  $i^{\text{th}}$  observation. Note that each  $y_i$  could be a vector, say,  $y_i \in R^p$ , in which case  $m = \ell \times p$ . For the general non linear estimation problem, one would have a dynamical system represented by

$$\dot{X}(t) = F(X(t), w(t), t) \quad (2.3)$$

and measurements given by

$$Y_i = G(X(t_i), t_i) + \varepsilon_i, \quad i = 1, 2, \dots, \ell \quad (2.4)$$

where  $F(\cdot)$  and  $G(\cdot)$  are nonlinear functions of the state  $X(t)$ .

Then Eqs. (2.1) and (2.2) would correspond to a linearized system obtained by expanding Eqs. (2.3) and (2.4) about some reference solution,  $X^*(t)$ . The matrices  $A(t)$  and  $\tilde{H}_i$  would be obtained from  $F(\cdot)$  and  $G(\cdot)$  by the following definitions:

$$A(t) = \left. \frac{\partial F}{\partial X} \right|_{X = X^*(t)} \quad \text{and} \quad \tilde{H}_i = \left. \frac{\partial G}{\partial X} \right|_{X_i = X^*(t_i)}$$

Accordingly,  $x(t)$  in Eq. (2.1) represents the deviation from a reference trajectory  $X^*(t)$  satisfying Eq. (2.3), where  $w(t) = 0$  and  $X(t_0) = X_0^*$ , a known vector, and  $y_i$  in Eq. (2.2) is the linearized observation deviation from the reference value  $G(X^*(t_i), t_i)$ . The term  $B(t)w(t)$  in Eq. (2.1) is the process noise term added to compensate for the incomplete modeling.

Given the observation set  $Y^\ell = \{Y_1, Y_2, \dots, Y_\ell\}$ , the estimate of the state may be desired either at some particular epoch, say  $t_0$ , which we will call the batch solution  $\hat{x}_0 = \hat{x}(t_0/t_\ell)$  or estimates of the state may be desired at each time point  $t_i$ , ( $t_1 \leq t_i \leq t_\ell$ ), based on all the observations up to that time,  $Y^i = \{Y_1, \dots, Y_i\}$ . This latter solution is referred to as the filtered solution  $\hat{x}_i = \hat{x}(t_i/t_i)$ . To compute the batch estimate, Eqs. (2.2) are expressed in terms of the state at the epoch  $t_0$ , as

$$y_i = H_i x_0 + \eta_i, \quad i = 1, \dots, \ell \quad (2.5)$$

where

$$H_i = \tilde{H}_i \Phi(t_i, t_0)$$

$$\eta_i = \tilde{H}_i \int_{t_0}^{t_i} \Phi(t_i, \tau) B(\tau) w(\tau) d\tau + \epsilon_i \quad (2.6)$$

The  $n \times n$  matrix  $\Phi(t_i, t_j)$  is referred to as the state transition matrix for the matrix  $A(t)$  [2] [3]. The batch solution for a linear dynamical system with the process noise  $w(t)$ , has exactly the same structure as the solution to the system with  $w(t) = 0$  (see Appendix A). Hence, for the purpose of reviewing the theory, we consider only the homogeneous part of Eq. (2.1), namely the system:

$$\dot{x}(t) = A(t) x(t) . \quad (2.7)$$

Then,  $\eta_i = \epsilon_i$  in Eq. (2.6) and Eq. (2.5) becomes

$$y_i = H_i x_0 + \epsilon_i, \quad i = 1, \dots, \ell \quad (2.8)$$

This sequence of observations can be collected into a single matrix as follows:

$$y = H x_0 + \epsilon \quad (2.9)$$

where

$$y = \begin{bmatrix} y_1 \\ \cdot \\ \cdot \\ \cdot \\ \cdot \\ y_\ell \end{bmatrix}, \quad H = \begin{bmatrix} H_1 \\ \cdot \\ \cdot \\ \cdot \\ \cdot \\ H_\ell \end{bmatrix}, \quad \text{and} \quad \epsilon = \begin{bmatrix} \epsilon_1 \\ \cdot \\ \cdot \\ \cdot \\ \cdot \\ \epsilon_\ell \end{bmatrix}$$

Now the problem reduces to solving the linear system in Eq. (2.9)

for  $x_0$ .

Because of the noise present in the observations, it is not possible to compute  $x_0$  from  $y$  deterministically and some criterion must be used to obtain a solution. Using the principle of least squares, [2] [3] the optimal estimate of  $x_0$  is selected to minimize

the sum of the squares of the observation residuals, calculated from an assigned value of  $x_o$ . In this approach, the quantity  $\epsilon_i$  is interpreted not as a random noise but as an error arising from linearization mismodeling and/or the specification of an incorrect value for  $x_o$ . The solution is obtained by solving a deterministic optimization problem for which the performance index is some function of the errors  $\epsilon_i$ . The commonly defined performance index is the weighted sum of the errors  $\epsilon_i$ , expressed as

$$J = \epsilon^T R^{-1} \epsilon \quad (2.10)$$

where  $R$  is the inverse of the weights assigned to the observation. For the minimum variance or maximum likelihood estimates,  $R$  is the covariance matrix associated with the set of observation errors,  $\epsilon$ . The result of minimizing  $J$ , as defined in Eq. (2.10), leads to the following estimate [3],

$$\hat{x}_o = (H^T R^{-1} H)^{-1} (H^T R^{-1} y) \quad (2.11)$$

In order to avoid possible numerical difficulties and to make use of previous knowledge, a priori information can be included in the solution. This is equivalent to considering a performance index

$$J = \epsilon^T R^{-1} \epsilon + (x_o - \bar{x}_o)^T \bar{P}_o^{-1} (x_o - \bar{x}_o) \quad (2.12)$$

where  $\bar{x}_o$  and  $\bar{P}_o$  are the a priori state and the state error covariance respectively. These statistics represent all information on the estimate of the state prior to obtaining the observation set,  $y$ . The solution obtained by using the a priori information is given by

$$\hat{x}_0 = (H^T R^{-1} H + \bar{P}_0^{-1})^{-1} (H^T R^{-1} y + \bar{P}_0^{-1} x_0) \quad (2.13)$$

This estimate of the state deviation,  $\hat{x}_0$ , is added to the a priori state  $X_0^*$ , to obtain the least squares batch estimate for the initial state of the nonlinear system at epoch  $t_0$ , i.e.,

$$\hat{X}_0 = X_0^* + \hat{x}_0 \quad (2.14)$$

Eq. (2.13) could be the solution to a parameter estimation problem, or to the problem of state estimation of a linear dynamical system at some specified time epoch. More often the best estimate of the state of a dynamical system may be desired at different time points rather than at a single epoch. Though this could be obtained with Eq. (2.13) at desired time points, a powerful recursive algorithm designed by Kalman [1], is the most widely used technique due to its efficiency in processing the measurements sequentially. This algorithm can be derived in several different ways based on different principles. In the most direct approach, it can be derived from Eq. (2.13) using an identity in matrix algebra known as the Schurr identity, [10] which can be stated as follows:

$$(BA^{-1}B^T + C^{-1})^{-1} = C - CB(B^T CB + A)^{-1}B^T C \quad (2.15)$$

Suppose that the estimate  $\hat{x}(k/k)$  of the state at a time  $t_k$ , ( $t_1 \leq t_k \leq t_\ell$ ) based on observations up to  $t_k$ ,  $y^k$ , is to be computed recursively from the estimate  $\hat{x}(k-1/k-1)$  and its covariance  $P(k-1/k-1)$  at time  $t_{k-1}$ .  $\hat{x}(0/0)$  and  $P(0/0)$  are assumed to be given. Then the estimate and covariance at  $t_{k-1}$  are propagated according to Eq. (2.7) to obtain the a priori estimate  $\hat{x}(k/k-1)$  and

its covariance  $P(k/k-1)$  as

$$\bar{x}_k = \hat{x}(k/k-1) = \Phi(k,k-1)\hat{x}(k-1/k-1) \quad (2.16)$$

$$\bar{P}_k = P(k/k-1) = \Phi(k,k-1)P(k-1/k-1)\Phi^T(k,k-1) \quad (2.17)$$

Now, Eq. (2.15) can be applied to Eq. (2.13) if the matrices  $H$ ,  $R$ ,  $\bar{P}_0$ ,  $y$  and  $\bar{x}_0$  are replaced by the appropriate quantities; in other words, Eq. (2.13) is rewritten as

$$\hat{x}(k/k) = (\tilde{H}_k^T R_k^{-1} \tilde{H}_k + \bar{P}_k^{-1})^{-1} (\tilde{H}_k^T R_k^{-1} y_k + \bar{P}_k^{-1} \bar{x}_k) \quad (2.13a)$$

which implies that the new measurement  $y_k$  with an error  $\epsilon_k$  whose covariance is  $R_k$ , is combined with the a priori estimate,  $\bar{x}_k$ , by minimizing an appropriate performance index similar to the one defined in Eq. (2.12). Application of Eq. (2.15) to (Eq. 2.13a) leads after some algebraic manipulation, to the following expression. [3]

$$\hat{x}(k/k) = \bar{x}_k + K_k (y_k - \tilde{H}_k \bar{x}_k) \quad (2.18)$$

where

$$K_k = \bar{P}_k \tilde{H}_k^T (\tilde{H}_k \bar{P}_k \tilde{H}_k^T + R_k)^{-1} \quad (2.19)$$

The error covariance of this estimate is given by

$$P(k/k) = \bar{P}_k - K_k \tilde{H}_k \bar{P}_k \quad (2.20)$$

Equations (2.16) through (2.20) define the equations needed for the recursive filtering algorithm derived by Kalman [1]. The estimate  $\hat{X}(k/k)$  of the state for the nonlinear system is computed by adding the estimate of the deviation  $\hat{x}(k/k)$  from Eq. (2.18) to the

nominal value  $\dot{X}^*(k)$  obtained by integrating  $\dot{X}$  in Eq. (2.3) from  $t_{k-1}$  to  $t_k$  with  $\dot{X}^*(k-1)$ .  $\dot{X}^*(0)$  is assumed to be given.

The Extended Kalman Filter is the same as the above algorithm except for the reference trajectory and Eq. (2.18). The reference trajectory is updated, after processing each observation, with the estimate of the deviation. In other words  $\dot{X}$  in Eq. (2.3) is integrated from  $t_{k-1}$  to  $t_k$  with  $\hat{X}(k-1/k-1)$  instead of  $\dot{X}^*(k-1)$ , to obtain  $\bar{X}(k)$  which is updated by the estimate of the deviation

$$\hat{x}(k/k) = K_k y_k \quad (2.21)$$

and the estimate at  $t_k$ , then is

$$\hat{X}(k/k) = \bar{X}(k) + \hat{x}(k/k) \quad (2.22)$$

It should be noted that the measurement partials  $\tilde{H}_k$  are to be evaluated using the state,  $\bar{X}(k)$ . Thus the EKF algorithm is given by Eqs. (2.16), (2.17) and (2.19) through (2.22).

The least-squares solution given in Eq. (2.13) involves the inversion of an  $n \times n$  matrix,  $n$  being the dimension of the state vector, (usually  $R$  is assumed to be a diagonal matrix and, hence, involves only scalar inversion) and on many occasions due to the ill-conditioned nature of the  $n \times n$  matrix,  $(H^T R^{-1} H + P_0^{-1})$ , its inversion will result in an inaccurate solution. This numerical difficulty can be circumvented if the least-squares problem is formulated in a different way. The solution represented by Eq. (2.13) is based on the 'normal equations' formed by minimizing the performance index in Eq. (2.12). An alternate least-squares solution to the problem can be obtained if one uses the 'data equations' involving the

information matrix  $(H^T R^{-1} H + P_0^{-1})$ . This solution, discussed in Ref. [11] and [12] is based on the use of a sequence of orthogonal transformation matrices to triangularize the information matrix. The solution to the estimation problem is obtained by a sequence of back substitutions. For the scenarios considered in this investigation, we did not encounter any serious problem in matrix inversion, partly due to the word length of the Cyber 170/750 computer used for the study. Consequently, we do not present numerical results obtained with this approach. However, in an actual target tracking application where a computer with a smaller word length must be used, the matrix triangularization approach can lead to a more accurate solution than the normal matrix approach. Hence, a brief account of the approach is given in the following discussion and a useful computational algorithm is described in Chapter 5. The method could be obtained by requiring that the performance index,  $J$ , be minimized, where

$$J = \epsilon^T \epsilon$$

Then if  $T$  is an  $m \times m$  orthogonal matrix [11], it follows that

$$\begin{aligned} J &= (y - Hx_0)^T T^T T (y - Hx_0), \quad T \text{ orthogonal,} \\ &= \|\|TY - THx_0\|\|^2 \end{aligned}$$

If furthermore,  $T$  is selected so that  $TH = \begin{bmatrix} \hat{R} \\ 0 \end{bmatrix}$  where, the  $n \times n$  matrix  $\hat{R}$ , is upper triangular, it follows that

$$\begin{aligned} J &= \|\| \begin{bmatrix} \hat{R} \\ 0 \end{bmatrix} x_0 - \begin{bmatrix} \hat{z} \\ \hat{e} \end{bmatrix} \|\|^2 \\ &= \|\| (z - \hat{R}x_0) \|\|^2 + \|\|\hat{e}\|\|^2 \end{aligned} \quad (2.23)$$

$J$  is minimum when  $\hat{z} - \hat{R}x_0 = 0$  and thus the solution is obtained from the relation.

$$\hat{R}\hat{x}_0 = \hat{z} \quad (2.24)$$

The sum of the observation residuals is given by the remainder in Eq. (2.23), i.e.,  $J = \sum r_1^2 = \|\hat{e}\|^2$ . Since orthogonal matrix  $T$  is chosen such that the matrix  $\hat{R}$  is an  $n \times n$  upper triangular matrix Eq. (2.24) can be used to obtain  $\hat{x}_0$  by back substitution. When there is a weighting matrix  $R^{-1}$  in the performance index as in Eq. (2.10), the observation vector  $y$  and the matrix  $H$  are normalized by multiplying each by  $R^{-1/2}$  which amounts to scaling the  $H$  and  $y$  matrices by the standard deviations of the observations. This approach can be extended in a straight forward manner to include the information contained in the a priori estimate and covariance matrix. The a priori estimate  $\bar{x}_0$  and  $\bar{P}_0$  is converted into a data equation by writing  $\bar{P}_0$  in terms of its square root matrix  $U$ , such that  $\bar{P}_0 = UU^T$ . Using the Cholesky decomposition method [11],  $U$  can be determined as an upper triangular matrix, and if  $\tilde{R} = U^{-1}$ , then the data equation corresponding to the a priori information is

$$\tilde{z} = \tilde{R}x_0 + \tilde{\epsilon} \quad (2.25)$$

where  $\tilde{z} = \tilde{R}\bar{x}_0$ . This is combined with the observation Eq. (2.9), after normalization, as follows.

$$\begin{aligned} J &= \epsilon^T \epsilon + \tilde{\epsilon}^T \tilde{\epsilon} \\ &= (y - Hx_0)^T (y - Hx_0) + (\tilde{z} - \tilde{R}x_0)^T (\tilde{z} - \tilde{R}x_0) \\ &= \|Y - Hx_0\|^2 + \|\tilde{z} - \tilde{R}x_0\|^2 \end{aligned}$$

$$\begin{aligned}
&= \left\| \begin{pmatrix} \tilde{z} \\ y \end{pmatrix} - \begin{pmatrix} \tilde{R} \\ H \end{pmatrix} x_0 \right\|^2 \\
&= \left\| T \begin{pmatrix} \tilde{z} \\ H \end{pmatrix} - T \begin{pmatrix} \tilde{R} \\ H \end{pmatrix} x_0 \right\|^2 \\
&= \left\| \begin{pmatrix} \hat{z} \\ \hat{e} \end{pmatrix} - \begin{pmatrix} \hat{R} \\ 0 \end{pmatrix} x_0 \right\|^2 \\
&= \left\| \hat{z} - \hat{R} x_0 \right\|^2 + \left\| \hat{e} \right\|^2
\end{aligned}$$

which is again the same as Eq. (2.23) and, hence, the solution is still of the form given in Eq. (2.24). There are two types of orthogonal matrices which will produce the same result of matrix triangularization, namely, Householder transformation [11] [12] and the Givens rotation [11]. It is important to note that the above method of triangularization by orthogonal matrices will hold, only if the information array  $H$  and the observations  $y$  are normalized so that the error  $\varepsilon$  has zero mean and unit variance; however, the method can be readily extended to the case where the observation covariance matrix is not the identity matrix,  $I$ .

As is obvious, the solution by use of orthogonal transformation matrices, has been described above for the least-square problem. The method can be extended to the sequential estimation process also. Besides numerical accuracy, another attractive aspect of the orthogonal rotation method is that the orthogonal matrix  $T$ , required to convert the  $m \times n$  matrix  $H$  into the  $n \times n$  upper triangular matrix,  $\hat{R}$ , does not have to be computed and stored explicitly. The transformation is implicit and it is performed recursively on the columns of the information array. For a detailed discussion of the numerical characteristics of this method, one may refer to Lawson and Hansen [11] and Bierman [12].

### 3. Dynamical Model for a Maneuvering Target

The best strategy for the solution of the problem of estimating the trajectory of a moving target, using passive sonar frequency measurements and bearing angle measurements obtained by a set of observers, is discussed in this chapter. The target under consideration is assumed to be a slow moving object incapable of making complicated maneuvers within a short period of time. However, it can accelerate (decelerate) and can execute certain patterns of maneuvers. The maneuvers are of unknown magnitude and direction and occur at unknown times. At a given instant, the target could be in any one of the following states - it could be at rest or it could be moving with constant velocity or it could be executing a maneuver. Any proposed dynamic model must be able to accommodate all the states of motion and the state of rest. It is obviously impossible to assume an expression for the acceleration which will describe all possible maneuvers. However, a mathematical model has to be assumed which is simple enough to allow efficient computations and which can be used to estimate the general characteristics of an accelerating target. A simple model which satisfies these requirements is described below.

The problem of modeling unknown accelerations in a different practical situation has been considered by Tapley and Ingram [7], Tapley and Schutz [8] and Tapley and Hagar [9] among others. Since a deterministic expression cannot be found for the unknown acceleration, it is assumed to be a random process with known statistics. The acceleration components in a rectangular coordinate system, for example, can be modeled as (1) Brownian motion processes (zeroth order

Gauss Markov processes) or as (2) first order adaptive Gauss Markov processes driven by white noise or as (3) second order adaptive Gauss Markov process driven by white noise. These models are of increasing complexity in the order mentioned above. The first and second order adaptive Gauss Markov process models are nonlinear dynamic models whereas the Brownian motion model is a linear dynamic model. Further, the dimension of the state vector and hence the computation time increases with the order of the acceleration model. Large dimension of the state vector could cause numerical difficulties in matrix inversion. Based on these considerations we model the acceleration components as Brownian motion.

The target motion is assumed to occur in two dimensions only and the estimation state vector will contain the position, velocity and acceleration components. Use of sensor frequency measurements in the estimation process, involves assumption of a reference frequency  $f_0$ . Since the reference frequency may not be known exactly, it is necessary to include  $f_0$  in the estimation state vector. Thus, for the model considered in this investigation the state vector will have seven components - two each for position, velocity and acceleration of the target and one for the reference frequency. Under these assumptions, the equations of motion and their solution are given in the following.

The time rate of change of acceleration components are modeled as zero mean Gaussian white noise, namely,

$$\dot{a}_x = w_1 \quad (3.1)$$

$$\dot{a}_y = w_2 \quad (3.2)$$

where  $w_i \sim N(0, q_i)$ ,  $i = 1, 2$ . That is, each acceleration component is assumed to be a zero mean Gaussian process with variance,  $q_i$ . Then the solution (in the mean) to the equations of motion will be given by [2]

$$\begin{aligned}
 x(t) &= x(0) + v_x(0)t + \frac{1}{2} a_x(0)t^2 \\
 y(t) &= y(0) + v_y(0)t + \frac{1}{2} a_y(0)t^2 \\
 v_x(t) &= v_x(0) + a_x(0)t \\
 v_y(t) &= v_y(0) + a_y(0)t \\
 a_x(t) &= a_x(0) \\
 a_y(t) &= a_y(0)
 \end{aligned}
 \tag{3.3}$$

The components of position, velocity and acceleration and the reference frequency are arranged in the estimation state vector as shown below:

$$X = \begin{bmatrix} x(1) \\ x(2) \\ x(3) \\ x(4) \\ x(5) \\ x(6) \\ x(7) \end{bmatrix} = \begin{bmatrix} f_o \\ x \\ y \\ v_x \\ v_y \\ a_x \\ a_y \end{bmatrix}
 \tag{3.4}$$

The reference frequency  $f_o$  is basically a constant value. Since the value is not known exactly, its time rate of change is also assumed to be a white noise and is modeled as,

$$\dot{f}_o = w_f \quad \text{with} \quad w_f \sim N(0, q_f) \quad (3.5)$$

Then the equations of motion of the target can be written as a set of first-order differential equations

$$\begin{aligned} \dot{f}_o &= w_f \\ \dot{x} &= v_x \\ \dot{y} &= v_y \\ \dot{v}_x &= a_x \\ \dot{v}_y &= a_y \\ \dot{a}_x &= w_1 \\ \dot{a}_y &= w_2 \end{aligned}$$

which can be written in matrix form as

$$\dot{X} = AX + w \quad (3.6)$$

where

$$A = \begin{bmatrix} 0 & 0 & 0 & 0 & 0 & 0 & 0 \\ 0 & 0 & 0 & 1 & 0 & 0 & 0 \\ 0 & 0 & 0 & 0 & 1 & 0 & 0 \\ 0 & 0 & 0 & 0 & 0 & 1 & 0 \\ 0 & 0 & 0 & 0 & 0 & 0 & 1 \\ 0 & 0 & 0 & 0 & 0 & 0 & 0 \\ 0 & 0 & 0 & 0 & 0 & 0 & 0 \end{bmatrix} \quad \text{and} \quad w = \begin{bmatrix} w_f \\ 0 \\ 0 \\ 0 \\ 0 \\ w_1 \\ w_2 \end{bmatrix} \quad (3.7)$$

Note that the first-order matrix differential equation of motion for the target is linear and the state equation linearization associated with many non-linear estimation applications is not necessary. In particular, Eq. 3.6 does not have to be linearized to use the estimation algorithms described in Ch. 2. In the present problem, as modeled above, the nominal trajectory can be computed in a straight forward manner using the state-transition matrix for the matrix A given above, which is

$$\Phi(t, t_0) = \begin{bmatrix} 1 & 0 & 0 & 0 & 0 & 0 & 0 \\ 0 & 1 & 0 & (t-t_0) & 0 & \frac{1}{2}(t-t_0)^2 & 0 \\ 0 & 0 & 1 & 0 & (t-t_0) & 0 & \frac{1}{2}(t-t_0)^2 \\ 0 & 0 & 0 & 1 & 0 & (t-t_0) & 0 \\ 0 & 0 & 0 & 0 & 1 & 0 & (t-t_0) \\ 0 & 0 & 0 & 0 & 0 & 1 & 0 \\ 0 & 0 & 0 & 0 & 0 & 0 & 1 \end{bmatrix} \quad (3.8)$$

Thus considering the state  $X$  as a random vector governed by the differential equation (3.6), its mean is propagated as

$$\bar{X}(t) = \Phi(t, t_0) \bar{X}(t_0) \quad (3.9)$$

and its covariance is propagated according to [2] [3]

$$P(t) = \Phi(t, t_0) P_0 \Phi^T(t, t_0) + \int_{t_0}^t \Phi(t, \tau) Q \Phi^T(t, \tau) d\tau \quad (3.10)$$

where  $\bar{X}(t_0)$  and  $P_0$  are the a priori state and covariance at time  $t_0$  and  $Q$  is a  $7 \times 7$  matrix with zeros everywhere except  $q_1$ ,  $q_2$  and  $q_f$  on the second, third and seventh diagonal elements respectively.

#### 4. Measurement Model

##### Introduction

Measurements of two basic types are available for use in estimating the motion of a maneuvering target. These measurements are 1) the frequency of the received signal and 2) the bearing angle between the signal source and some arbitrary reference direction. The changes in the bearing angle and frequency are assumed to be related to the motion of the target. In the treatment discussed here, the effects of multipath, medium inhomogeneities and measurement bias are neglected.

##### Frequency Measurement

The mathematical model for the frequency measurement processed in the estimation algorithm, is based on the principle of the Doppler effect [13]. When both the observer and the sound source are stationary, the observer receives the true frequency,  $f_o$ , transmitted by the source. If the observer or the source or both are in motion, then the observer receives either a greater or smaller number of cycles per unit of time, depending on the relative motion between the observer and the source. This difference in frequency between the received and the transmitted wave, is known as the Doppler effect [13]. A mathematical relation exists between this frequency shift and the relative speed of the observer with respect to the source. Thus by measuring the frequency of a signal and knowing its actual frequency an observer can calculate the relative speed of the source. Depending on whether the source is moving and the observer is stationary or vice-versa, there are two different expressions for this frequency shift:

For the moving source/stationary observer case,

$$f = \frac{f_o}{1 + \frac{\dot{\rho}}{c}} \quad (4.1)$$

For the moving observer/stationary source case

$$f = f_o \left(1 - \frac{\dot{\rho}}{c}\right) \quad (4.2)$$

In each of these expressions,  $f$  is the measured frequency,  $f_o$  is the reference (or actual) frequency,  $c$  is the speed of sound in the wave propagation medium, and  $\dot{\rho}$  is the time rate of change of the linear distance between the source and the observer. In the present investigation, the source will be assumed to be in motion with respect to the observer and Eq. (4.1) is applicable.

The observed frequency  $f$  is related to the state vector through the quantities  $f$  and  $\dot{\rho}$ . This relation is non-linear and hence must be linearized in order to be used in the estimation algorithm. The linearization of the non linear relation between the state  $X$  and the measurement  $f$ , denoted by the general relation,  $Y = G(X,t)$ , involves the computation of the first partials of  $G$  with respect to (the components of)  $X$ . For a single observation, these partials form a  $(1 \times n)$  row matrix, which will be denoted by  $\tilde{H}$ . For the frequency measurement, the partials are as follows.

Let  $(x_s, y_s)$  be the coordinates of an observer (which for this investigation will be a sonar buoy),  $(x, y)$ ,  $(\dot{x}, \dot{y})$  be the components of position and velocity of the target at a given instant and let  $f$  be the frequency received at that instant. Then the range and range rate are given by

$$\rho = [(x - x_s)^2 + (y - y_s)^2]^{1/2}$$

$$\dot{\rho} = \frac{(x - x_s)\dot{x} + (y - y_s)\dot{y}}{\rho}$$

With  $G = f_o / (1 + \dot{\rho}/c)$ , we have

$$\frac{\partial G}{\partial f_o} = \frac{1}{1 + \frac{\dot{\rho}}{c}} \quad (4.3a)$$

The remaining partials can be obtained as follows:

$$\begin{aligned} \frac{\partial G}{\partial x} &= \frac{\partial G}{\partial \dot{\rho}} \frac{\partial \dot{\rho}}{\partial x} \\ &= \frac{f_o}{(1 + \frac{\dot{\rho}}{c})^2} \frac{1}{c} \frac{\partial \dot{\rho}}{\partial x} \end{aligned}$$

where

$$\begin{aligned} \frac{\partial \dot{\rho}}{\partial x} &= \frac{1}{\rho^2} \{ \rho \dot{x} - [(x - x_s)\dot{x} + (y - y_s)\dot{y}] \frac{x - x_s}{\rho} \} \\ &= \frac{\rho \dot{x} - \dot{\rho}(x - x_s)}{\rho^2} \end{aligned}$$

Using this procedure, the remaining elements of  $\tilde{H}$  are determined as follows

$$\frac{\partial G}{\partial x} = n[\rho \dot{x} - \dot{\rho}(x - x_s)] \quad (4.3b)$$

$$\frac{\partial G}{\partial y} = n[\rho \dot{y} - \dot{\rho}(y - y_s)] \quad (4.3c)$$

$$\frac{\partial G}{\partial \dot{x}} = n\rho[x - x_s] \quad (4.3d)$$

$$\frac{\partial G}{\partial \dot{y}} = n\rho[y - y_s] \quad (4.3e)$$

$$\frac{\partial G}{\partial a_x} = 0 \quad (4.3f)$$

$$\frac{\partial G}{\partial a_y} = 0 \quad (4.3g)$$

where

$$n = \frac{-f_o}{c\rho^2 \left(1 + \frac{\dot{\rho}}{c}\right)^2} \quad (4.3h)$$

Collecting the partials from Eqs. (4.3a) to (4.3h), the  $\tilde{H}$  matrix corresponding to the frequency measurement is

$$\tilde{H}_f = \begin{bmatrix} \frac{\partial G}{\partial f_o} & \frac{\partial G}{\partial x} & \frac{\partial G}{\partial y} & \frac{\partial G}{\partial \dot{x}} & \frac{\partial G}{\partial \dot{y}} & 0 & 0 \end{bmatrix} \quad (4.4)$$

where the partial derivatives are defined by Eqs. (4.3). The partial derivatives are evaluated on some reference solution assumed to be near to the actual target motion.

#### Bearing Angle

The bearing angle of the target with respect to a sensor (observer) is another type of measurement used in the estimation algorithm. It is defined as the angle between the x-axis and the line joining the sensor and the target measured in a direction from the x-axis towards the y-axis, as shown in Fig. 1.2. It is given by

$$\beta = \sin^{-1} \left( \frac{y - y_s}{\rho} \right) = \sin^{-1} \left( \frac{y - y_s}{\sqrt{(x - x_s)^2 + (y - y_s)^2}} \right) \quad (4.5)$$

This measurement is also a non linear function of the state and hence

it must be linearized. The first partials of  $\beta$  with respect to the components of the state vector are as follows:

$$\frac{\partial \beta}{\partial f_0} = 0 \quad (4.6a)$$

$$\frac{\partial \beta}{\partial x} = -\frac{y - y_s}{\rho^2} \quad (4.6b)$$

$$\frac{\partial \beta}{\partial y} = \frac{x - x_s}{\rho^2} \quad (4.6c)$$

$$\frac{\partial \beta}{\partial \dot{x}} = \frac{\partial \beta}{\partial \dot{y}} = \frac{\partial \beta}{\partial a_x} = \frac{\partial \beta}{\partial a_y} = 0 \quad (4.6d)$$

Thus the  $\tilde{H}$  matrix corresponding to the bearing angle measurement is given by

$$\tilde{H}(\beta) = \begin{bmatrix} 0 & \left[ \frac{-(y - y_s)}{\rho^2} \right] & \left[ \frac{(x - x_s)}{\rho^2} \right] & 0 & 0 & 0 & 0 \end{bmatrix} \quad (4.7)$$

#### Effects of Measurement Noise

The noise in the measurement model is assumed to be additive; in other words, the measurement  $Y_i$  obtained at time  $t_i$  is assumed to be the sum of the true value and the noise due to instrument and to signal propagation. Since the true value is not known, it is assumed to be close to the value computed using the reference trajectory. The functional relation is given by

$$Y_i = G(X_i, t_i) + \epsilon_i$$

where

$$G(X_i, t_i) = f = \frac{f_0}{\left(1 + \frac{\dot{\rho}}{c}\right)}$$

for the frequency measurement from Eq. (4.1) and

$$G(X_i, t_i) = \beta = \sin^{-1} \left( \frac{y - y_s}{\rho} \right)$$

for the bearing angle measurement from Eq. (4.5).  $\epsilon_i$  is assumed to be a zero mean Gaussian random variable. Though in reality,  $\epsilon_i$  is indirectly dependent on the range  $\rho$ , here it is assumed to be independent of the state vector and hence it remains unaltered as an additive term in the linearized equation also, as in Eq. (2.2). For real observations, the variance of the measurement error is a function of the signal to noise ratio which depends on the relative range and other parameters. For the present investigation we have assumed constant values for the measurement noise variance.

## 5. The Estimation Algorithms

### Introduction

For a target estimation problem of the type considered in this report, an on-line sequential filter is a natural choice. The Extended Kalman-Bucy Filter (EKF) is chosen to reduce the effect of non linearities on the accuracy of the estimate. The EKF may not perform well following a target maneuver or when the filter gains become very small. Further, it may not always be possible to guess a reasonable a priori value for the initial state. One way to overcome such difficulties, would be to use a batch algorithm to process an initial set of observations. The estimate obtained by the batch processor can be used, then, to start (or restart) the extended sequential filter from the time epoch. Such a hybrid combination of batch and sequential filter holds promise as the best strategy for estimating the motion of a maneuvering target with the simple model discussed in Ch. 3 and the computational algorithms for both of these filters are presented in the following sections. The numerical ill-conditioning problem often encountered in a batch solution is eliminated by use of orthogonal transformation applied to the information matrix, and the steps involved in computing the batch solution by this approach are also given. Finally, the conventional batch estimation algorithm is modified to include the effects of process noise.

### The Least-Squares Algorithm

For the computation of the least-squares solution given in Eq. (2.11) or Eq. (2.13), the matrices  $H^T R^{-1} H$  and  $H^T R^{-1} y$  must be formed using all the measurements available in a given batch. In

the case of the conventional least-squares solution for a system without the random disturbance  $w$  in the dynamics, these matrices can be formed by simple matrix additions corresponding to each observation. After processing all the observations, either Eq. (2.11) or Eq. (2.13), depending on whether a priori information is to be included or not, is used to calculate the batch solution for a given time epoch. The steps involved in this computation are as follows.

Algorithm A -- Let  $\bar{X}_0$  be the given initial state vector, and  $m$  be the number of measurement to be processed. The a priori error  $\bar{x}_0$  in the initial state and the a priori error covariance  $\bar{P}_0$  are optionally assumed to be given. The following steps lead to the estimate of the state.

0. Initialize the matrices,  $M$ , ( $n \times n$ ), where  $n$  is the dimension of the state vector and  $L$ , ( $n \times 1$ ). Set  $M = 0$ ,  $L = 0$  and  $k = 1$ .
1. Read the observation:  $t$ ,  $Y$ ,  $\sigma$ , the time, the measurement and the measurement standard deviation. Let

$$t_k = t \quad ; \quad Y_k = Y \quad ; \quad \sigma_k = \sigma \quad \text{and} \quad \Delta t = t_k - t_{k-1} .$$

2. Compute the state-transition matrix  $\Phi(t_k, t_0)$ .
3. Integrate  $\dot{X} = AX$  to get  $X(t_k)$ .  
i.e., compute  $X(t_k) = \Phi(t_k, t_0)\bar{X}_0$
4. Compute the measurement partials

$$H_k = \left. \frac{\partial G(X, t)}{\partial X} \right|_{X = X(t_k)} \quad \text{and} \quad \tilde{H}_k = \tilde{H}_k \Phi(t_k, t_0)$$

5. Compute the observation  $Y_{c_k}$  and the observation deviation,  $y_k$

where

$$y_k = Y_k - Y_{c_k}$$

6. Compute the weight:  $R_k = \sigma_k^2$
7. Update the matrices  $M$  and  $L$ :

$$M = M + H_k^T R_k^{-1} H_k$$

$$L = L + H_k^T R_k^{-1} y_k$$

8. Increment  $k$ :  $k = k+1$

If  $k \leq m$  go to step 1

9. Otherwise compute the solution  $\hat{x}_0$  as

$$\hat{x}_0 = M^{-1}L, \text{ if a priori is not to be added}$$

$$\hat{x}_0 = (M + \bar{P}_0^{-1})^{-1}(L + \bar{P}_0^{-1}\bar{x}_0) \text{ if a priori is to be added.}$$

10. Then,  $\hat{X}_0 = \bar{X}_0 + \hat{x}_0$

11. Replace  $\bar{X}_0$  with  $\hat{X}_0$  and go to step 0 for the next iteration.

With the solution  $\hat{X}_0$  one can construct the trajectory of the target, provided the assumed acceleration model adequately describes all the target maneuvers during the entire observation interval. The target maneuver acceleration model assumed for this investigation is a constant acceleration, and hence will not describe even simple maneuvers such as a steady turn with constant speed. Consequently, if the target executes a maneuver within the time span,  $\Delta T$ , over which the  $m$  observations were taken, then the solution  $\hat{X}_0$  will deviate from the true state at the epoch time due to the unmodeled acceleration. Under such circumstances, one approach to obtain a reasonable trajectory for the target would be to split the whole observation set, consisting of  $m$  observations, into several (say  $\ell$ ) batches, each consisting of a subset of the original  $m$  measurements, and then compute a least-squares solution for each batch successively

by propagating the solution from one time epoch to the time epoch of the next batch. Fig. 5.1 illustrates this idea. The arcs can be divided based on equal time intervals or an equal number of observations (i.e.,  $n_1 = n_2 = \dots = n_l$ ). In either case the number of observations in each arc,  $n_i$ , should be selected so that the information matrix  $(H_i^T R_i^{-1} H_i)$  is full rank and does not lead to numerical difficulties while computing the matrix inverse. However, the time span of each arc should not be long compared to the possible maneuver intervals. In the work reported here, we have assumed individual arcs having a constant number of observations, i.e.,  $n_i = \text{NBATCH}$ ,  $i=1, \dots, l$ .

Algorithm A is applied to each arc by replacing  $m$  by  $n_i$ , and  $\hat{X}_o$  by  $\hat{X}_{o_i}$ , and then, iterating the individual arc solution if desired. The solution of arc  $i$  at the epoch  $t_{o_i}$  is then propagated to the epoch time  $t_{o_{i+1}}$  of the next arc by the equation

$$\bar{X}_{o_{i+1}} = \phi(t_{o_{i+1}}, t_{o_i}) \hat{X}_{o_i}, \quad i = 1, 2, \dots, l - 1 \quad (5.1)$$

Thus, the initial state for the arc  $(i+1)$  will be  $\bar{X}_{o_{i+1}}$  with a priori error being zero. The a priori error covariance matrix for this initial state is computed as

$$\bar{P}_{o_{i+1}} = \phi(t_{o_{i+1}}, t_{o_i}) (H_i^T R_i^{-1} H_i + \bar{P}_{o_i}^{-1})^{-1} \phi^T(t_{o_{i+1}}, t_{o_i}) \quad (5.2)$$

The estimate, covariance pair  $[\hat{X}_{o_i}, (H_i^T R_i^{-1} H_i + \bar{P}_{o_i}^{-1})^{-1}]$  provide the estimate of the trajectory at a certain interval of time which is analogous to the extended sequential filter solution. Since the solutions  $\hat{X}_{o_i}$  are obtained by the least-squares method, the resulting trajectory may be called a 'batch-sequential' solution.

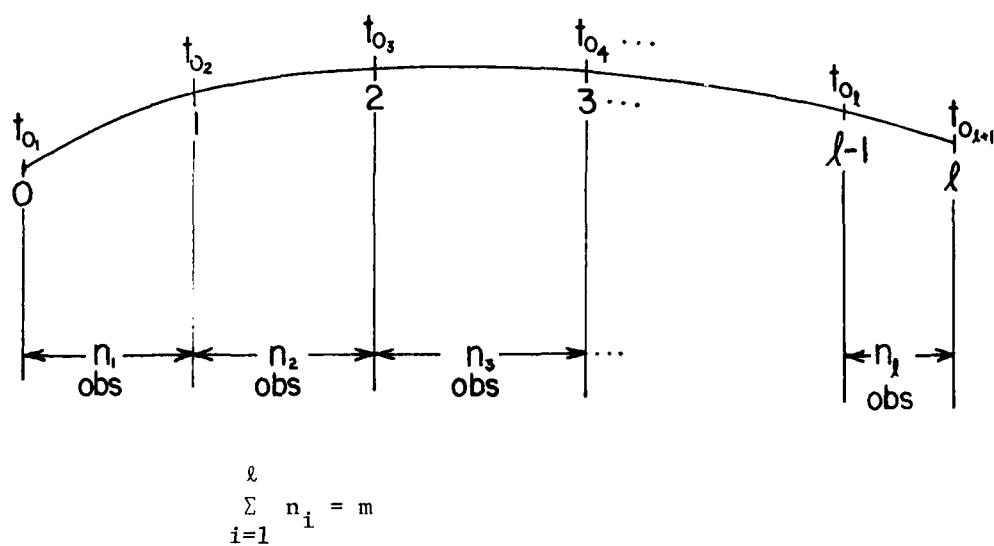


Fig. 5.1 Symbolic Representation of Dividing the Complete Observation Set into Several Batches

### Batch Estimate with Process Noise

Inclusion of the effects of process noise,  $w(t)$ , in the batch or batch-sequential solution is the next step to be considered. The solution to Eq. (2.1) with  $w \neq 0$ , is given, formally, as

$$x_{k+1} = \Phi(t_{k+1}, t_k)x_k + \int_{t_k}^{t_{k+1}} \Phi(t_{k+1}, \tau)\beta(\tau)w(\tau)d\tau \quad (5.3)$$

Presence of the second term complicates the computation of the least-squares solution. One simplifying assumption would be to consider the noise  $w(\tau)$  as a piece-wise random constant function of time with zero mean and specified covariance for each time segment. Further assumptions and the derivation of the batch solution in the presence of process noise are given in Appendix A. The computation algorithm for this case is as follows.

Algorithm B -- Given the initial state  $\bar{X}_0$ , the measurement set,  $Y_1, \dots, Y_m$ , to be processed, the a priori error  $\bar{x}_0$  in the initial state and the a priori covariance  $\bar{P}_0$ :

0. Initialize an  $n \times n$  ( $n$  being the dimension of the state vector) and an  $n \times 1$  matrices  $M = 0$  and  $L = 0$  respectively.  $k = 1$

1. Read the observation:  $t, y, \sigma$

Let  $t_k = t$  ;  $Y_k = Y$  ;  $\sigma_k = \sigma$

$$\Delta t = t_k - t_{k-1}$$

2. Compute  $\Phi(t_k, t_0)$

3. Compute  $X(t_k) = \Phi(t_k, t_0)\bar{X}_0$

4. Compute  $\tilde{H}_k = \left. \frac{\partial G(X, t)}{\partial X} \right|_{X=X(t_k)}$



This procedure forms the information arrays

$$H = \begin{bmatrix} H(1) \\ H(2) \\ \cdot \\ \cdot \\ H(m) \end{bmatrix} \quad \text{and } y = \begin{bmatrix} y(1) \\ y(2) \\ \cdot \\ \cdot \\ y(m) \end{bmatrix}$$

and the associated inverse weighting matrix,  $\Gamma$ , is given as

$$\Gamma = \begin{bmatrix} \rho_{11} + R_1 & \rho_{12} & \cdot & \cdot & \cdot & \cdot & \cdot & \rho_{1m} \\ \rho_{21} & \cdot \\ \cdot & \cdot \\ \cdot & \cdot \\ \cdot & \cdot \\ \cdot & \cdot \\ \rho_{m1} & \cdot & \cdot & \cdot & \cdot & \cdot & \cdot & \rho_{mm} + R_m \end{bmatrix}$$

With  $H$ ,  $y$ , and  $\Gamma$  determined, the solution is given by the expression

$$\hat{x}_o = (H^T \Gamma^{-1} H + \bar{P}_o^{-1})^{-1} (H^T \Gamma^{-1} y + \bar{P}_o^{-1} x_o),$$

$$\hat{P}_o = (H^T \Gamma^{-1} H + \bar{P}_o^{-1})^{-1}$$

An approximation to Algorithm B, which saves some of computation time required to invert the  $m \times m$  matrix,  $\Gamma$ , is obtained by neglecting all the non-diagonal terms in the  $\Gamma$  matrix. For such an assumption  $\Gamma^{-1}$  is obtained by  $m$  scalar divisions. This will be exactly the same as Algorithm A except for Step 6. Thus, an approximation to algorithm B, denoted as algorithm C can be obtained as follows.

Algorithm C -- All steps are exactly the same as in Algorithm A, except

Step 6 which is as follows. Compute the new weight  $R_k^{-1}$  for the

measurement:  $R_k = \sigma_k^2 + \rho_{kk}$  where

$$\rho_{kk} = \tilde{H}_k^T \left\{ \sum_{i=1}^k \left( \int_{t_{i-1}}^{t_i} \Phi(k, \tau) B(\tau) d\tau \right) Q_{i-1}^{-1} \left( \int_{t_{i-1}}^{t_i} B^T(\tau) \Phi^T(k, \tau) d\tau \right) \right\} \tilde{H}_k^T$$

All of the above algorithms can be used in either a batch or a batch-sequential solution.

#### Least-Square Solution by Matrix Triangularization

Since the theory for the approach was outlined briefly in Chapter 2, attention in this section will be devoted to the computational algorithm. Again the approach can be adapted to obtain either a batch or a batch-sequential solution. Furthermore, this method can be applied to each of the three cases discussed in the previous section, and we will denote the corresponding algorithms as Algorithm A', B', C', respectively.

Algorithm A' and C' -- Given  $\bar{x}_0, \{Y_1, \dots, Y_m\}, \bar{x}_0, \bar{P}_0$ , perform the following computations

0. Set  $m_0 = 0$ 
  - If there is no a priori  $\{\bar{x}_0, \bar{P}_0\}$ , then go to Step 1. Otherwise, compute the upper triangular square root matrix  $U$  of  $\bar{P}_0$  using the Cholesky decomposition method so that  $\bar{P}_0 = UU^T$ .
  - Invert  $U$  and let  $\tilde{R} = U^{-1}$
  - Compute  $\tilde{z} = \tilde{R}\bar{x}_0$
  - Move the upper triangular matrix  $\tilde{R}$  and the vector  $\tilde{z}$  to the information array  $\tilde{A}$ .

$$\tilde{A} = \begin{bmatrix} \tilde{R} & \tilde{z} \\ \hline & \\ 0 & 0 \\ \hline n & 1 \end{bmatrix}$$

$$\bullet m_0 = n$$

1. Set  $k = 1$

2. Read observation:  $t, Y, \sigma$

$$\text{Let } t_k = t ; Y_k = Y ; \sigma_k = \sigma$$

$$\Delta t = t_k - t_{k-1}$$

3. Compute  $\phi(t_k, t_0)$

4. Compute  $X(t_k) = \phi(t_k, t_0) \bar{X}_0$

5. Compute  $\tilde{H}_k = \left. \frac{\partial G(X, t)}{\partial X} \right|_{X = X(t_k)}$

6. Compute the observation  $Y_{c_k}$  and the residual (0-c)  $y_k = Y_k - Y_{c_k}$

7. Compute the scale factor to normalize the observation partials and the residuals (0-c):

$$\text{Algorithm A' -- } \alpha^* = \frac{1}{\sigma_k}$$

$$\text{Algorithm C' -- } \alpha^* = \frac{1}{\sqrt{\sigma_k^2 + \rho_{kk}}}$$

where

$$\rho_{kk} = \tilde{H}_k \left\{ \sum_{i=1}^k \left( \int_{t_{i-1}}^{t_i} \phi(k, \tau) B(\tau) d\tau \cdot Q_{i-1} \int_{t_{i-1}}^{t_i} B^T(\tau) \phi^T(k, \tau) d\tau \right) \right\} \tilde{H}_k^T$$

8. Stack the measurement partials and the scaled observation deviations:

$$H(k) = \alpha_k^{*\sim} H_k \phi(t_k, t_0)$$

$$y(k) = \alpha_k^* y_k$$

9. Increment  $k$ :  $k = k+1$

If  $k \leq m$ , go to Step 1

10. Compute the solution  $\hat{x}_0$ :

- (a) Move the matrices  $H$  and  $y$  to  $\tilde{A}$  such that

$$\tilde{A}(m_0+1, 1) = H(1) \quad \text{and} \quad \tilde{A}(m_0+1, n+1) = y(1)$$

Then depending on whether a priori is added or not, we have

$$\tilde{A} = \begin{array}{c|c} \tilde{R} & \tilde{z} \\ \hline H & y \\ \hline n & 1 \end{array} \quad \text{or} \quad \tilde{A} = \begin{array}{c|c} [H & y] \\ \hline n & 1 \end{array} \begin{array}{l} n \\ m \end{array}$$

- (b) Apply Givens Transformation [11] to  $A$  to obtain

$$T\tilde{A} = \begin{array}{c|c} \hat{R} & \hat{z} \\ \hline 0 & \hat{e} \\ \hline n & 1 \end{array} \begin{array}{l} n \\ m+m_0-n \end{array}, \quad \text{where } T \text{ is orthogonal}$$

- (c) The solution is computed as  $\hat{x}_0 = \hat{R}^{-1}\hat{z}$  and the covariance of the solution is,  $\hat{P}_0 = \hat{R}^{-1}\hat{R}^{-T}$

Algorithm B' -- This algorithm proceeds exactly same as Algorithm A' up through step 5. Then,

6. Stack the measurement partials matrix and the observation deviation  $y_k$  as

$$H(k) = \tilde{H}_k \phi(t_k, t_0)$$

$$y(k) = y_k$$

7. Compute (part of) the inverse weighting matrix  $\rho$ :

$$\rho = \begin{bmatrix} \rho_{11} + R_1 & \rho_{12} & \dots & \rho_{1k} \\ \vdots & \ddots & \ddots & \vdots \\ \rho_{k1} & & & \rho_{kk} + R_k \end{bmatrix}$$

where  $R_i = \sigma_i^2$ . That is, for  $i = 1, \dots, k$ , compute

$$\rho_{ik} = \tilde{H}_i \left\{ \sum_{\ell=1}^i \left( \int_{t_{\ell-1}}^{t_{\ell}} \phi(i, \tau) B(\tau) d\tau \cdot Q_{\ell-1} \int_{t_{\ell-1}}^{t_{\ell}} B^T(\tau) \phi^T(k, \tau) d\tau \right) \right\} \tilde{H}_k^T$$

8. Increment  $k$ :  $k = k+1$

If  $k \leq m$  go to Step 1

9. Compute the solution  $\hat{x}_0$ :

The arrays  $H$  and  $y$  have to be normalized using the  $m \times m$  inverse weighting matrix,  $\Gamma$ , where

$$\Gamma = \begin{bmatrix} \rho_{11} + R_1 & \rho_{12} & \dots & \rho_{1m} \\ \rho_{21} & \ddots & \ddots & \vdots \\ \vdots & & & \vdots \\ \rho_{m1} & & & \rho_{mm} + R_m \end{bmatrix}$$

- (a) To accomplish this task, compute the Cholesky decomposition of  $\Gamma = U_{\rho} U_{\rho}^T$  so that

$$\Gamma^{-1} = U_{\rho}^{-T} U_{\rho}^{-1}$$

- (b) Compute  $\bar{A} = U_{\rho}^{-1} H$  and  $\bar{z} = U_{\rho}^{-1} y$

- (c) Move the matrices  $\bar{A}$  and  $\bar{z}$  to (the information array)  $\tilde{A}$  such that

$$\tilde{A}_{(m_0+1, 1)} = \bar{A}_{(1, 1)} \quad \text{and} \quad \tilde{A}_{(m_0+1, n+1)} = \bar{z}_{(1)}$$

Then, depending on whether a priori is added or not, we have

$$\tilde{A} = \begin{bmatrix} \tilde{R} & | & \tilde{z} \\ \hline \bar{A} & | & \bar{z} \end{bmatrix} \begin{matrix} n \\ m \\ n \quad 1 \end{matrix} \quad \text{or} \quad \tilde{A} = \begin{bmatrix} \bar{A} & | & \bar{z} \\ \hline & & \end{bmatrix} \begin{matrix} m \\ n \quad 1 \end{matrix}$$

- (d) Apply Givens Transformation to  $\tilde{A}$  to obtain

$$T\tilde{A} = \begin{bmatrix} \hat{R} & | & \hat{z} \\ \hline 0 & | & \hat{e} \end{bmatrix} \begin{matrix} n \\ m+m_0-n \\ n \quad 1 \end{matrix}$$

- (e) The solution is given by  $\hat{x}_0 = \hat{R}^{-1} \hat{z}$  and its error covariance is given by  $\hat{P}_0 = \hat{R}^{-1} \hat{R}^{-T}$

### Sequential Filtering

As pointed out previously, for the problem of estimating the trajectory of a moving target, the most appropriate algorithm appears to be the Extended Kalman Filter algorithm given in Eq. (2.21), rather than the standard Kalman Filter solution given in Eq. (2.18). In the Extended Kalman Filter solution, after processing each

observation, the trajectory will be rectified using the estimate of the state. In accordance with the dynamic model given in Eq. (3.6), the covariance propagation from one time point to the next is given by

$$\bar{P}_k = \Phi(t_k, t_{k-1}) \hat{P}_{k-1} \Phi^T(t_k, t_{k-1}) + \Gamma_k \quad (5.4)$$

where

$$\begin{aligned} \bar{P}_k &= P(k/k-1) \\ \hat{P}_{k-1} &= P(k-1/k-1) \\ \Gamma_k &= \int_{t_{k-1}}^{t_k} \Phi(t_k, \tau) Q(\tau) \Phi^T(t_k, \tau) d\tau \end{aligned} \quad (5.5)$$

Assuming  $Q(t)$  to be a constant diagonal matrix and using the state transition matrix given in Eq. (3.8), the integral in Eq. (5.5) can be carried out analytically, to obtain

$$\Gamma_k = \begin{bmatrix} q_f(\Delta t) & 0 & 0 & 0 & 0 & 0 & 0 \\ 0 & q_1 \frac{(\Delta t)^5}{20} & 0 & q_1 \frac{(\Delta t)^4}{8} & 0 & q_1 \frac{(\Delta t)^3}{6} & 0 \\ 0 & 0 & q_2 \frac{(\Delta t)^5}{20} & 0 & q_2 \frac{(\Delta t)^4}{8} & 0 & q_2 \frac{(\Delta t)^3}{6} \\ 0 & q_1 \frac{(\Delta t)^4}{8} & 0 & q_1 \frac{(\Delta t)^3}{3} & 0 & q_1 \frac{(\Delta t)^2}{2} & 0 \\ 0 & 0 & q_2 \frac{(\Delta t)^4}{8} & 0 & q_2 \frac{(\Delta t)^3}{3} & 0 & q_2 \frac{(\Delta t)^2}{2} \\ 0 & q_1 \frac{(\Delta t)^3}{6} & 0 & q_1 \frac{(\Delta t)^2}{2} & 0 & q_1 (\Delta t) & 0 \\ 0 & 0 & q_2 \frac{(\Delta t)^3}{6} & 0 & q_2 \frac{(\Delta t)^2}{2} & 0 & q_2 (\Delta t) \end{bmatrix} \quad (5.6)$$

where  $\Delta t = t_k - t_{k-1}$  and  $q_f, q_1, q_2$  are defined in Eqs. (3.5) and (3.2). The computational algorithm for the extended sequential solution can be expressed as follows.

Algorithm D -- Given the initial state  $\bar{X}_0$ , number of measurements  $m$  to be processed, a priori estimate of the error in initial state  $\bar{x}_0$ , and the a priori error covariance matrix,  $\bar{P}_0$ ,

0. Initialize the state and the covariance matrix:

$$\hat{X}_0 = \bar{X}_0 + \bar{x}_0$$

$$\hat{P}_0 = \bar{P}_0 ; \text{ set } k = 1$$

1. Read the observation:  $t, Y, \sigma$

$$\text{Let } t_k = t ; Y_k = Y ; \sigma_k = \sigma \text{ and } \Delta t_k = t_k - t_{k-1}$$

2. Compute the state transition matrix  $\phi(t_k, t_{k-1})$

3. Compute  $\Gamma_k$

4. Propagate the state and the covariance:

$$\bar{X}_k = \phi(t_k, t_{k-1})\hat{X}_{k-1}$$

$$\bar{P}_k = \phi(t_k, t_{k-1})\hat{P}_{k-1}\phi^T(t_k, t_{k-1}) + \Gamma_k$$

5. Compute measurement partials:

$$\tilde{H}_k = \left. \frac{\partial G(X, t)}{\partial X} \right|_{X = \bar{X}_k}$$

6. Compute the observation  $Y_{c_k}$  and the observation deviation  $y_k$ ,

where

$$y_k = Y_k - Y_{c_k}$$

7. Compute the gain and the estimate:

$$K_k = \bar{P}_k \tilde{H}_k^T (\tilde{H}_k \bar{P}_k \tilde{H}_k^T + \sigma_k^2)^{-1}$$

$$\hat{x}_k = K_k y_k$$

8. Update the state and covariance matrix:

$$\hat{X}_k = \bar{X}_k + \hat{x}_k$$

$$\hat{P}_k = (I - K_k \tilde{H}_k) \bar{P}_k$$

9. Increment:  $k = k+1$

If  $k \leq m$  go to Step 1, otherwise stop.

#### Adaptive Sequential Filtering

Though in general the Extended Kalman Filter is very stable, in some cases where a non linear dynamic model is in error or incomplete, the filter performance, will degrade and in some cases the estimate will diverge from the true trajectory. One of the remedies for such a problem is to adapt an 'adaptive filtering' method which forces a lower bound on the unreliably decreasing state error covariance matrix by introducing fictitious noise in the dynamics, to 'cover' the model error. The variances of such fictitious state noise are estimated using the filter residuals. The method is described by Jazwinsky [14]. The dynamic model considered for the problem discussed in this report, though not non linear, is an unstable linear model and is incomplete so far as the target maneuvers are concerned. Hence, application of the Extended Kalman Filter algorithm may encounter the above mentioned divergence for some scenarios. As a

consequence, adaptive filter equations described in [14] have been implemented in the computer simulation program. The equations used for coding the algorithm are summarized in Appendix B. Since at the present the performance of the filter with the adaptive state noise compensation has not been completely evaluated, this topic will not be considered further.

## 6. Numerical Results

### Simulation Procedure

The measurement simulation is performed as follows. A representative configuration of positions for a set of sensors is assumed in a rectangular coordinate system. A trajectory for the target, with typical maneuvers, is obtained by integrating the equations of motion with an assumed acceleration model and initial conditions. At selected intervals of time, the doppler frequency and the bearing angles with respect to the sensors are computed. To obtain simulated measurements, which are representative of real observations, the computed measurements are corrupted by additive Gaussian random noise. The Gaussian noise is obtained from a sequence of numbers which are computed as follows. The random number generator RANF, which is a Fortran Library Function on the Cyber 170/750 system at the University of Texas, is used to obtain a random number  $\xi$  which is uniformly distributed over the interval (0,1). According to the Central Limit Theorem, the sum of a large number of independent and identically distributed random variables is a Gaussian random variable [15]. Since  $\xi$  has a mean of 1/2 and variance 1/12, the random variable

$$\zeta = \sum_{i=1}^N \xi_i - N/2$$

is considered Gaussian with zero mean and unit variance for  $N = 12$ . Thus, calling the RANF function twelve times and adding the returned values to  $-6.0$ , a zero mean Gaussian random number with unit variance is obtained, which is then multiplied by the given measurement standard deviation ( $\sigma_f$  for frequency and  $\sigma_\beta$  for bearing angle). The resulting random number is added to the computed

measurement to obtain the simulated observation. Other methods of generating random numbers are discussed in Reference [16].

Two basic maneuver histories are considered in this investigation. Fig. 6.1 shows the first of the target maneuver trajectory and the sensor locations. As mentioned earlier, the target motion is considered in two dimensions only. The target is assumed to have zero acceleration along the straightline paths and travels with constant speed. Consequently, during the turn and the circular motion it will have non-zero acceleration components. Thus, the trajectory shown in Fig. 6.1 represents a target moving with a constant speed of 5 m/sec along a straightline path through the origin of the coordinate system. After maintaining a steady course for 500 seconds, the first maneuver executed is a  $45^\circ$  turn. The  $45^\circ$  turns are executed with constant values for acceleration components maintaining the magnitude of the velocity to be 5 m/sec. The circular motion is executed with a constant turn rate of 0.5 deg/sec and speed 5 m/sec. The total simulation time is 1900 seconds.

Variations of the frequency and bearing angle measurements with time, computed along such a trajectory, are shown in Figures 6.2 and 6.3, respectively. These measurements are computed from the array of sensors located 2 km apart, along the sides of a right triangle, as shown by dots in Fig. 6.1 and the middle sensor of the array (sensor No. 3) is at 10 km from the origin. The coordinates of the sensor locations for this case are given in Table 6.1. It can be seen clearly (at least in the frequency plot) that the different segments of each curve correspond to the various maneuvers or straightline motions of the target. Note that for the first 500 seconds, there are

only three distinct lines in the frequency plot; this is due to the symmetry of the sensor locations with respect to the first segment of the target trajectory. In other words, during this time period, the range rate and hence the frequency from sensors 1 and 5 are equal and those from sensors 2 and 4 are equal.

Though the frequency and the bearing angle measurements are computed with respect to all the sensors simultaneously, as shown in Figures 6.2 and 6.3, observations corresponding to a specified selection of sensors and to specified intervals of time could be saved for processing. Such a capability allows one to study the effects of measurement interval and the number of measurements from different sensors on the accuracy of the estimate. The simulated observations consisting of frequency measurements from all five sensors and bearing angle measurements from only two sensors (sensor No. 1 and sensor No. 5) are processed as a nominal case. The frequency measurements are sampled every 10 seconds, whereas bearing angle measurements are sampled every 30 seconds. This amounts to a total of 955 frequency measurements and 128 measurements over a period of 1900 seconds. Variations in sensor locations and in data rate are considered to study the effects of geometry on the trajectory estimation. For all cases considered, a standard deviation of  $\sigma_f = 0.1$  Hz for the frequency measurement and  $\sigma_\beta = 5$  degrees for the bearing angle measurement are assumed to compute Gaussian random numbers. It should be remarked that the noise variance for the angle measurement depends on the relative range between the target and the sensor and that for the frequency measurement depends on the relative range and the

resolution of the measuring device. The quality of the measurements degrades with increasing range [17]. The measurement standard deviations attainable in practice vary from 3 degrees to 6 degrees for angle measurements and from 0.002 Hz to 0.2 Hz for frequency measurements. For the scenario described above, the relative range lies between approximately 2.4 km and 10 km during the entire period of simulation and hence the assumed constant values of 5 degrees for the angle and 0.1 Hz for the frequency measurement standard deviations can be considered to be realistic to pessimistic. The reference frequency for the Doppler shift measurement is assumed to be 300 Hz, and the speed of sound,  $c$ , in the ocean is assumed to be 1530 m/sec.

#### Numerical Results

Fig. 6.4 compares the estimated trajectory (the solid line) with the true trajectory (the dashed line) for the case described above, which is referred to as Case A.1. The estimated trajectory is obtained by the Extended Kalman Filter. The initial conditions for the state propagation are the same as those used for trajectory simulation, and the measurement noise standard deviations used for processing are also the same ( $\sigma_\beta = 5$  degrees,  $\sigma_f = 0.1$  Hz) as those used for observation simulation. The initial state, the diagonal elements of the a priori state error covariance matrix and the process noise covariance matrix, which were used to obtain the estimated trajectory in Fig. 6.4, are tabulated in Table 6.2. The error in the estimate ( $\hat{X}_i - X_{i_{\text{true}}}$ ,  $i = 2, \dots, 7$ ) for the components of position, velocity and acceleration are shown in Figures 6.5 through 6.10. The dashed lines in all these

figures, which are symmetric about the time-axis, represent the one-sigma standard deviations ( $\pm \sigma$ ) for the errors in the respective components. The errors in the position and velocity components are random and bounded by the one-sigma boundary except for occasional peaks. The errors in the acceleration components are also random, but show a definite trend in the mean, which can be correlated to the accelerations of the target during its various maneuver phases. The times of occurrence of maneuvers and the accelerations during these maneuvers, that were used to stimulate the trajectory, are shown also in Figures 6.9 and 6.10. It is clear that the simple Brownian motion model for the dynamics is able to follow the trends in the actual acceleration, and a close inspection of the Figures 6.4 through 6.10 indicates that, for this scenario, the accuracy of the estimated trajectory is quite satisfactory.

#### The Effect of Sensor Geometry

In order to see the effects of the sensor location geometry, the distance between consecutive sensors is reduced from 2 km to 700 m, and simulated observations for this case were obtained, holding all other parameters constant. The sensor No. 3 is at a distance of 10 km from the origin. Sensor No. 3 is kept at the same location and the others are moved symmetrically towards it as indicated by the stars in Fig. 6.1. The coordinates for these sensor locations are given in Table 6.3. The result obtained by processing the observation set obtained with this geometry (Case A.2) is shown in Fig. 6.11. Comparing Fig. 6.4 and Fig. 6.11, it is obvious that the wider the sensors are spread, the

better the tracking results. For the sensor locations selected for Case A.2, another observation set (referred to as Case A.3) was generated by including bearing angle measurements from all the 5 sensors every 10 seconds, instead of every 30 seconds from only two sensors. Consequently, this set consists of 955 frequency and 128 angle measurements for Case A.1 and Case A.2. The result obtained when Case A.3 observation set was used, is shown in Fig. 6.12. A significant improvement in the estimated trajectory, compared to the one shown in Fig. 6.11, is obtained. The same sets of values for  $X_o$ ,  $P_o$  and  $Q$  given in Table 6.2 were used for Case A.2 and Case A.3. Comparisons between the above three cases indicate that in terms of estimation accuracy and the cost of acquiring and processing observations, it is better to spread the sensor locations as far as feasible than to obtain more measurements from closely located sensors.

Keeping the same orientation of the sensor locations, the whole array is moved away from the starting position of the target, so that the sensor No. 3 is 15 km away from the origin. For this scenario (which is the same as Case A.1), three cases with the sensors 2 km apart (Case A.4), sensors 700 m apart (Case A.5) and sensors 700 m apart but bearings from all sensors every 10 seconds (Case A.6), were considered. The results are shown in Figures 6.13 through 6.15. The values for  $X_o$ ,  $P_o$  and  $Q$  in Table 6.2 are used for all three cases. Sensor location coordinates for Case A.4 are given in Table 6.4 and those for Case A.5 and Case A.6 can be found in Table 6.5. Figures 6.13 through 6.15 confirm the conclusion reached in the previous paragraph. Further, it is to be noted that an increase in range leads

to an effective decrease in the angular resolution obtained by the sensor array and hence the estimated trajectories shown in Figures 6.13 through 6.15 are much worse compared to the ones shown in Fig. 6.4, 6.11 and 6.12, respectively.

#### Effects of Errors in the Initial Estimates

In each of the above cases, a perfect initial state is assumed to compute the estimated trajectory and the estimates show the ability of the algorithms to track the motion, once an acceptable trajectory has been obtained. The results demonstrate the applicability of the maneuver model and the sequential estimation algorithm to the problem of tracking the motion of a maneuvering target. The trajectory and the errors in the estimates of the position components shown in Figures 6.16 through 6.18 are the result of processing the first observation set (Case A.1), but with errors in initial state and are to be compared with those shown in Figures 6.4 through 6.6. An initial state with errors of -300 m in the x-component and -1000 m in the y-component of the position and -3.535534 m/sec in each of the velocity components, was used to initiate the filtering process. The values of the initial state ( $X_0$ ) of the diagonal elements of the a priori state error covariance matrix ( $Q$ ) used for this case are given in Table 6.6. As can be seen from Figures 6.17 and 6.18, it takes about 120 seconds or so for the transients to disappear, and from then on, the estimated trajectory stays close to the true trajectory, as in the case of Fig. 6.4. The noncircular loops in Fig. 6.16 as opposed to the circular loops in Fig. 6.4 are due to the fact that the x- and y-axis are drawn to different scales in the former, whereas the scales are the

same in the latter. Note the change in scale for the vertical axes in Figures 6.5 and 6.6. Similar perturbations in initial state will be considered for the second type of target maneuver history in order to demonstrate the stability of the Extended Kalman Filter.

#### Comparison of Algorithm Performance

In order to compare the filter methods described in Chapter 5, a second scenario with a different trajectory and sensor orientation is considered. A simulated observation tape, corresponding to the trajectory and sensor locations (indicated by dots) shown in Fig. 6.19, was obtained from Tracor, Inc. As part of a joint effort to analyze filtering techniques for target trajectory estimation, this scenario was used to evaluate the filter algorithms described in Chapter 5. However, in order to be able to vary some parameters in the analysis, noisy measurements simulated at the University of Texas for the same trajectory, as shown in Fig. 6.19, are used to obtain the results shown in Figures 6.22 through 6.30. Values for the measurement noise standard deviations, reference frequency, speed of sound, and the turning rate are all the same as before, but the speed is 8 m/sec instead of 5 m/sec. Thus, the trajectory is computed assuming zero acceleration along the straight line paths. The initial position of the target is at (+ 10 km; - 5.6 km); the target moves along a straight path parallel to y-axis at a constant speed of 8 m/sec for the first 700 seconds and then makes a  $45^{\circ}$  turn with the above speed and a constant turn rate of 0.5 deg/sec. The acceleration components will be nonzero during this turn. After completing the turn, it proceeds

along the  $45^{\circ}$  line, as shown in Fig. 6.19, at the same constant speed. The sensor location coordinates are given in Table 6.7. The total simulation time is 1800 seconds. Frequency measurement sampled at every 10 seconds from all the sensors and bearing angle measurements sampled at every 30 seconds from sensor No. 1 and sensor No. 5 are saved for processing and consequently the observation set will have a total of 905 frequency measurements and 122 bearing angle measurements. The observation set simulated for the scenario described above will be referred to as Case B.1.

The frequency and bearing angle measurements simulated in Case B.1 have been plotted (without the noise being added) against time and are shown in Figures 6.20 and 6.21, respectively. The frequency, being a function of the range rate of the target (see Eq. 4.1), varies as the range rate changes. The range rates corresponding to all the sensors are negative to start with, and increase steadily as the target moves, and hence the computed values of the frequencies decrease continuously. The sharp corners are due to the jump in the values for the accelerations components occurring at the start (700 sec.) and at the end (790 sec.) of the target maneuver, and the steep linear increase in the frequency values occurs during the turn. The line joining the sensors 3, 4, and 5 is perpendicular to the trajectory at a point towards the end, at which the range rates of the target with respect to these sensors become zero. Hence, the frequency curves corresponding to these sensors concur at a point with the ordinate 300 cycles/sec., as can be observed in Fig. 6.20. The bearing angles (measured from positive x-axis towards positive y-axis) with respect to all the sensors

increase continuously, as the target moves along the trajectory, and are shown in Fig. 6.21. Taking the bearing angle as modulo  $2\pi$  causes the discontinuities in the curve, which occur when the target crosses from one quadrant to the next for the respective sensors. Finally, note that in this figure also, the curves corresponding to the sensors 3, 4, and 5 intersect at one point due to the fact that the position of the target at this time lies on the same line joining these three sensors.

Trajectory solutions obtained by processing the above observation set Case B.1. using the Extended Kalman Filter and the "batch-sequential" filter are shown in Figures 6.22 through 6.24 in order to compare the two filter algorithms. The initial state  $X_0$ , the a priori state error covariance matrix  $P_0$ , and the process noise covariance matrix  $Q$  used to obtain the estimated trajectories shown in the above three figures, are tabulated in Table 6.8. The initial state is the same as that used for simulating the true trajectory (shown by dashed lines), and the measurement noise standard deviations used for processing the measurements are also the same as those used for simulation of the observations. One common feature among all the three figures is that the estimated trajectories stay closer to the true trajectory in the earlier portion than during the rest of the estimation period. This can be explained by noting that the initial state for the estimation process is exact, yielding a perfect trajectory to start with, and also the filter gains are large in the beginning, which decrease when the state error covariance matrix decreases with time. Another common feature among the three figures is the large deviation of the estimated

trajectories from the true trajectory, occurring approximately around a point (10 km - 2.5 km). At this point, the frequency measurement becomes insensitive to the target position and velocity when the radius vector joining the target and a sensor is normal to the velocity vector of the target. Hence the frequency measurements from sensor No. 1 will have very little or no information about the target state when the y-coordinate of the target is near -1.4 km. This could be the reason for the above mentioned large deviation in the estimated trajectories. Fig. 6.22 shows a comparison between the true and the estimated trajectory obtained by using the Extended Kalman Filter, whereas the true and the estimated trajectories obtained by using "batch-sequential" algorithm are compared in Figures 6.23 and 6.24. The only difference between the latter two trajectories is that the one in Fig. 6.23 does not have process noise in the dynamics, whereas the one in Fig. 6.24 includes the effects of non-zero covariance for the process noise in the acceleration components. For both trajectories, the observation set (Case B.1) is divided into 34 small batches, each consisting of 30 observations and batch solutions are obtained for each sub-arc, as described in Algorithm B of Chapter 5. The solution of each sub-arc is iterated 4 times within the sub-arc and the estimate converges in 2 or 3 iterations for all arcs. Besides being not so accurate compared to the EKF estimates, these trajectories take an appreciable amount of computing time. For example, the execution times for the trajectories shown in Figures 6.22 through 6.24 are 10.8 sec., 59.6 sec., 210.7 sec., respectively. Comparing Fig. 6.23 with Fig. 6.24,

it is obvious that having process noise in the dynamics shows a definite improvement in the solution. From the above discussion of Figures 6.22 through 6.24, one can conclude that the performance of the EKF algorithm is comparable to the "batch-sequential" algorithm both in terms of accuracy and computing time.

In order to check the performance of the EKF, the initial conditions to the filter were perturbed and solutions were obtained. A few sets of initial errors were considered and the results of processing the observation set Case B.1, for one typical set of errors are shown in Figures 6.25 through 6.27. The initial state  $X_0$ , the a priori state error covariance matrix  $P_0$ , and the process noise covariance matrix  $Q$  used to obtain these figures, are given in Table 6.9. During the initial few seconds the error in the x-component of position oscillates between -3.3 km and 2.4 km and that in the y-component between -1.0 km and 1.9 km. These figures show that after about 90 seconds of initial transients, the estimated trajectory converges to the true trajectory, indicating that a reasonable error in initial state will not cause a total failure of the EKF algorithm. However, the performance of the filter is degraded in that the deviation of the estimated trajectory from the true trajectory shown in Fig. 6.25 is larger compared to that in Fig. 6.22. The increase trend in the later part of the one-sigma curve shown in Fig. 6.27 may not signify the divergence of the filter, since that in Fig. 6.26 decreases steadily and the errors in both the components of position are well-bounded within the one-sigma curves.

In order to verify the statement made earlier regarding sensor geometry for this scenario also, the sensor locations are spread over a wider area (as marked by the stars in Fig. 6.19 and the coordinates given in Table 6.10) and a set of simulated observations (Case B.2) were obtained. Using the set of values for  $X_0$ ,  $P_0$  and  $Q$  given in Table 6.9, i.e., with the same set of initial errors as for Figures 6.25 through 6.27, the results obtained by processing this observation set are shown in Figures 6.28 through 6.30. When compared with Fig. 6.25, a significant improvement can be noticed in the estimated trajectory shown in Fig. 6.28. Though in this case also it takes about 90 seconds for the initial transients to disappear, the errors in Figures 6.29 and 6.30 are bounded with the one-sigma curves and are smaller compared to those shown in Figures 6.26 and 6.27, respectively. (Note the difference in scale between the corresponding figures.) Hence, it can be concluded again that a wider station location geometry reduces estimation errors.

Table 6.1 Sensor Location Coordinates for Case A.1

sensor No.	x-coordinate (m)	y-coordinate (m)
1	7071.07	3071.07
2	7071.07	5071.07
3	7071.07	7071.07
4	5071.07	7071.07
5	3071.07	7071.07

Table 6.2 Values of  $X_o$ ,  $P_o$  and  $Q$  for Processing Case A.1 through Case A.6 (Figures 6.4 through 6.15)

Component of State	Initial State $X_o$	Diagonal of $P_o$	Diagonal of $Q$
$x_1$	300.0	1.0	0.0
$x_2$	0.0	1.0E+05	0.0
$x_3$	0.0	1.0E+05	0.0
$x_4$	3.535534	1.0E+01	0.0
$x_5$	3.535534	1.0E+01	0.0
$x_6$	0.0	1.0E-02	1.0E-05
$x_7$	0.0	1.0E-02	1.0E-05

Table 6.3 Sensor Location Coordinates for Cases A.2 and A.3

Sensor No.	x-Coordinate (m)	y-Coordinate (m)
1	7071.07	5671.07
2	7071.07	6371.07
3	7071.07	7071.07
4	6371.07	7071.07
5	5671.07	7071.07

Table 6.4 Sensor Location Coordinates for Case A.4

Sensor No.	x-Coordinate (m)	y-Coordinate (m)
1	10606.6	6606.6
2	10606.6	8606.6
3	10606.6	10606.6
4	8606.6	10606.6
5	6606.6	10606.6

Table 6.5 Sensor Location Coordinates for Cases A.5 and A.6

Sensor No.	x-Coordinate (m)	y-Coordinate (m)
1	10606.6	9206.6
2	10606.6	9906.6
3	10606.6	10606.6
4	9906.6	10606.6
5	9206.6	10606.6

Table 6.6 Perturbed Values of  $X_0$  and Values of  $P_0$  and  $Q$  for Case A.1 (figures 6.16 through 6.18)

Components of state	Initial state $X_0$	Diagonal of $P_0$	Diagonal of $Q$
$x_1$	300.0	1.0	0.0
$x_2$	-300.0	1.0E+08	0.0
$x_3$	-1000.0	1.0E+08	0.0
$x_4$	0.0	1.0E+02	0.0
$x_5$	0.0	1.0E+02	0.0
$x_6$	0.0	1.0E-02	1.0E-05
$x_7$	0.0	1.0E-02	1.0E-05

Table 6.7 Sensor Location Coordinates for Case B.1

Sensor No.	x-Coordinate (m)	y-Coordinate (m)
1	0.0	-1400.0
2	-700.0	-700.0
3	-1400.0	0.0
4	-700.0	700.0
5	0.0	1400.0

Table 6.8 Values of  $X_0$ ,  $P_0$ , and  $Q$  used for Case B.1

Components of state	Initial state $X_0$	Diagonal of $P_0$	Diagonal of $Q$
$x_1$	300.0	1.0	0.0
$x_2$	10000.0	1.0E+05	0.0
$x_3$	-5600.0	1.0E+05	0.0
$x_4$	8.0	1.0E+01	0.0
$x_5$	0.0	1.0E+01	0.0
$x_6$	0.0	1.0E-02	1.0E-05
$x_7$	0.0	1.0E-02	1.0E-05

Table 6.9 Perturbed Values of  $X_0$  and Values of  $P_0$  and  $Q$  for case B.1 and B.2 (Figures 6.25 through 6.30)

Components of state	Initial state $X_0$	Diagonal of $P_0$	Diagonal of $Q$
$x_1$	300.0	1.0	0.0
$x_2$	10000.0	1.0E+08	0.0
$x_3$	-6600.0	1.0E+08	0.0
$x_4$	0.0	1.0E+02	0.0
$x_5$	0.0	1.0E+02	0.0
$x_6$	0.0	1.0E-02	1.0E-05
$x_7$	0.0	1.0E-02	1.0E-05

Table 6.10 Sensor Location Coordinates for Case B.2

Sensor No.	x-Coordinate (m)	y-Coordinate (m)
1	0.0	-4000.0
2	-2000.0	-2000.0
3	-4000.0	0.0
4	-2000.0	2000.0
5	0.0	4000.0

SIMULATED SCENARIO A; CASE A  
 TRAJECTORY FOR OBSERVATION GENERATION

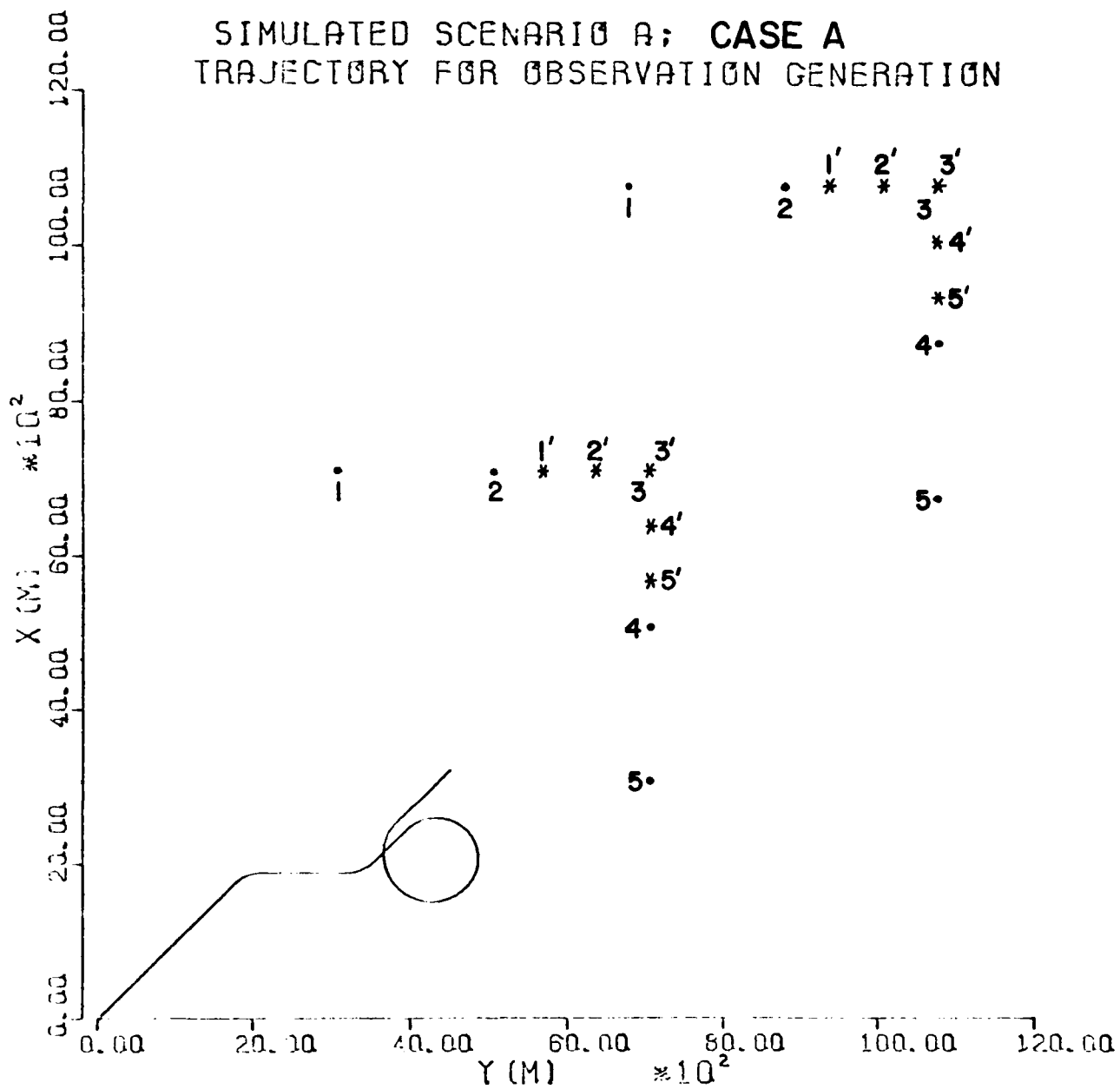


Fig. 6.1

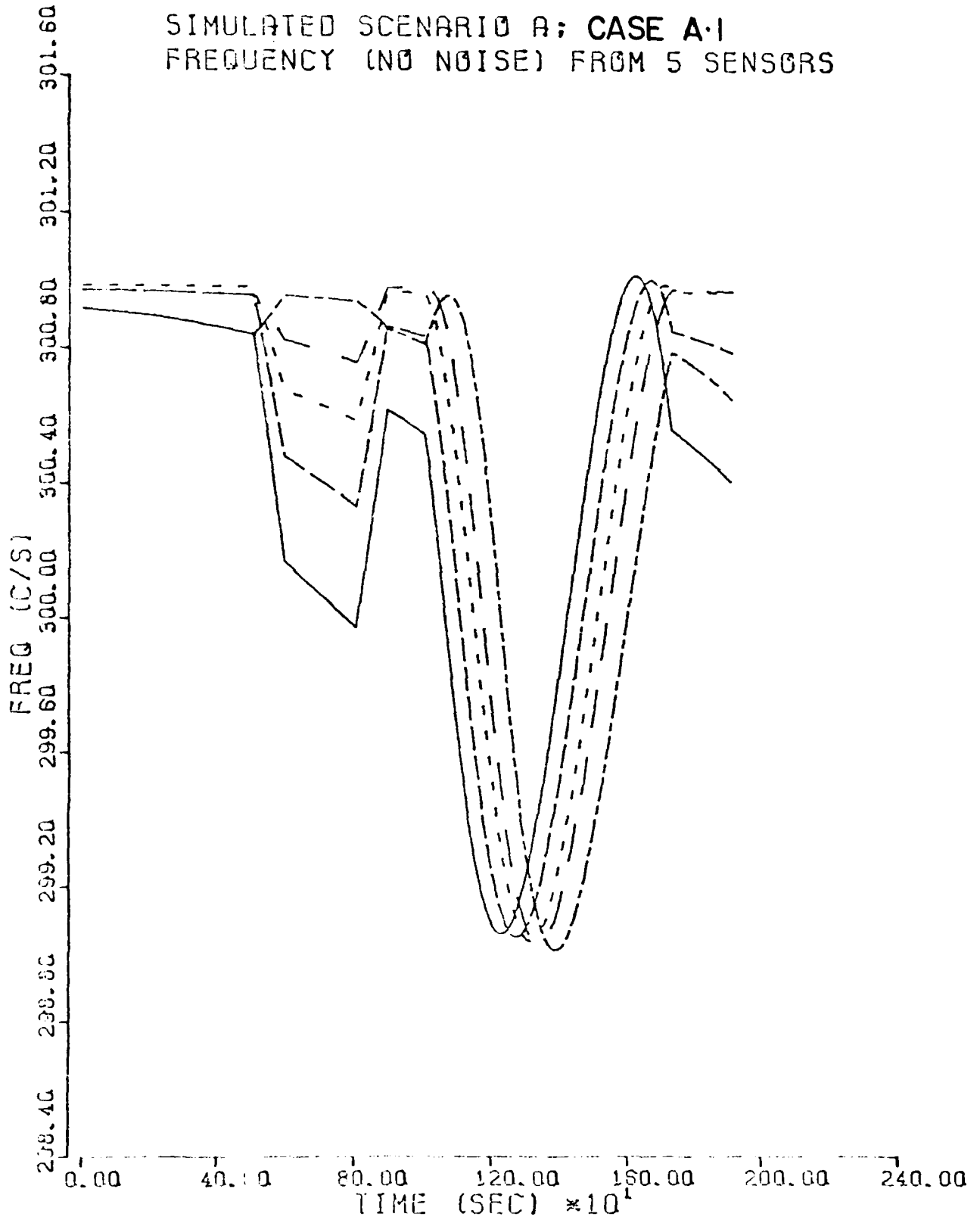


Fig. 6.2

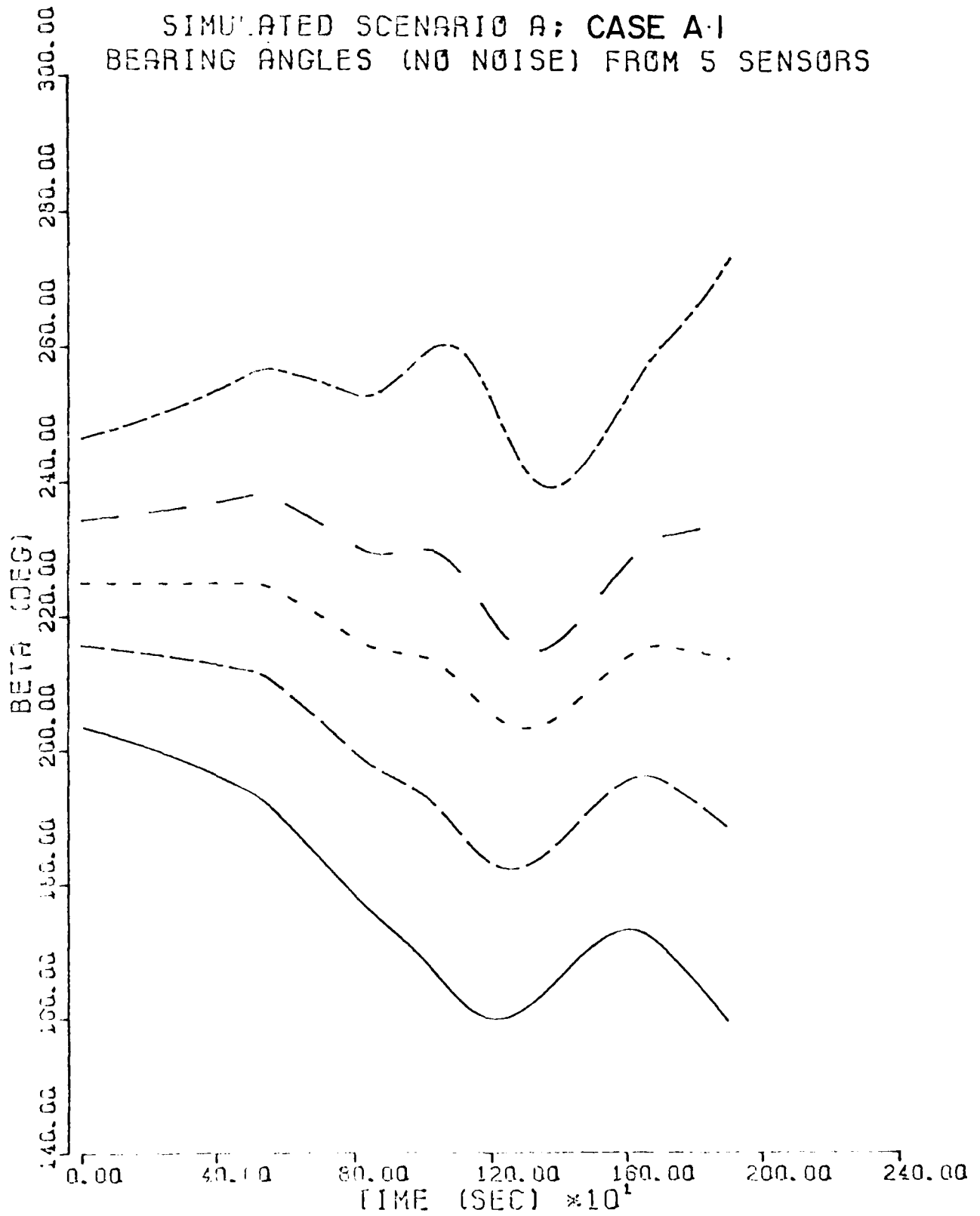


Fig. 6.3

SIMULATED SCENARIO A; CASE A-1  
EXTSEQ ONLY; EXACT X0; P0=E5; Q=E-5

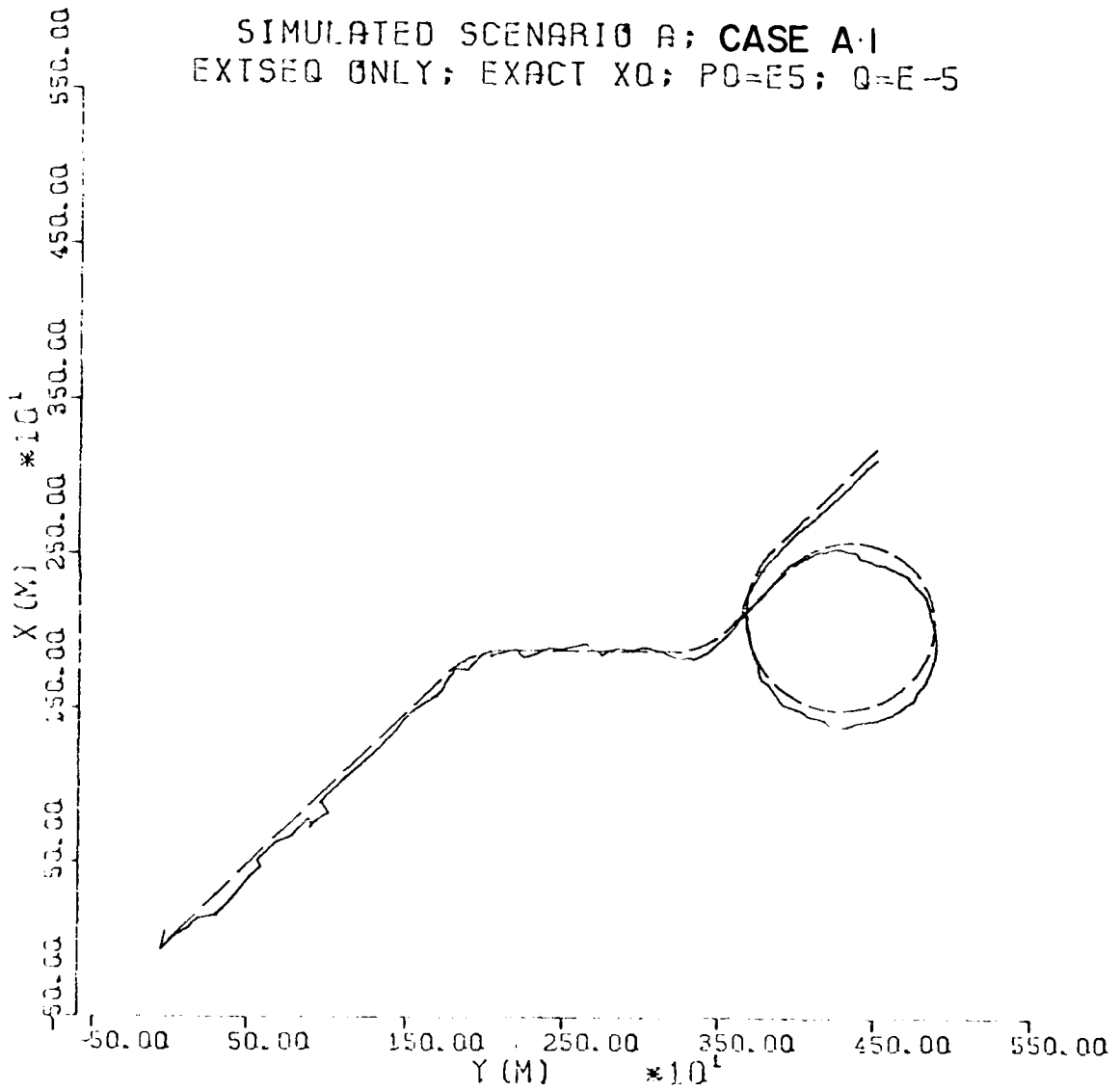


Fig. 6.4

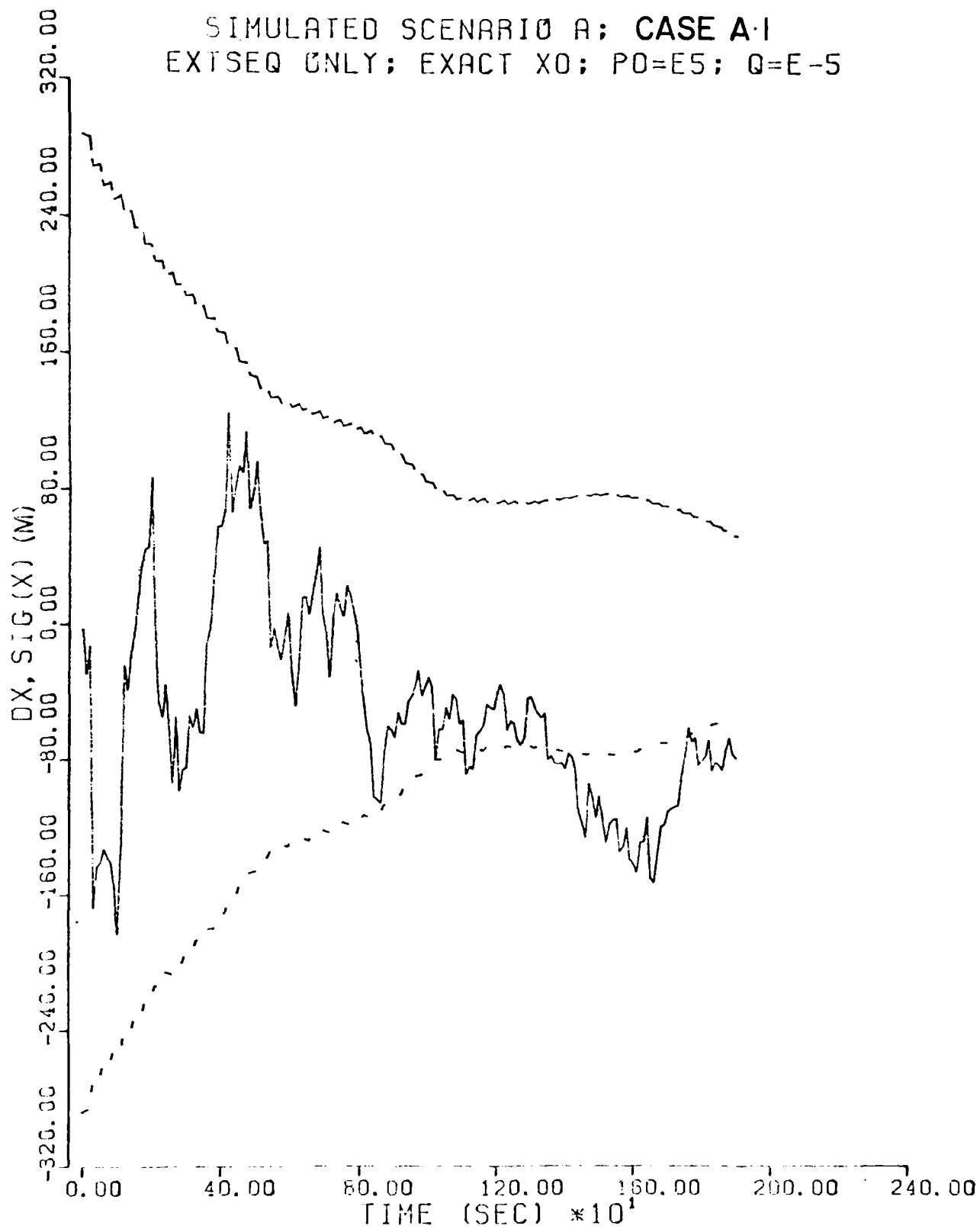


Fig. 6.5

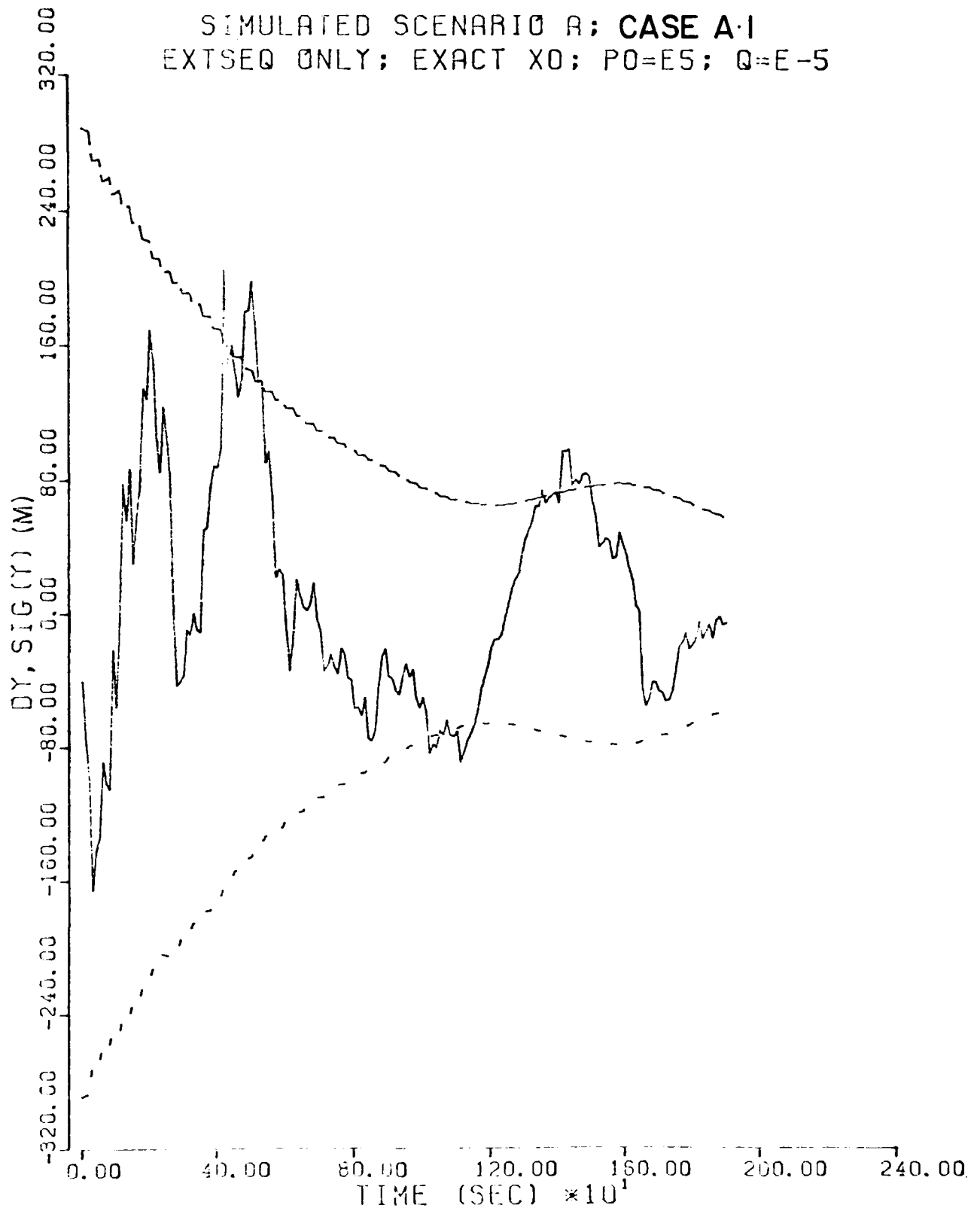


Fig. 6.6

SIMULATED SCENARIO A; CASE A-1  
EXTSEQ ONLY; EXACT X0; P0=E5; Q=E-5

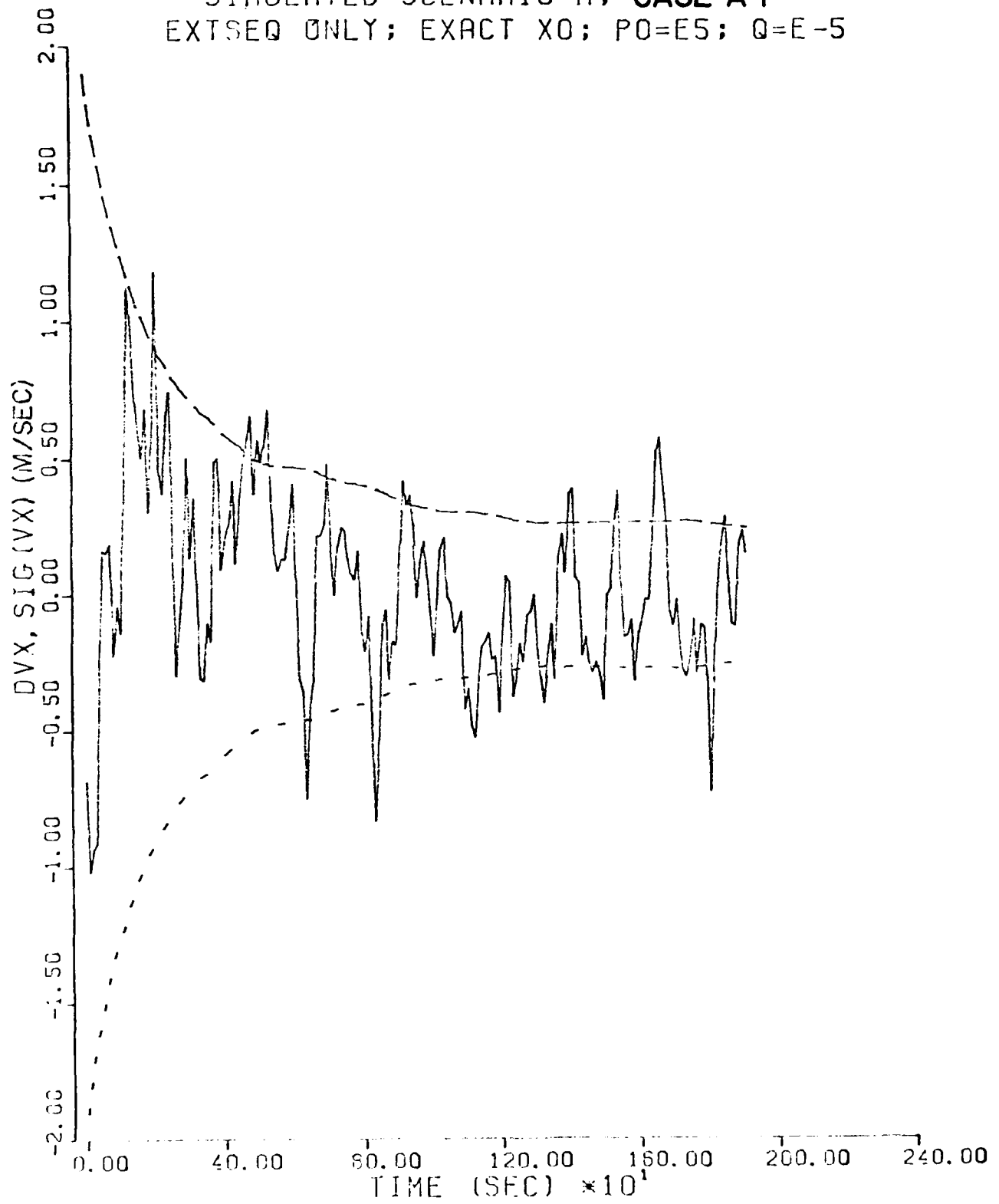


Fig. 6.7

SIMULATED SCENARIO A; CASE A-1  
EXTSEQ ONLY; EXACT X0; P0=E5; Q=E-5

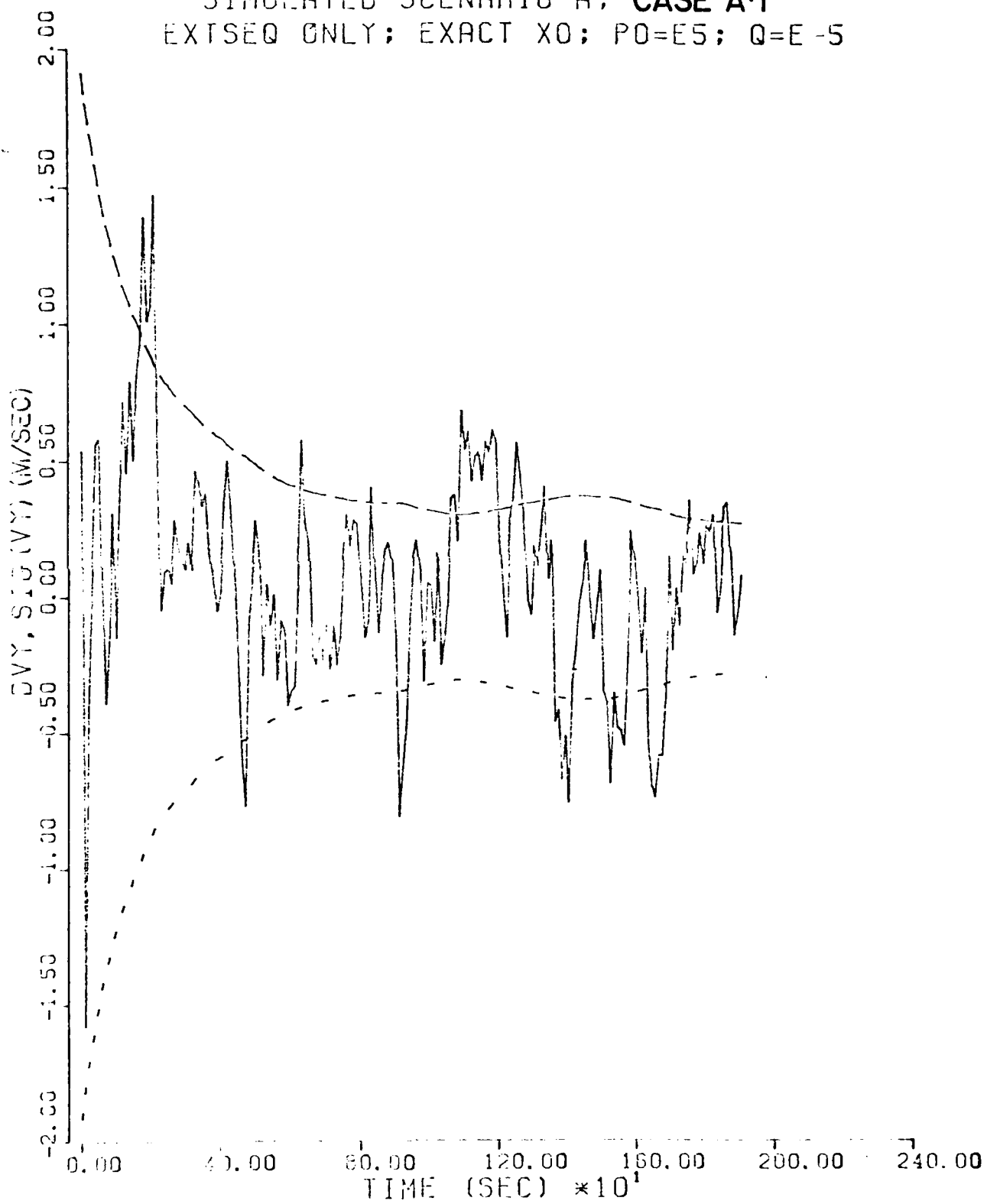


Fig. 6.8

SIMULATED SCENARIO A; CASE A-1  
EXTSEQ ONLY; EXACT X0; P0=E5; Q=E-5

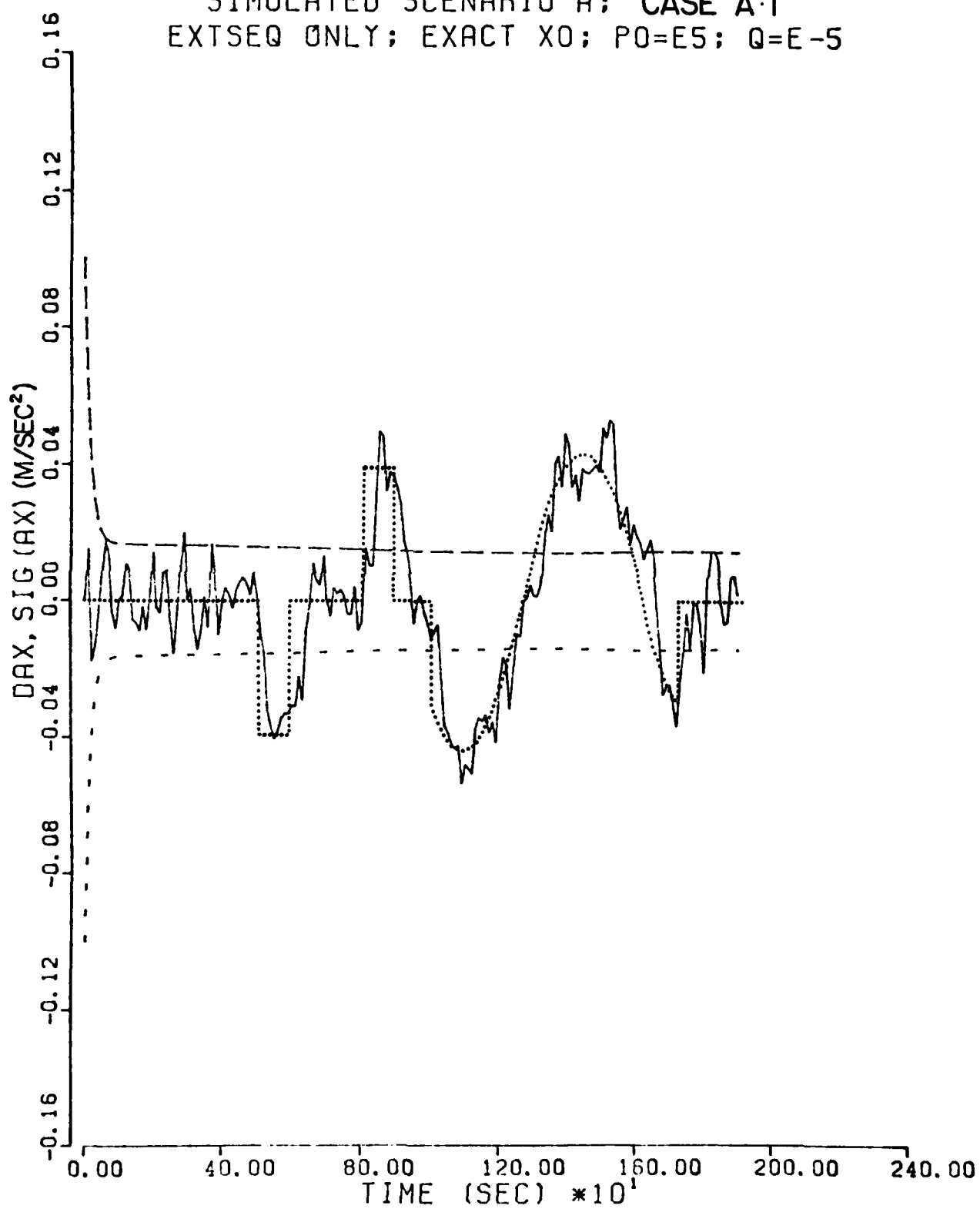


Fig. 6.9

SIMULATED SCENARIO A; CASE A.1  
EXTSEQ ONLY; EXACT X0; P0=E5; Q=E-5

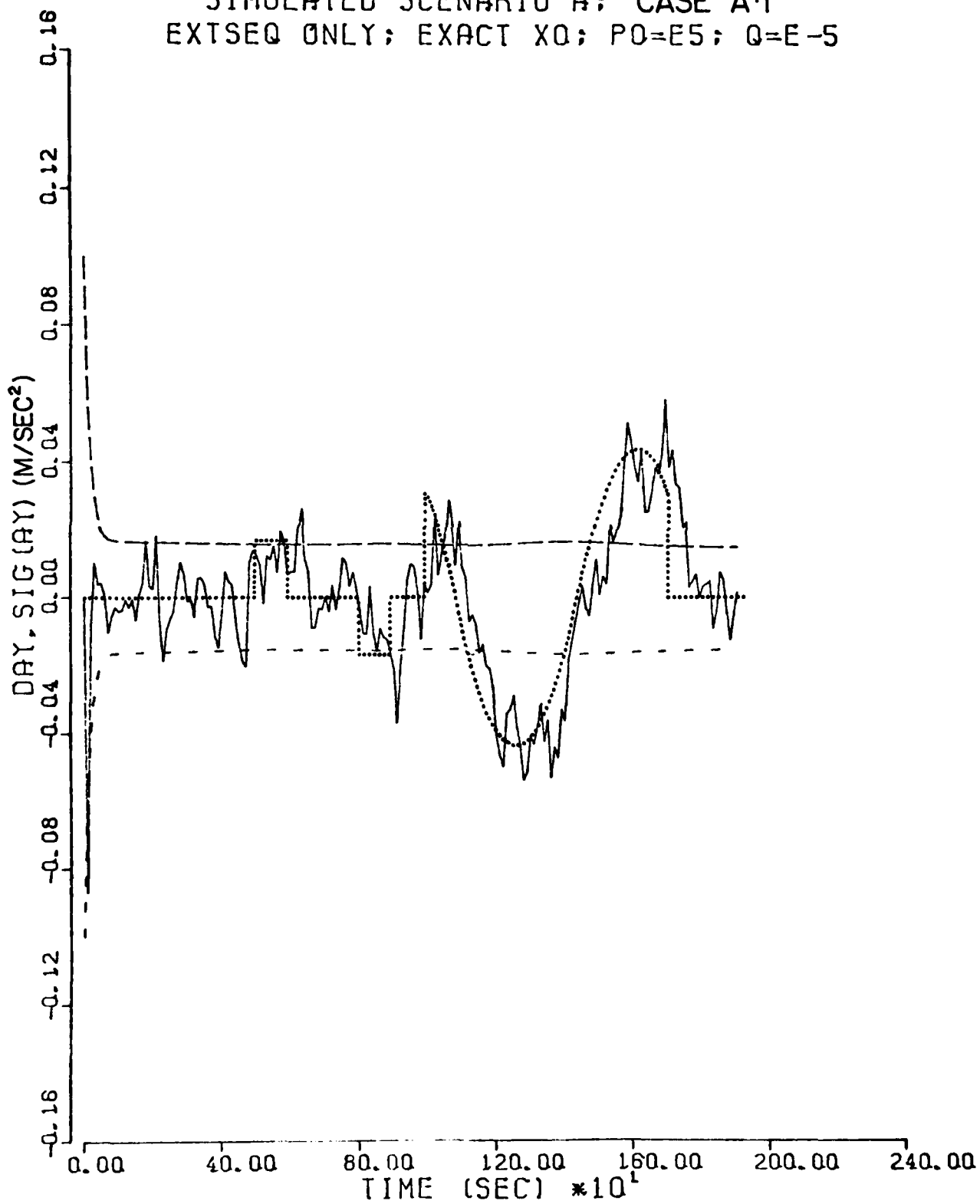


Fig. 6.10

SIMULATED SCENARIO A; CASE A-2  
EXTSEQ ONLY; EXACT X0; P0=E5; Q=E-5

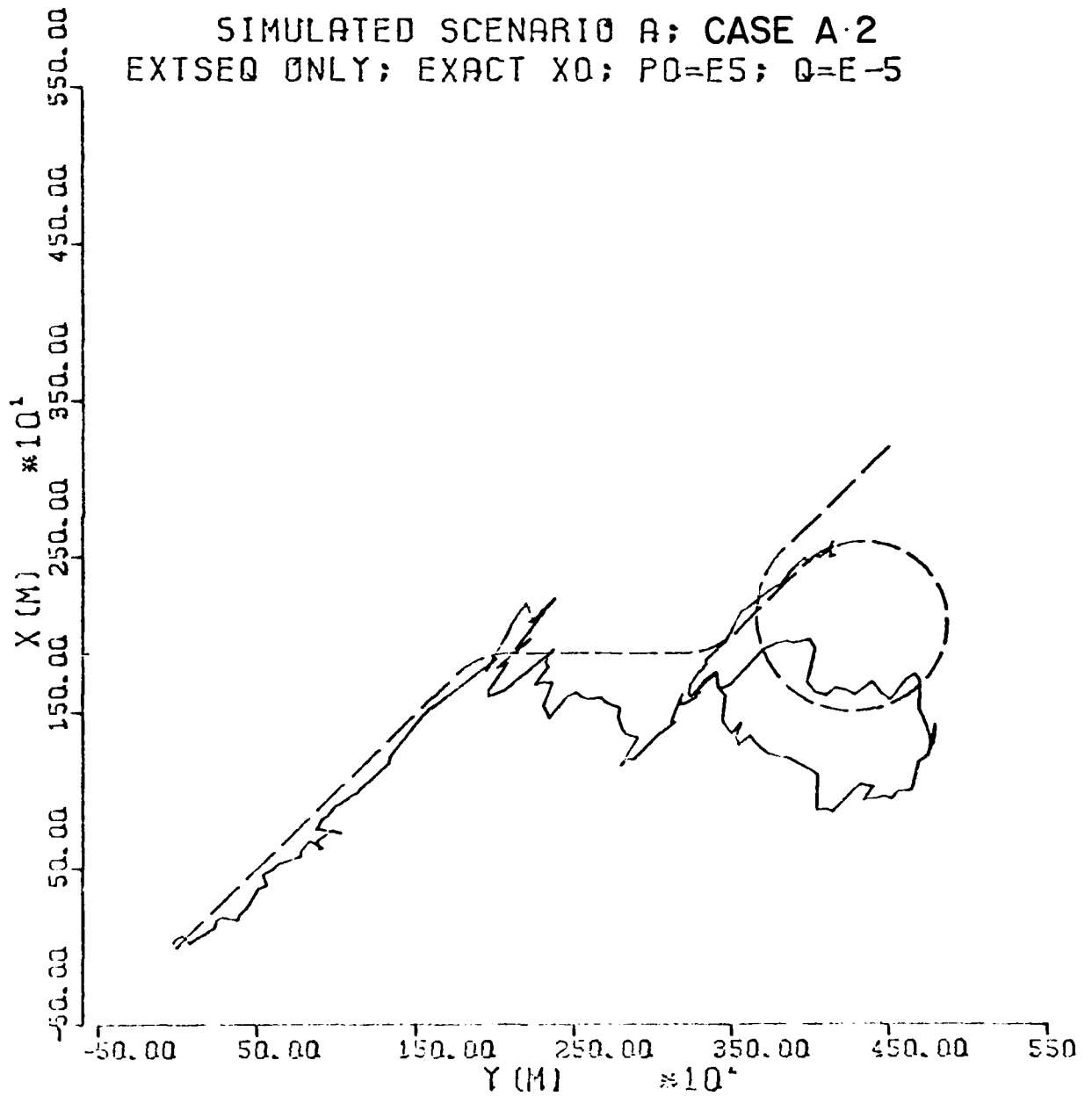


Fig. 6.11

SIMULATED SCENARIO A; CASE A-3  
EXTSEQ ONLY; EXACT X0; PO=E5; Q=E-5

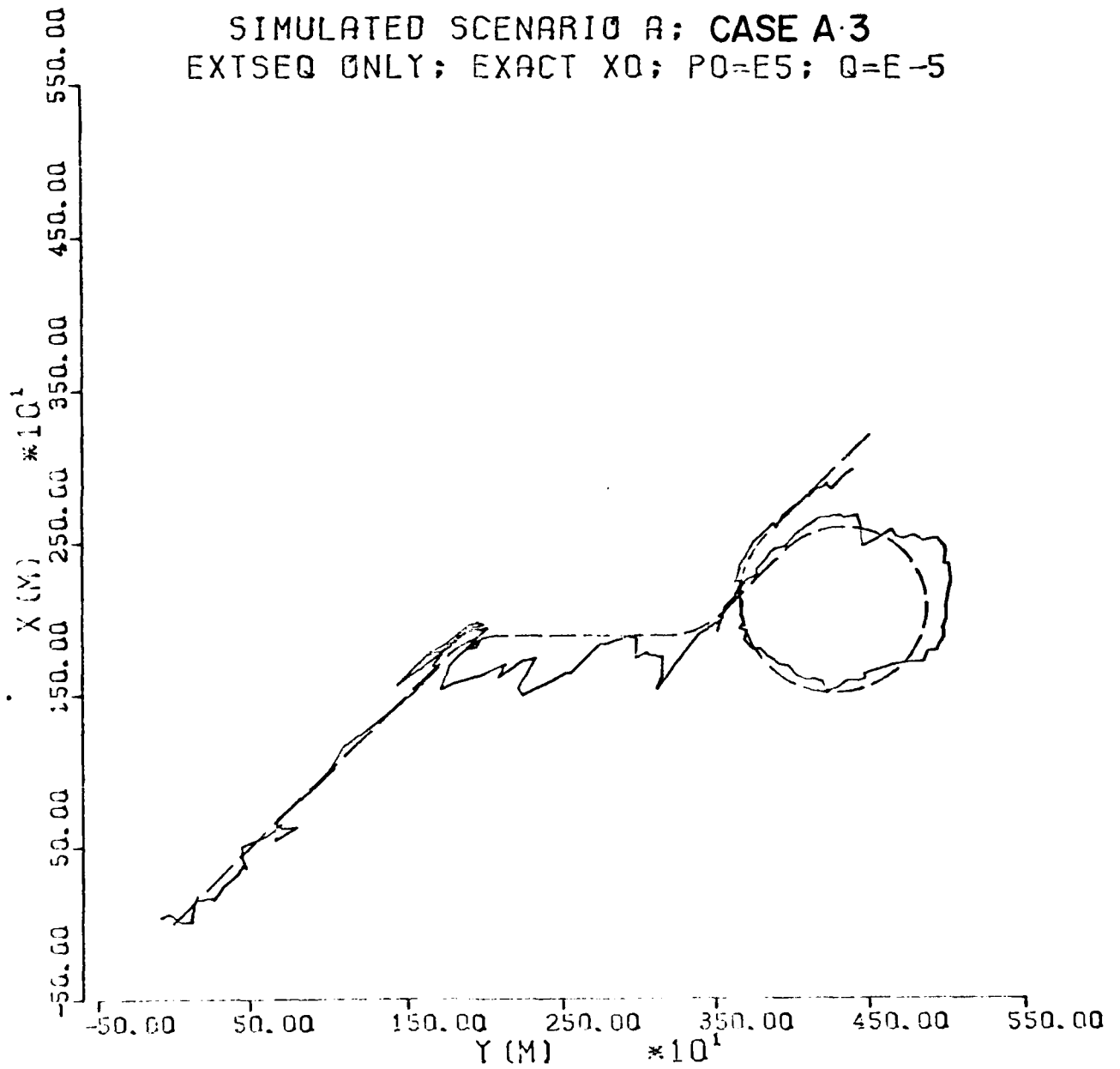


Fig. 6.12

SIMULATED SCENARIO A; CASE A-4  
EXTSEQ ONLY; EXACT X0; P0=E5; Q=E-5

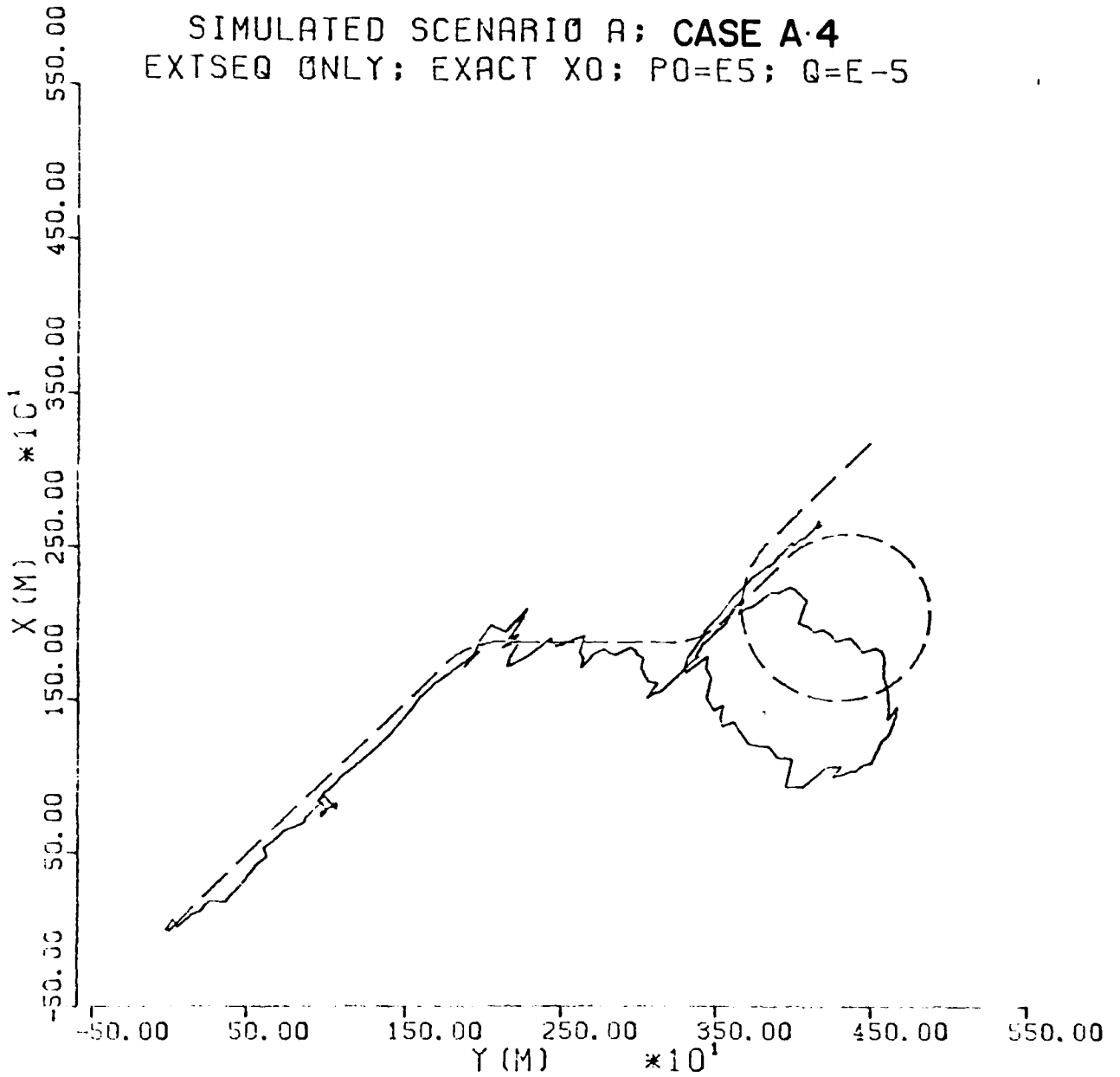


Fig. 6.13

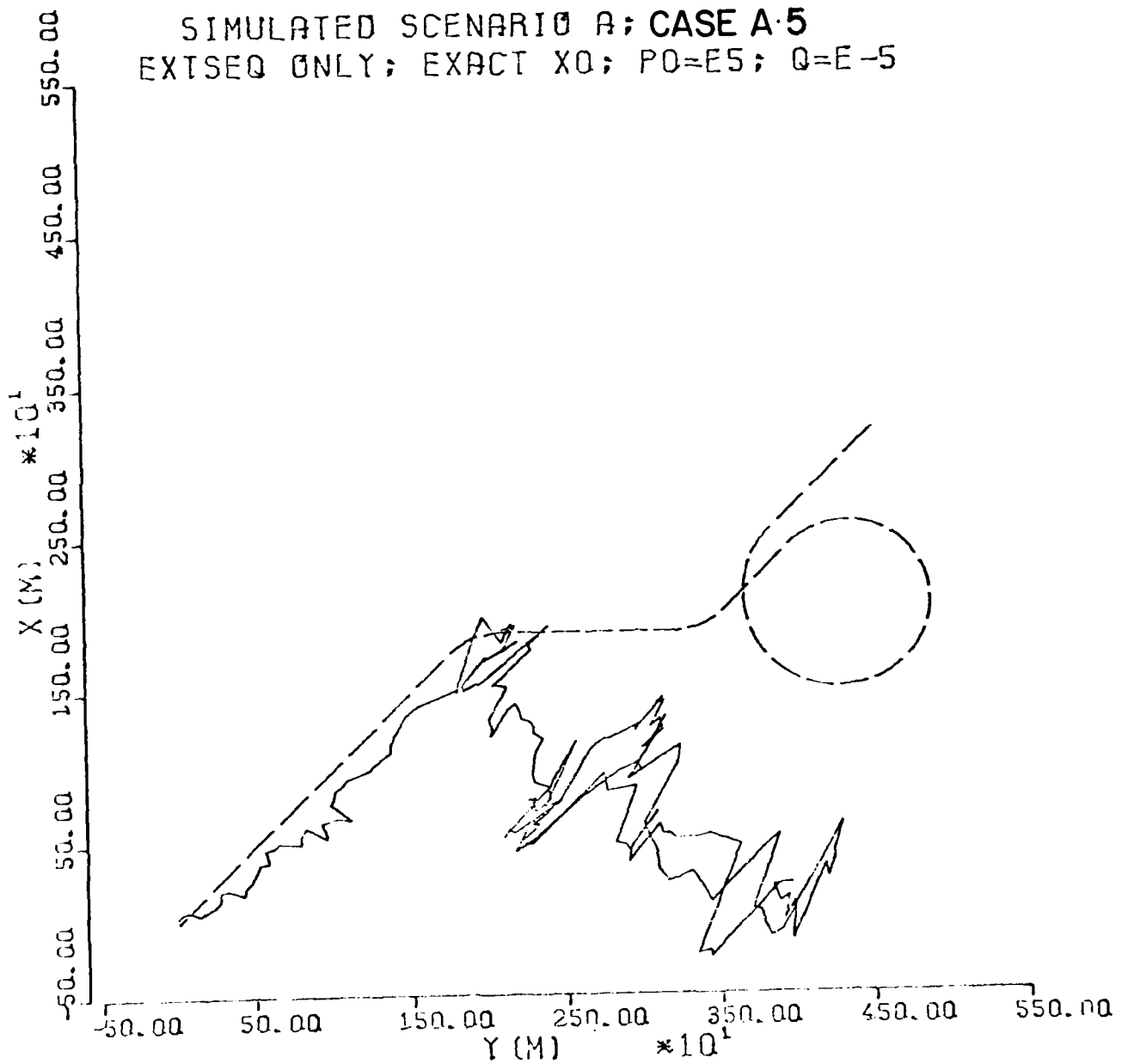


Fig. 6.14

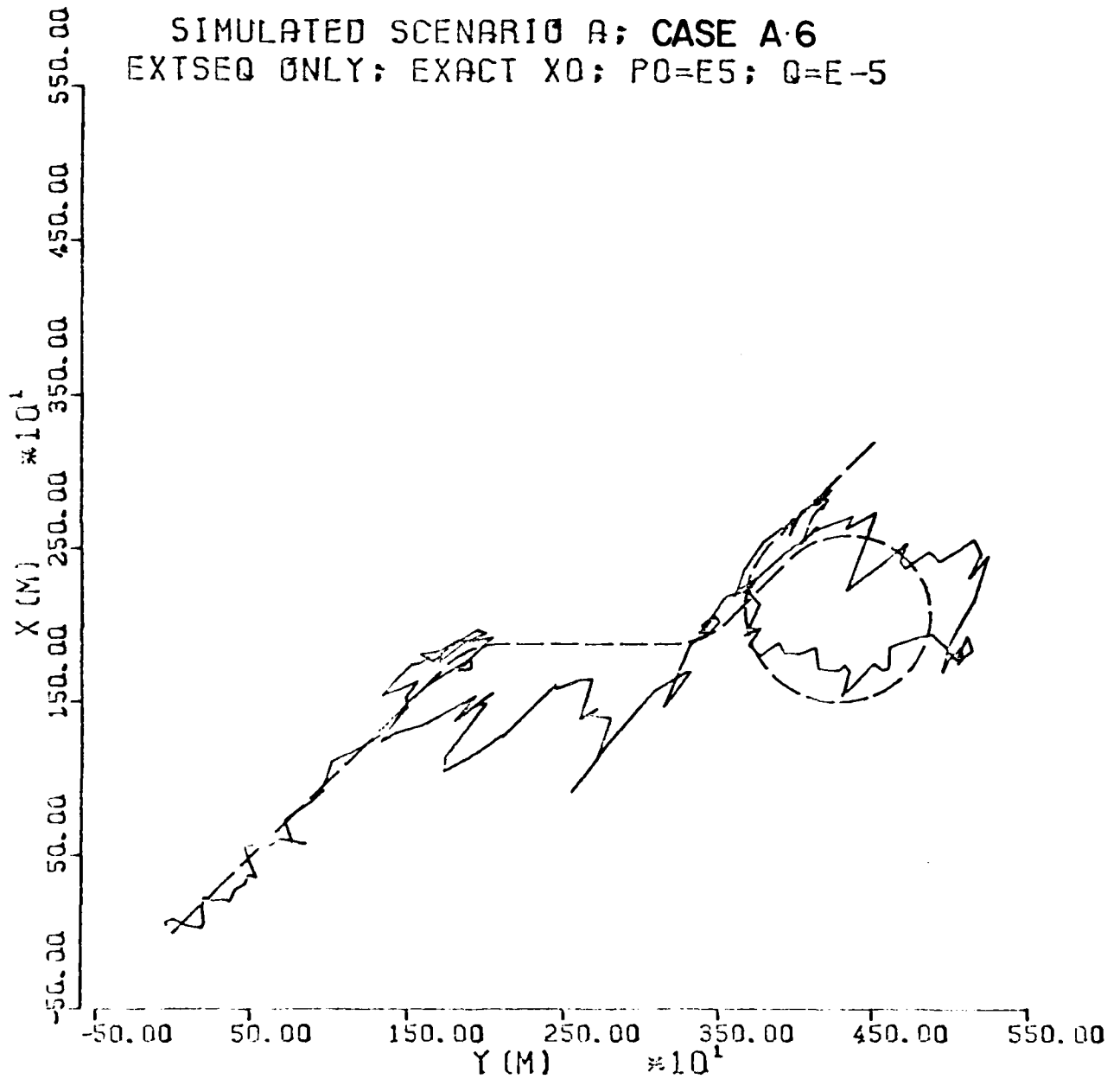


Fig. 6.15

SIM SCENARIO A; CASE A-1 PO=E8, Q=E-5  
EXTSEQ ONLY; DX0=-300, DY0=-1000, DVO=-5

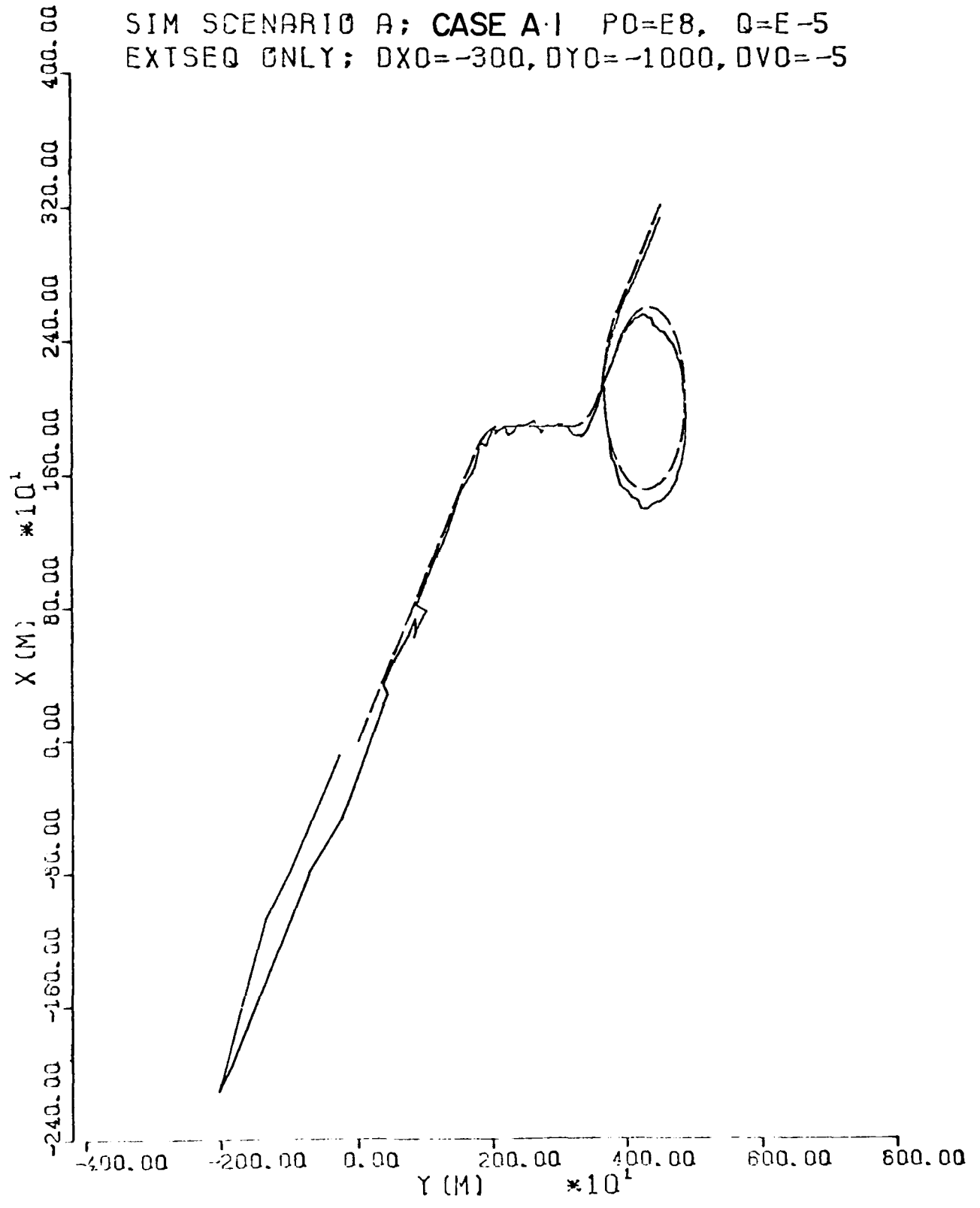


Fig. 6.16

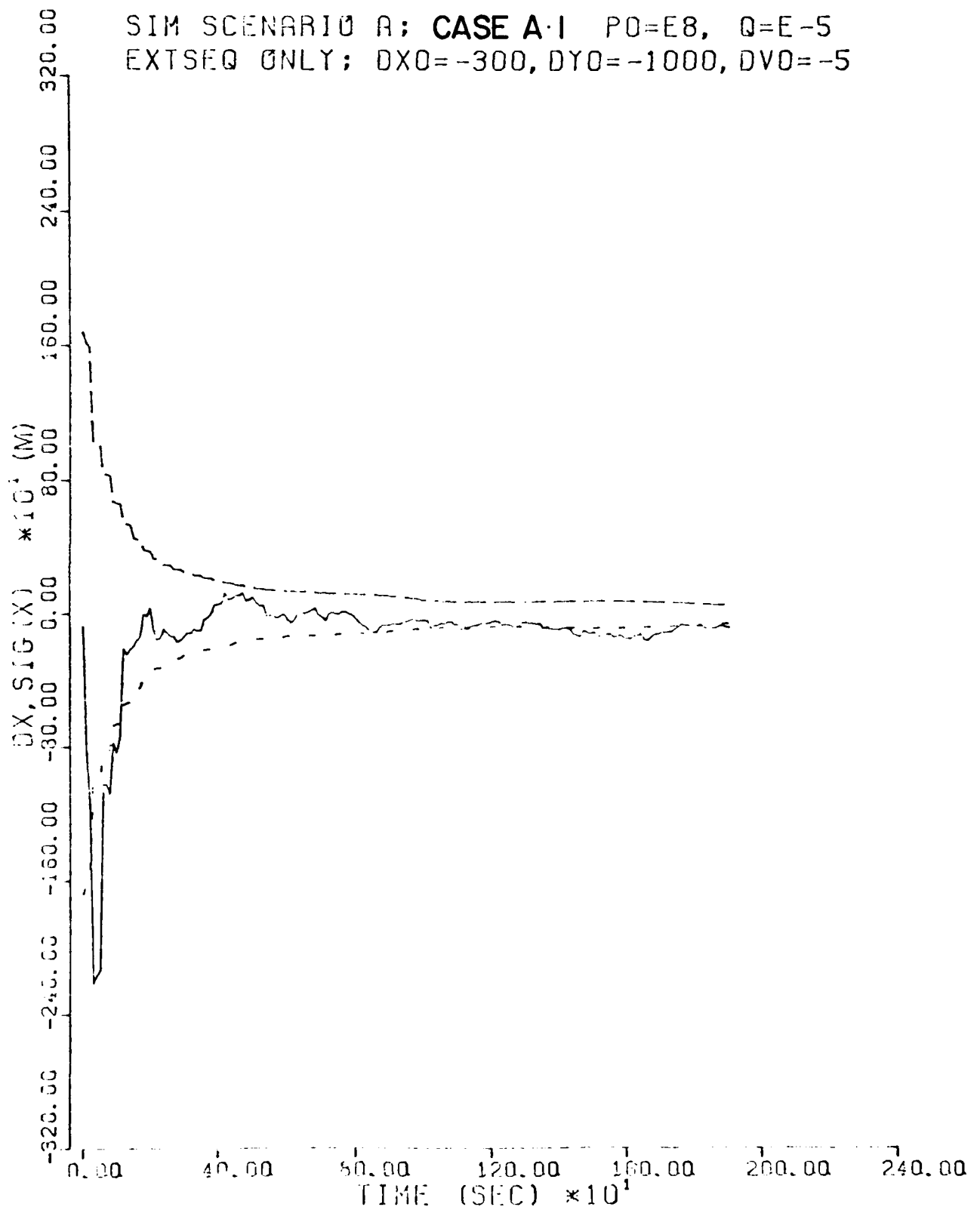


Fig. 6.17

SIM SCENARIO A; CASE A-1; PO=E8, Q=E-5  
EXTSEQ ONLY; DX0=-300, DY0=-1000, DVO=-5

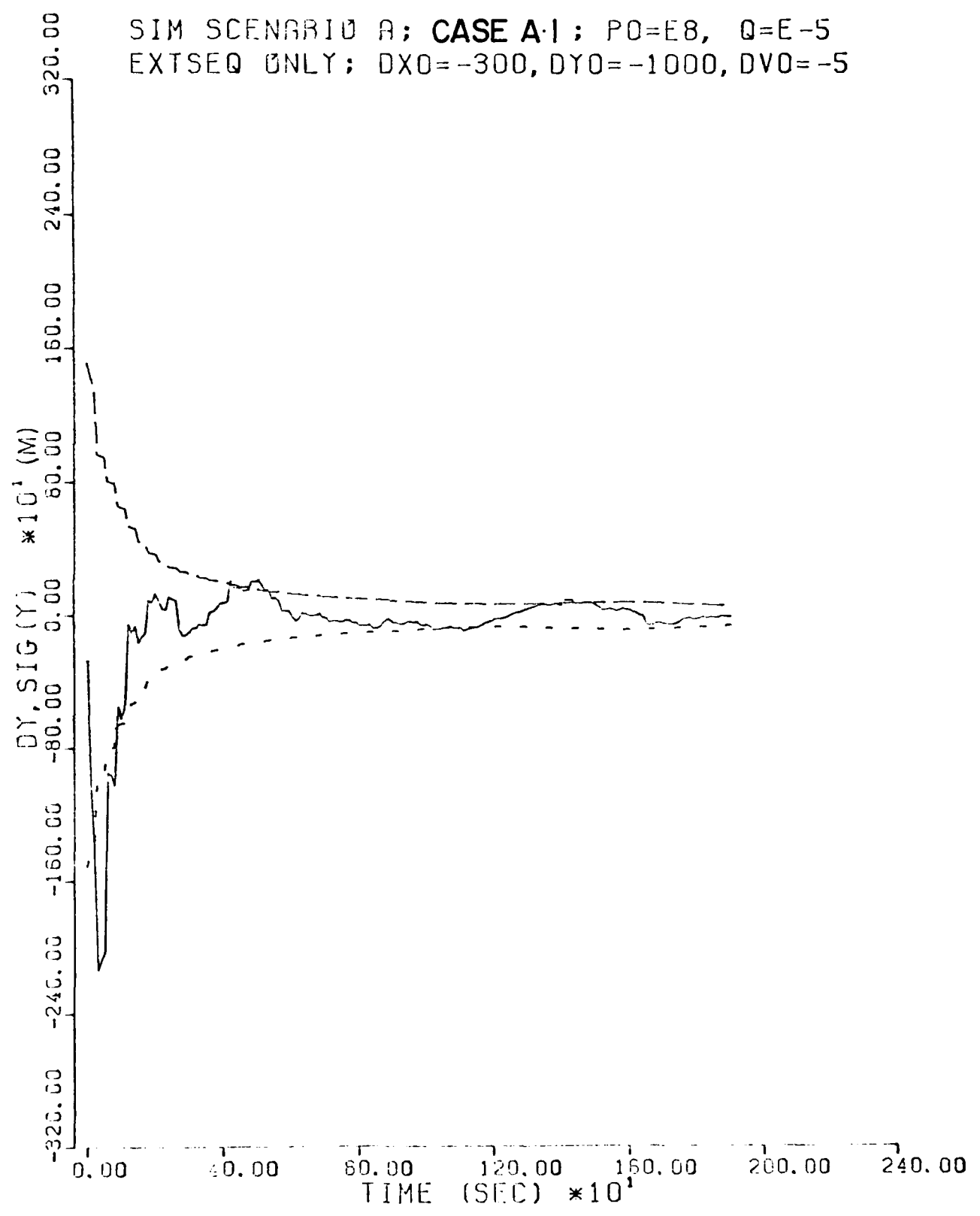


Fig. 6.18

SIMULATED SCENARIO; CASE B  
 TRAJECTORY FOR OBSERVATION GENERATION

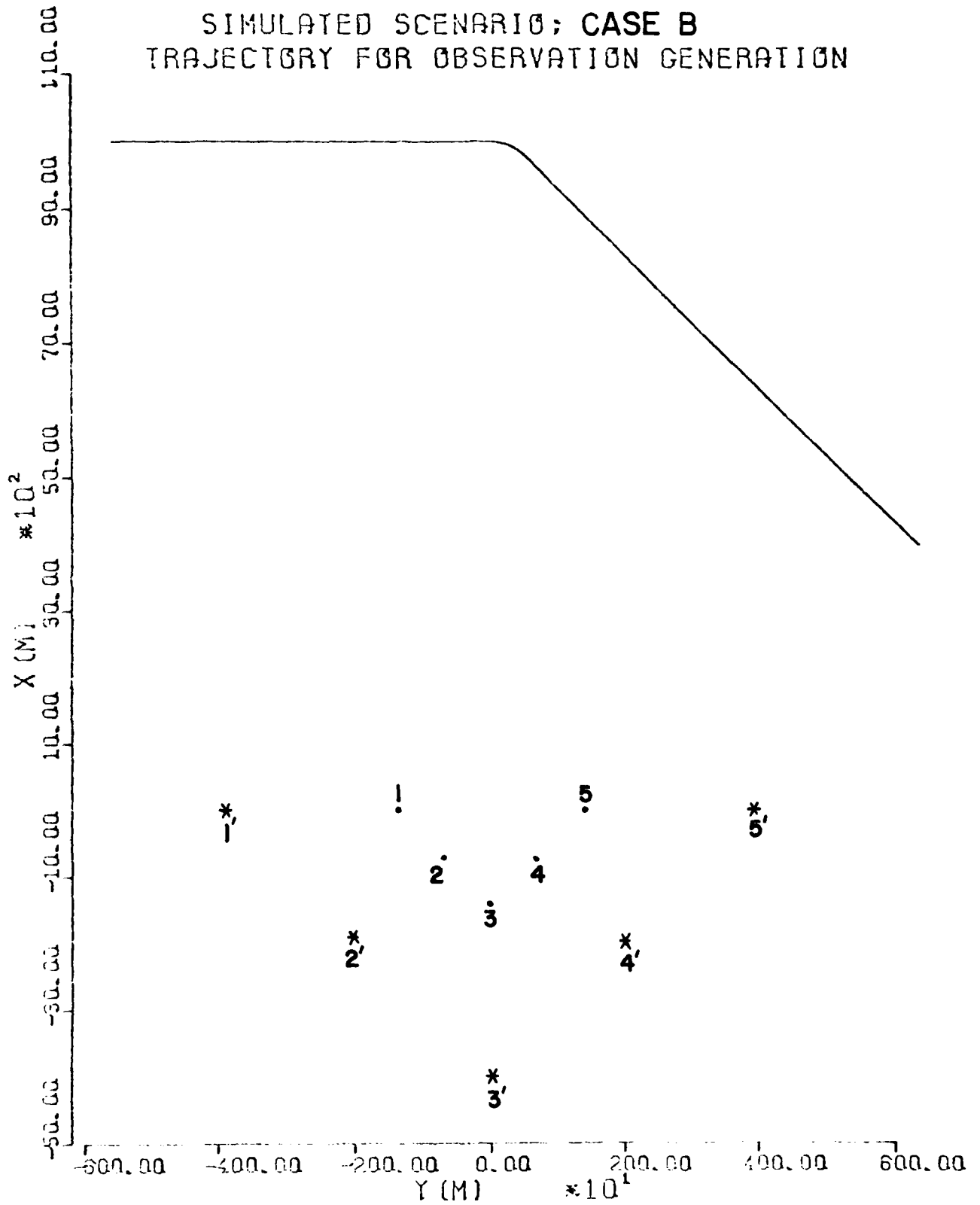


Fig. 6.19

SIMULATED SCENARIO; CASE B-1  
FREQUENCY (NO NOISE) FROM 5 SENSORS

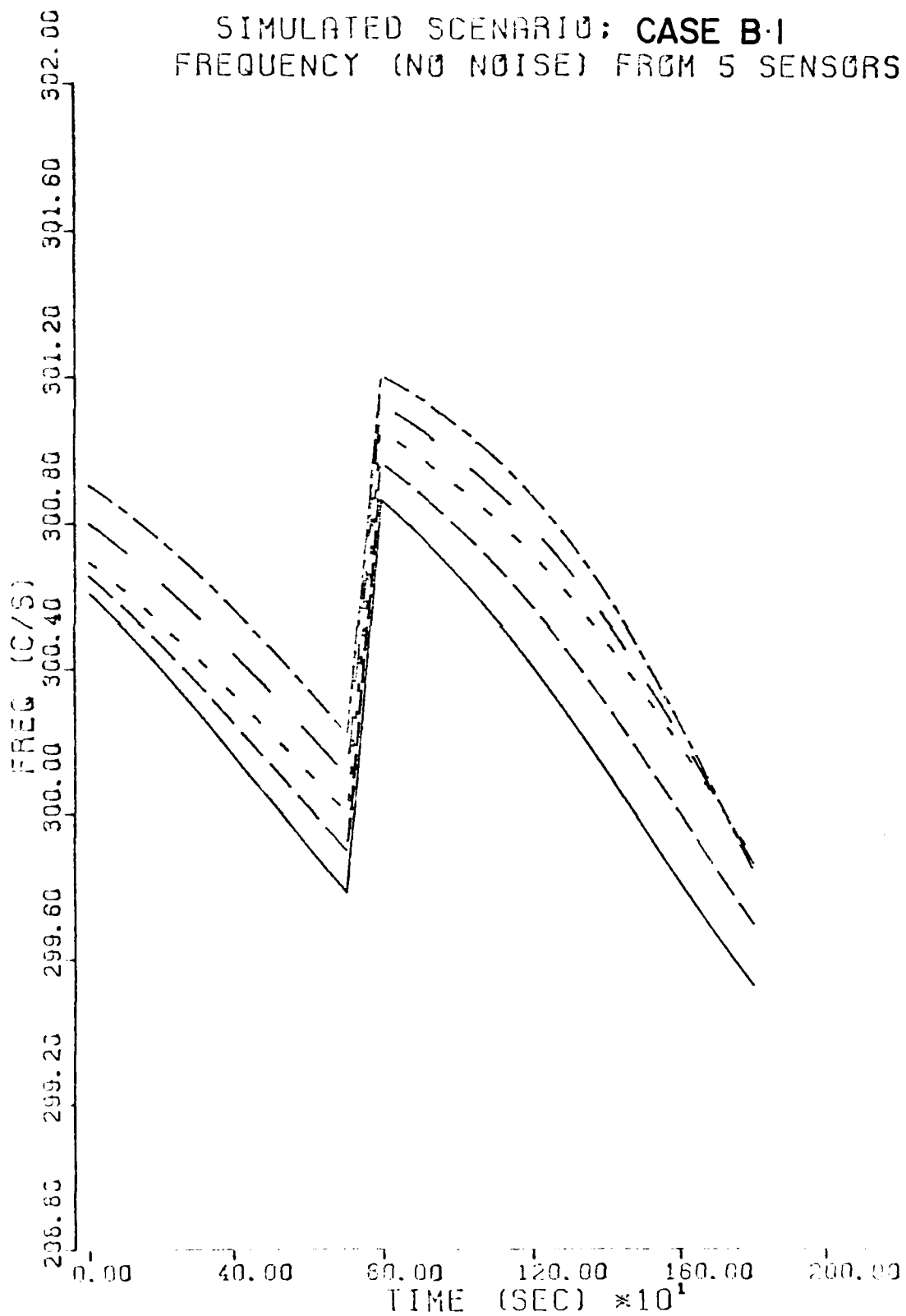


Fig. 6.20

AD-A095 184

TEXAS UNIV AT AUSTIN INST FOR ADVANCED STUDY IN ORBIT--ETC F/G 17/1  
ESTIMATING THE MOTION OF A MANEUVERING TARGETS USING PASSIVE ME--ETC(U)  
AUG 80 B D TAPLEY, P A ABUSALI, B E SCHUTZ N00014-78-C-0663  
IASOM-TR-80-2 NL

UNCLASSIFIED

2 of 2  
AD A  
D08104



END

DATE

FILED

3-81

DTIC

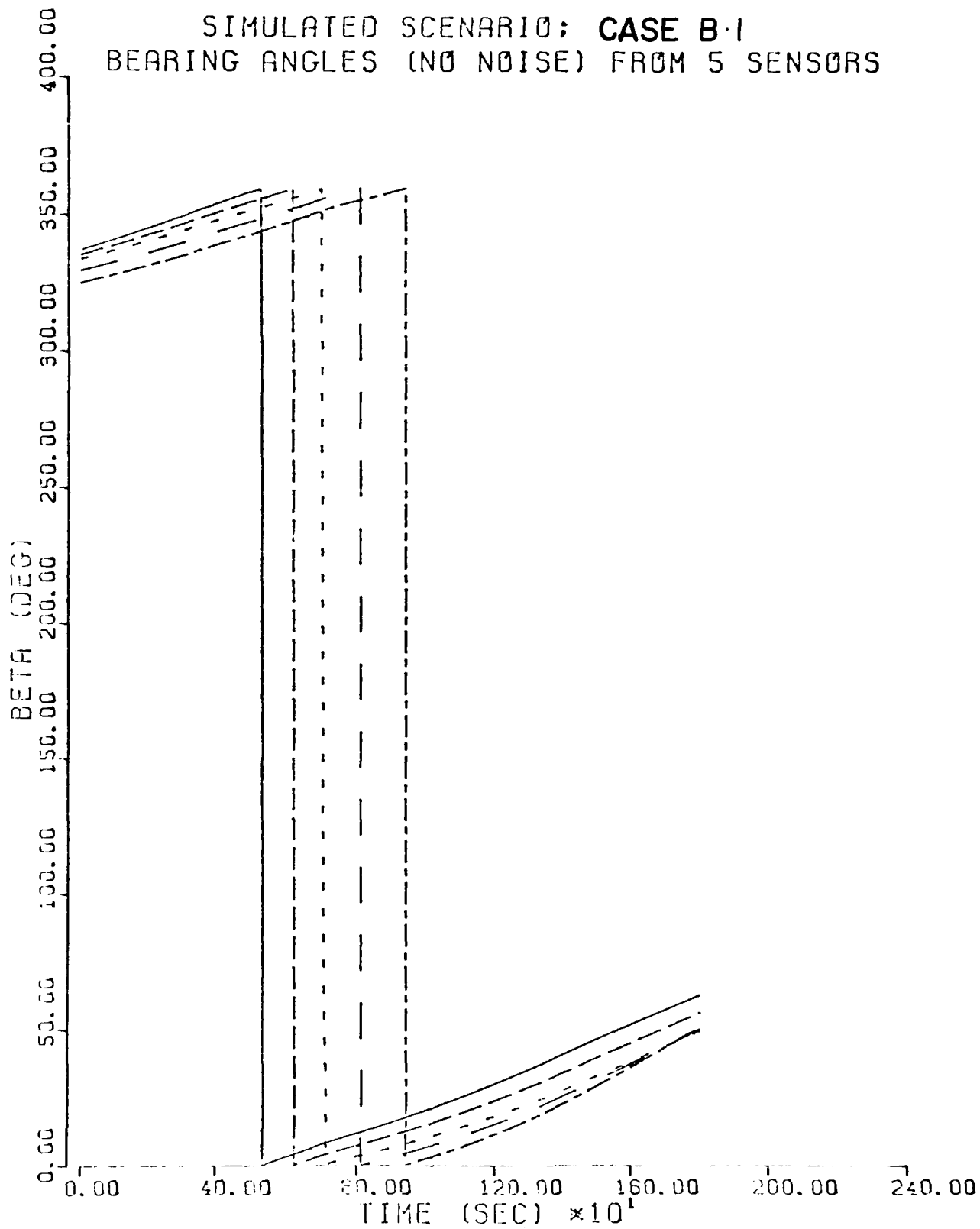


Fig. 6.21

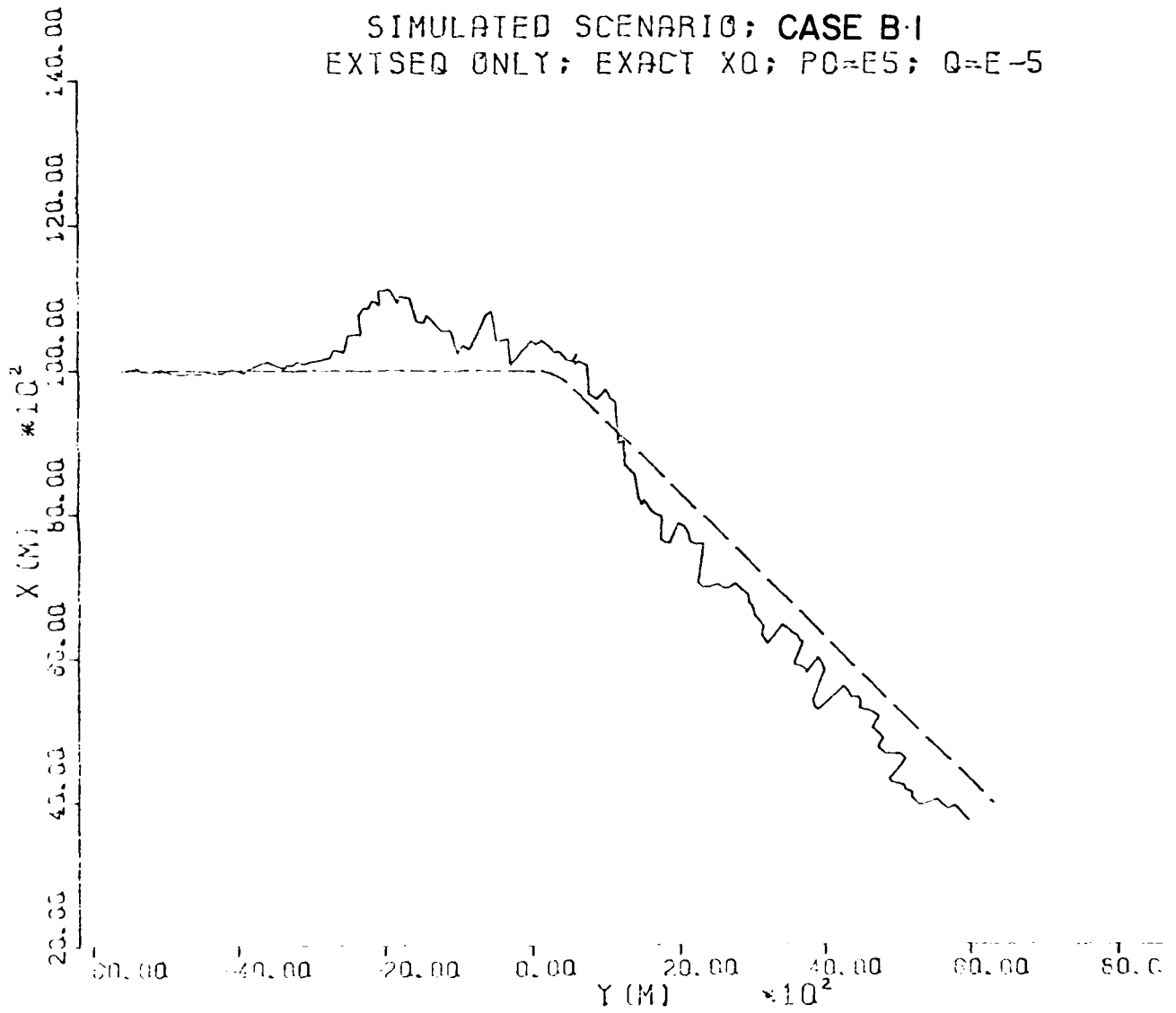


Fig. 6.22

SIMULATED SCENARIO; CASE B.1 OPT=1  
SEQBCH(34,30); EXACT X0; PO=E5

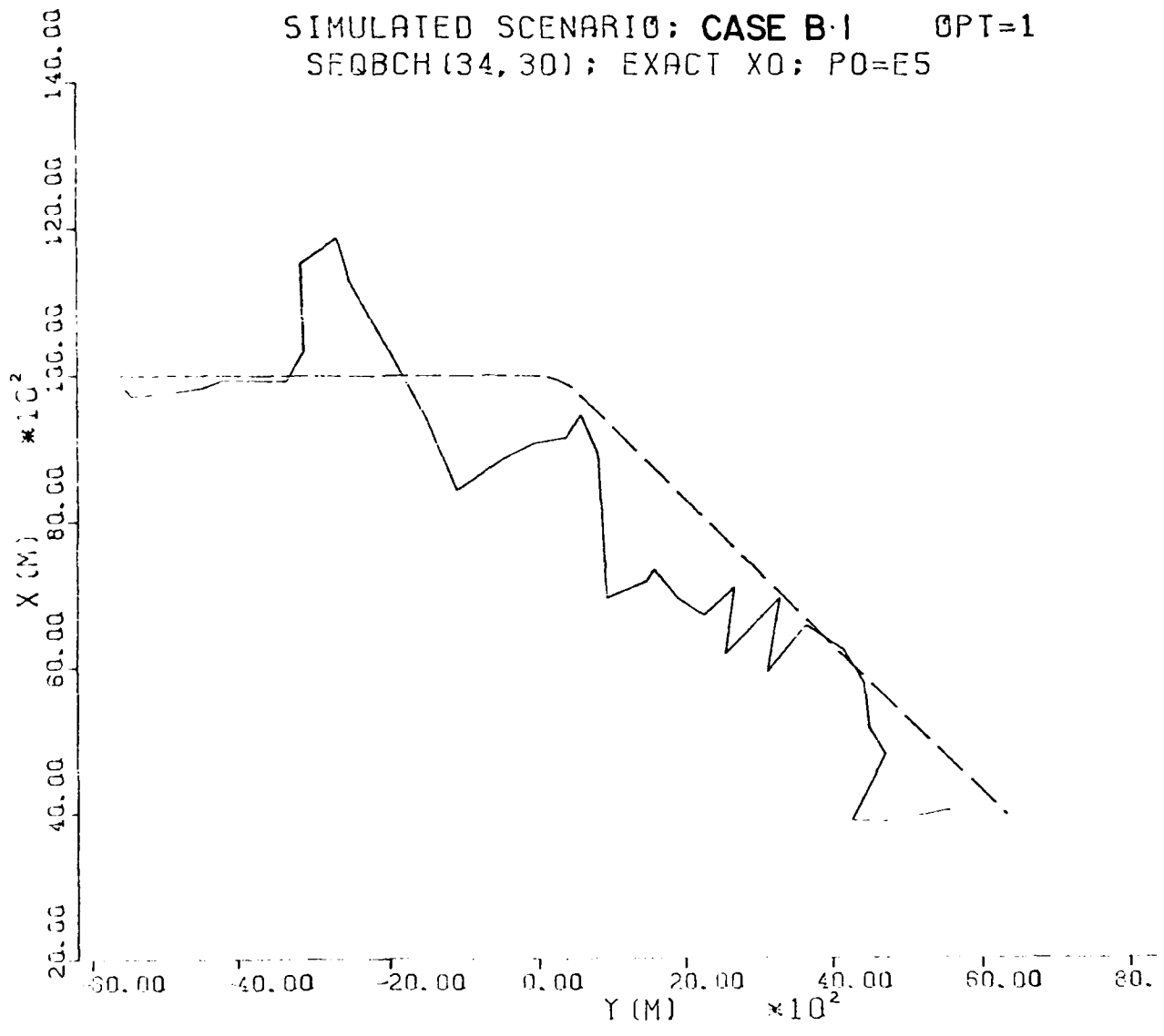


Fig. 6.23

SIMULATED SCENARIO; CASE B-1 OPT=3  
SEQBCH(34,30); EXACT XO; PO=E5; Q=2E-6

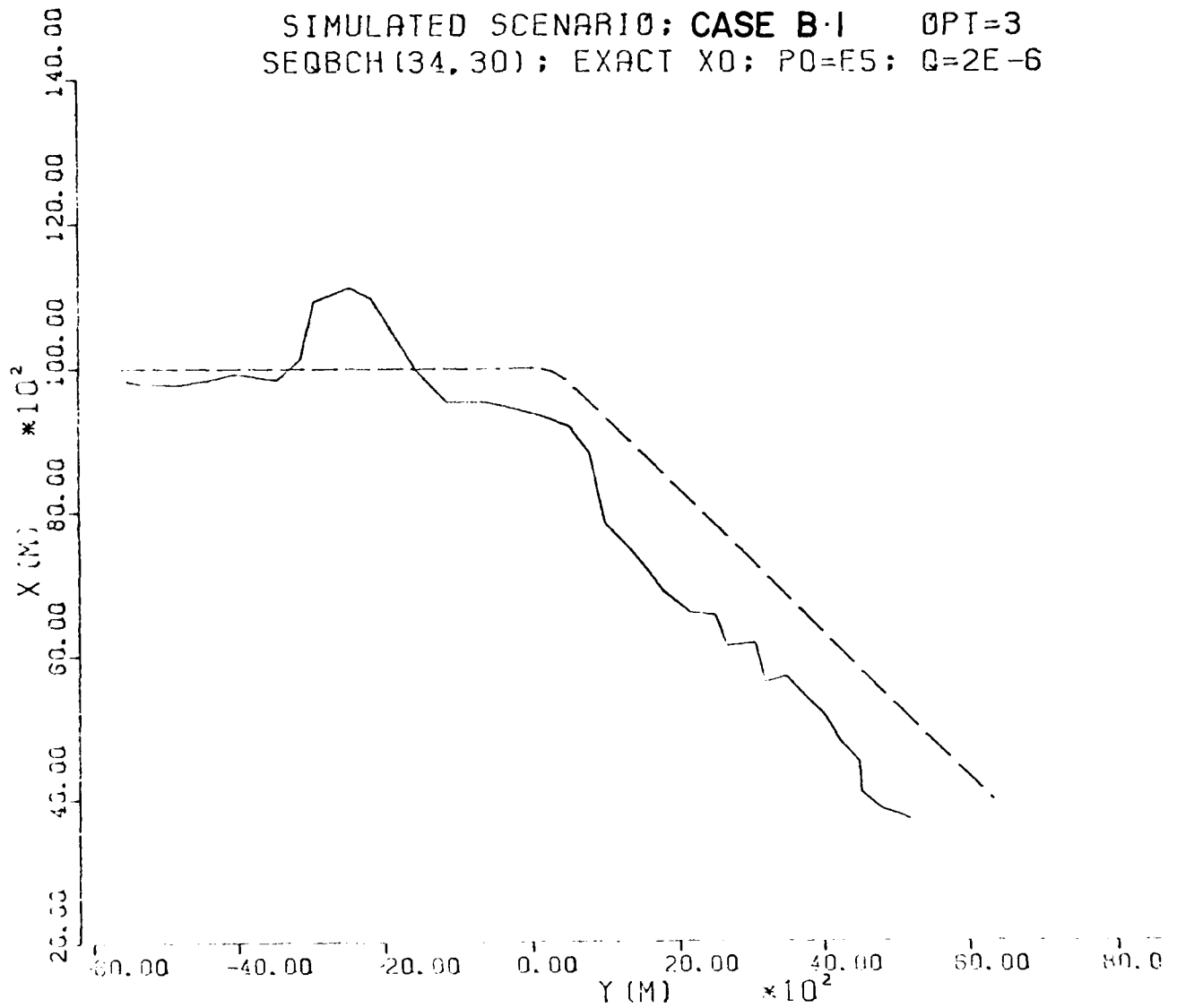


Fig. 6.24

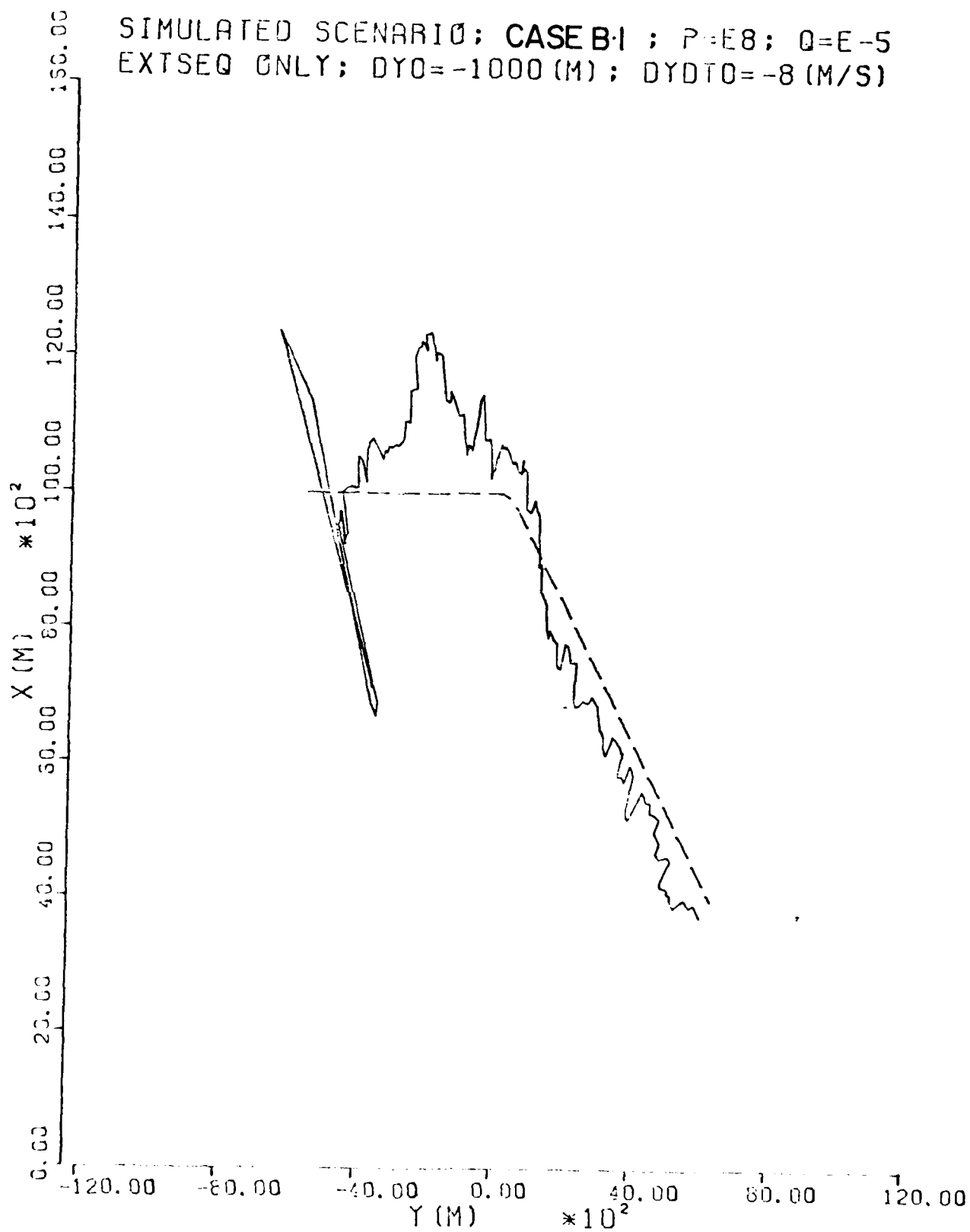


Fig. 6.25

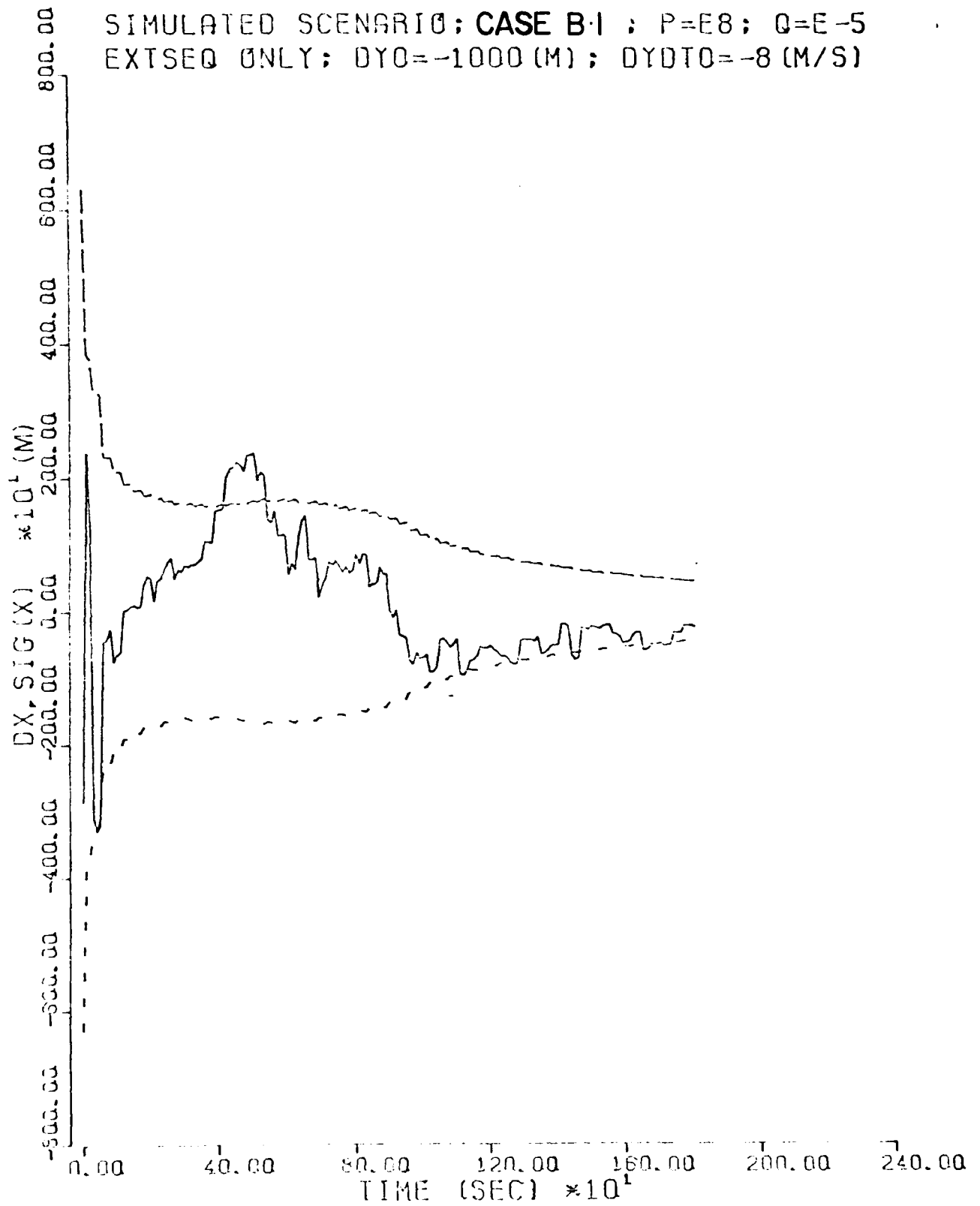


Fig. 6.26

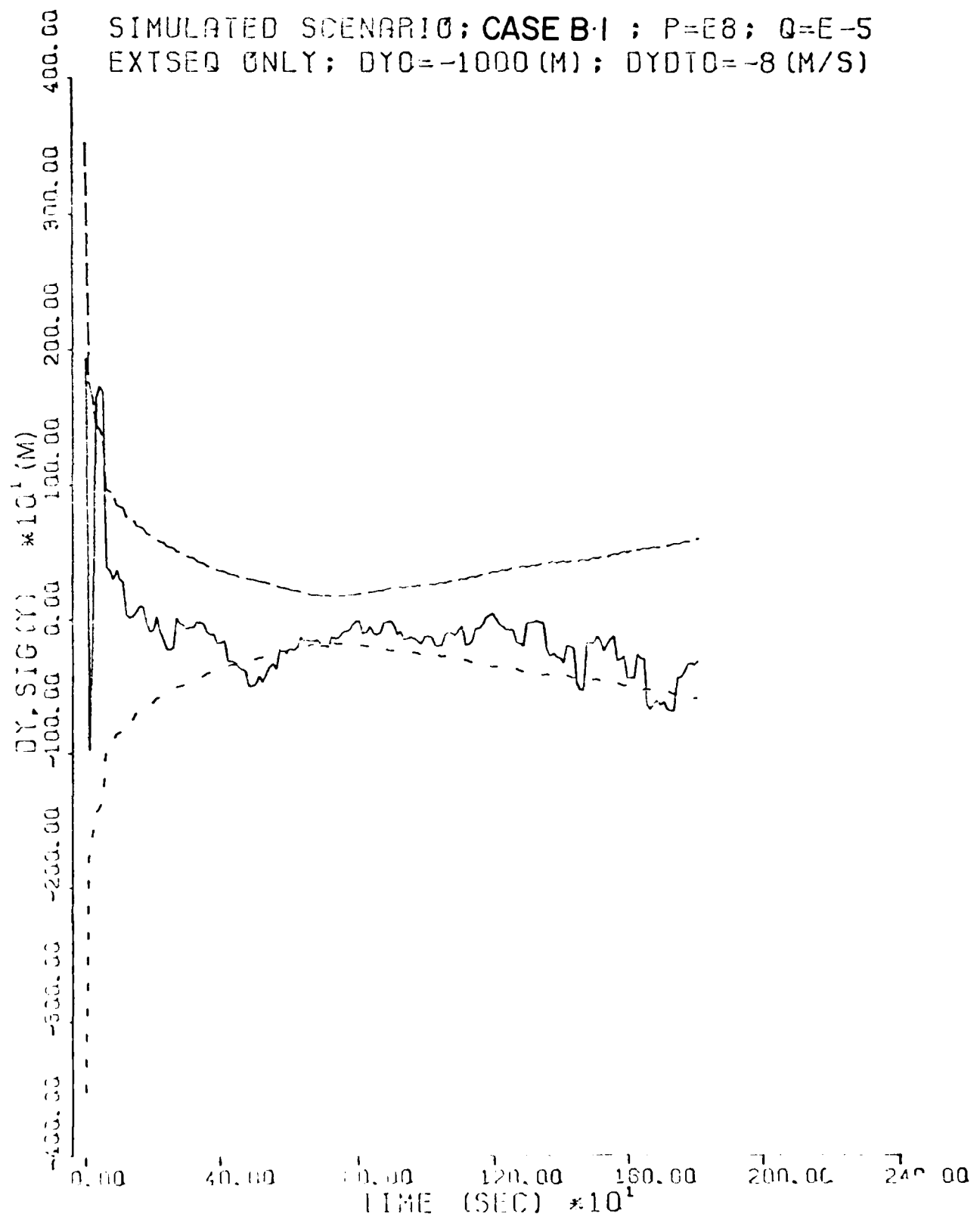


Fig. 6.27

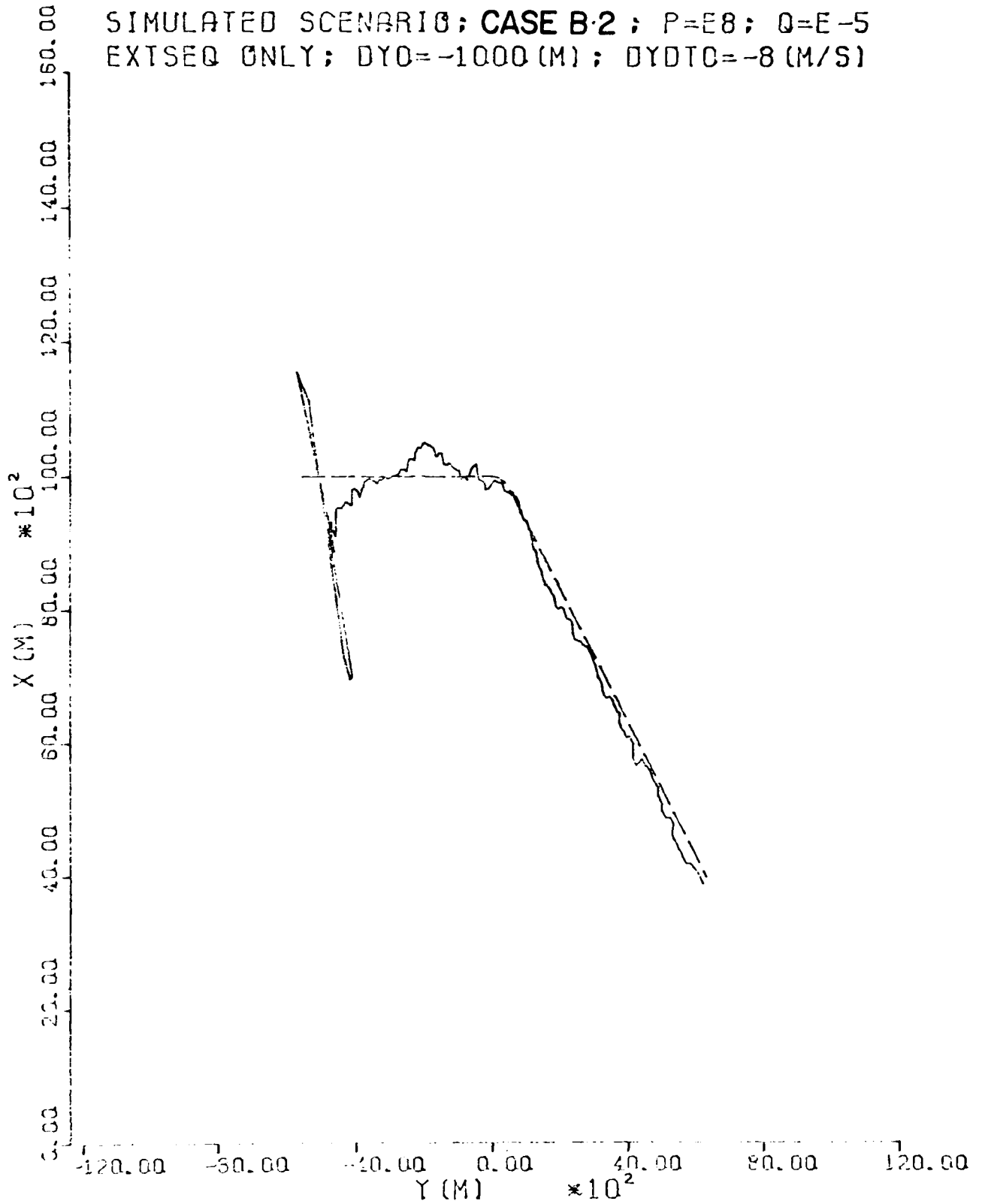


Fig. 6.28

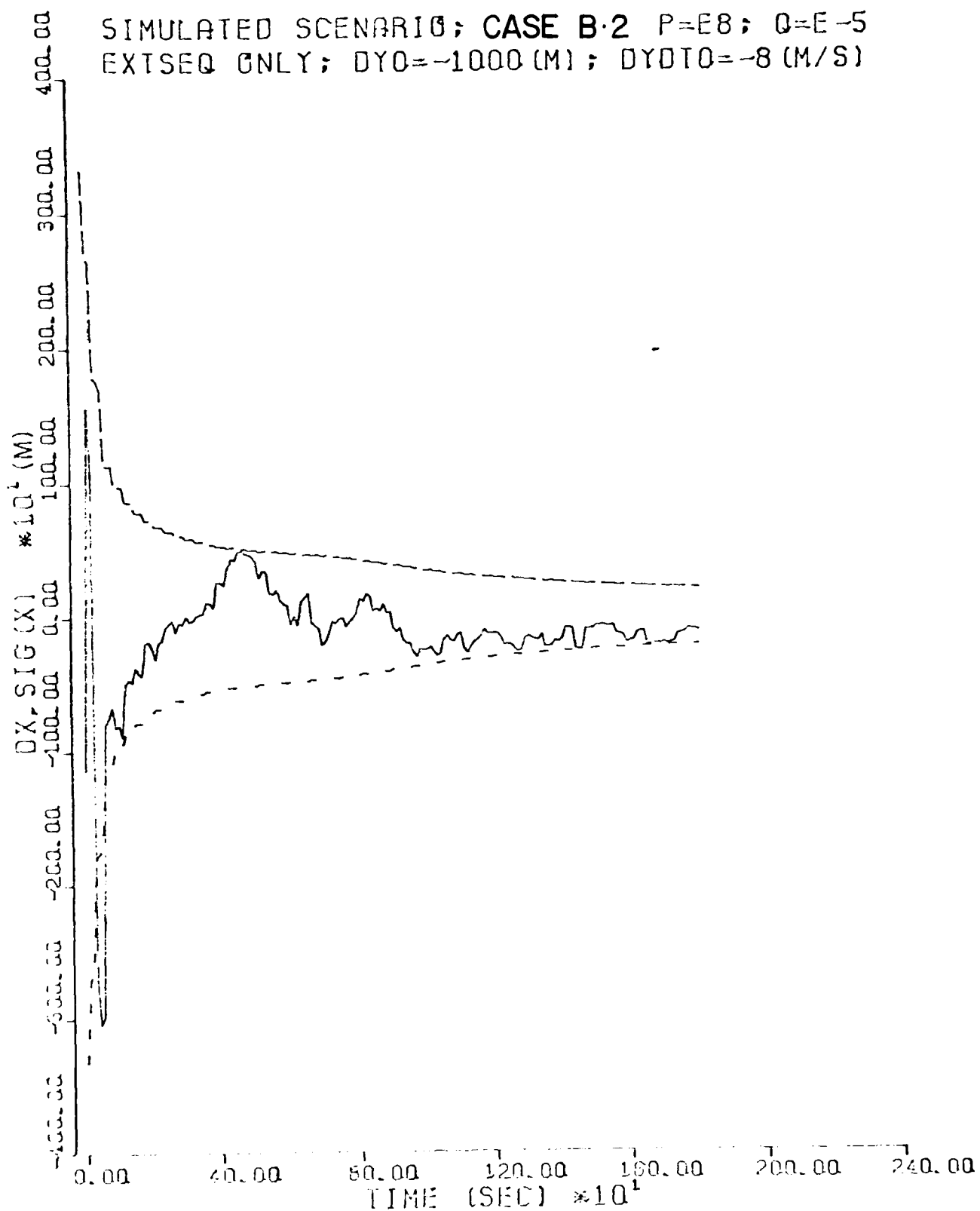


Fig. 6.29

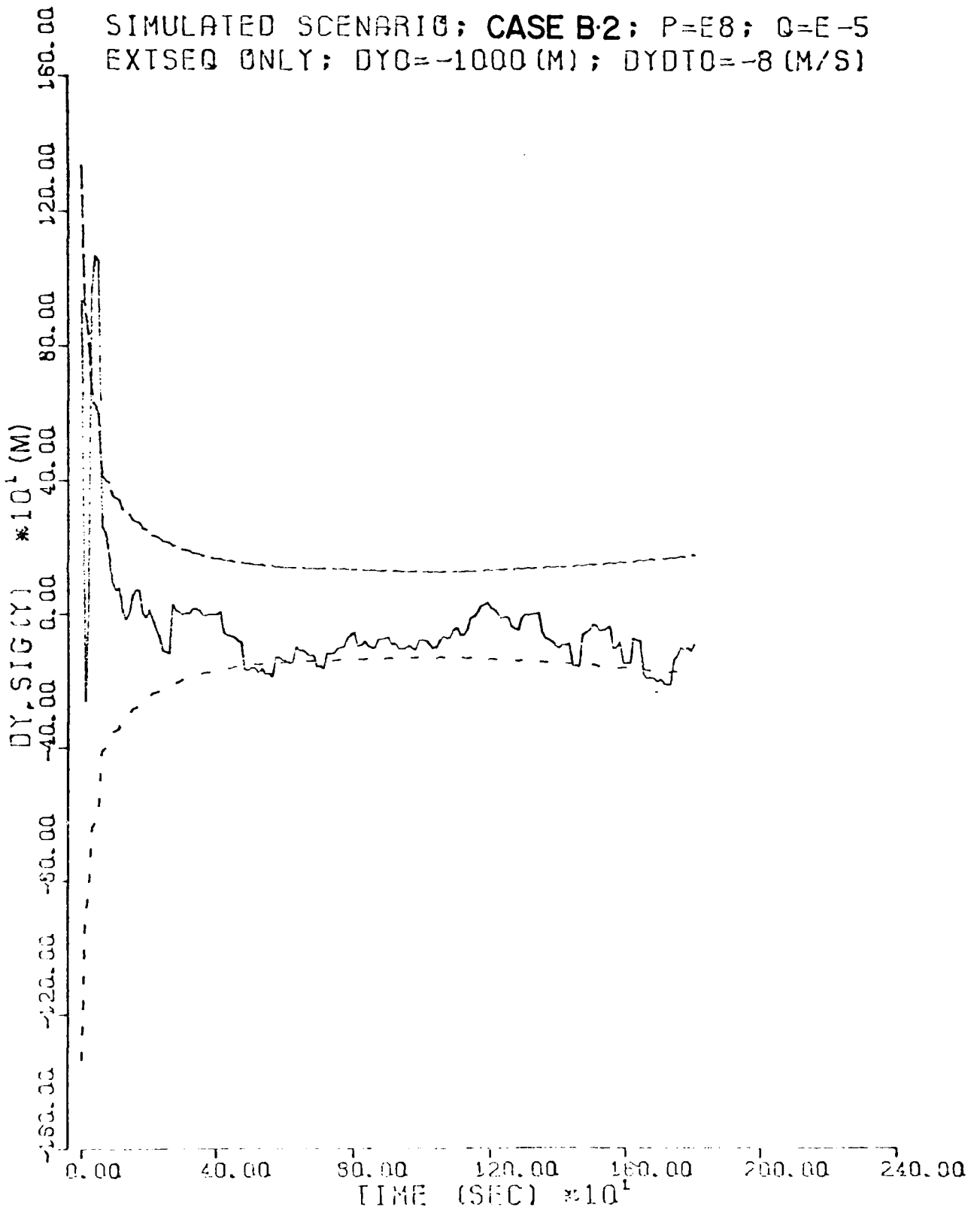


Fig. 6.30

## 7. Conclusions and Recommendations

The problem of estimating the trajectory of a slow moving maneuverable target using passive measurements from an array of stationary sensors, has been investigated in the previous chapters. Based on the results discussed in Chapter 6, the following conclusions can be drawn regarding the mathematical model and the algorithms used in the study. These are listed below along with recommendation of topics to be studied in the future.

### Conclusions

- The choice of a rectangular coordinate system is advantageous in that the target dynamics is linear for the acceleration model considered here.
- Modelling the acceleration components in rectangular coordinates as Brownian motion process is adequate to estimate the trajectory of the target executing typical maneuvers. Though it is a simple model, it is able to closely follow the actual maneuver acceleration curves when used with the EKF algorithm.
- The Extended Kalman Filter performs well for the scenarios considered and provides satisfactory results. It is especially well suited to tracking the targets motion once the estimation initiation transient has dissipated.
- The 'batch-sequential' filter method with the process noise modification estimates a trajectory which is in general agreement with the estimate obtained using EKF. However, the computation time for estimating the trajectory using this algorithm is larger than the EKF execution time by a factor of about 20.

When the process noise is not included in the 'batch-sequential' filter solution, the solution is not as accurate as the EKF solution during and following the maneuvers.

- Though the measurements were simulated with pessimistic values for the measurement noise standard deviations, the trajectory estimated by EKF converges to the true trajectory even when the initial state is perturbed. The errors in the initial state cause initial transients in the estimated trajectory, which disappear within a short time (about 5% of the total time period).
- The effect of sensor geometry is an important factor in the accuracy of the estimates of the target motion. Measurements made from sensors located as far apart as feasible, yield better estimates than those obtained from closely located sensors. The geometric orientation of its sensors is far more important than the number of observations.

#### Recommendations for Further Study

Further investigations must be made to understand the characteristics of the measurements. The dependence of the measurement standard deviations on the relative range is an important aspect that should be modeled in future simulation studies. The model formulation should be extended to three dimensions. The characteristic of the signal propagation in the medium, for example, the multi-path effects on the signal received at the sensors, should be studied. Initial results obtained with adaptive filtering wherein the process noise covariance is also estimated, appear promising and should be given a more thorough evaluation. Different models for the dynamics should be investigated;

for example, modelling the acceleration components as an adaptive first order Gauss-Markov process. This model will increase the dimension of the state vector, but allow a better estimate of the acceleration.

### References

1. Kalman, R.E., "A New Approach to Linear Filtering and Prediction Problems," Trans. ASME, J. Basic Engineering, Vol. 82, 1960, pp. 35-44.
2. Jazwinski, A.H., "Stochastic Processes and Filtering Theory," Academic Press, New York (1970).
3. Tapley, B.D., "Statistical Orbit Determination Theory," Recent Advances in Dynamical Astronomy, Edited by B.D. Tapley and V. Szebehely, D. Reidel Publishing Company, pp. 346-425 (1973).
4. Titus, H., (Ed), "Advances in Passive Target Tracking, Volume 1," NPS-62TS77071, Naval Postgraduate School, Monterey, CA (May 1977).
5. Alspach, D.L., "A Gaussian Sum Bayesian Approach to Passive Bearings - Only Tracking," Advances in Passive Target Tracking, Edited by H. Titus, Naval Postgraduate School, Monterey, CA (May 1977).
6. Moose, R.L. and D.H. McCabe, "Adaptive Target Tracking for Underwater Maneuvering Targets," Department of Electrical Engineering, Virginia Polytechnic Institute and State University, Blacksburg, Virginia (October 1979).
7. Tapley, B.D. and D.S. Ingram, "Orbit Determination in the Presence of Unmodeled Accelerations," IEEE Transactions on Automatic Control, Vol. AC-18, Aug. 1973, pp. 369-373.
8. Tapley, B.D. and B.E. Schutz, "Estimation of Unmodeled Forces on a Lunar Satellite," presented at the 23rd International Astronautical Congress Vienna, Austria (Oct. 1972).
9. Tapley, B.D. and H. Hagar, "Estimation of Unmodeled Forces on a Low-Thrust Space Vehicle," Journal of Spacecraft and Rockets, Vol. 12, No. 10, Oct. 1970, pp. 592-598.
10. Liebelt, P.B., "An Introduction to Optimal Estimation," Addison Wesley, Reading, Massachusetts (1967).
11. Lawson, C.L. and R.J. Hanson, "Solving Least Squares Problems," Prentice Hall, Englewood Cliffs, NJ (1974).
12. Bierman, G.J., "Factorization Methods for Discrete Sequential Estimation," Academic Press, New York (1977).
13. Joos, G. and I.M. Freeman, "Theoretical Physics," Hafner Publishing Company, New York (1950).

14. Jazwinski, A.H., "Adaptive Filtering," Automatica, Vol. 5, pp. 475-485 (1969).
15. Papoulis, A., "Probability, Random Variables, and Stochastic Processes," McGraw-Hill, New York (1965).
16. Eller, T.J., "Sequential Estimation of Random Thrust Errors for Solar Electric Propulsion Spacecraft," AMRL-1057, Applied Mechanics Research Laboratory, The University of Texas, Austin, Texas, (1974).
17. Urick, R.J., "Principles of Underwater Sound for Engineers," McGraw-Hill, New York (1975).

## Appendix A

### Batch Solution in the Presence of Process Noise

The linear dynamic model for the system with process noise is assumed in the form

$$\dot{x} = Ax + Bw \quad (\text{A.1})$$

where  $w$  is a zero mean white Gaussian process. If  $\Phi(t_1, t_2)$  is the state transition matrix for  $A$ , then the formal solution to Eq. (A.1) can be expressed as

$$x_k = \Phi(k, k-1)x_{k-1} + \int_{t_{k-1}}^k \Phi(k, \tau)B(\tau)w(\tau)d\tau \quad (\text{A.2})$$

In order to derive the batch solution including the effect of process noise on the propagation of the state, the white noise process  $w(t)$  in Eq. (A.2) is assumed to be the limit of a Gaussian white sequence. In other words,  $w(t)$  is considered as a random piecewise constant function, as shown in Fig. A.1, with covariance

$$E\{w(t_i)w^T(t_j)\} = Q(t_i)\delta_{ij} \quad (\text{A.3})$$

Then the integral in Eq. (A.2) can be evaluated after removing the constant  $w_{k-1}$  from the integral. If  $t_0$  is the epoch time at which the batch estimate is to be calculated, then all the state vectors can be expressed in terms of the epoch state  $x_0$ . So the state propagation equation, Eq. (A.2), can be written as

$$x_k = \Phi(k, 0)x_0 + \sum_{i=1}^k \left[ \int_{t_{i-1}}^{t_i} \Phi(k, \tau)B(\tau)d\tau \right] w_{i-1} \quad (\text{A.4})$$

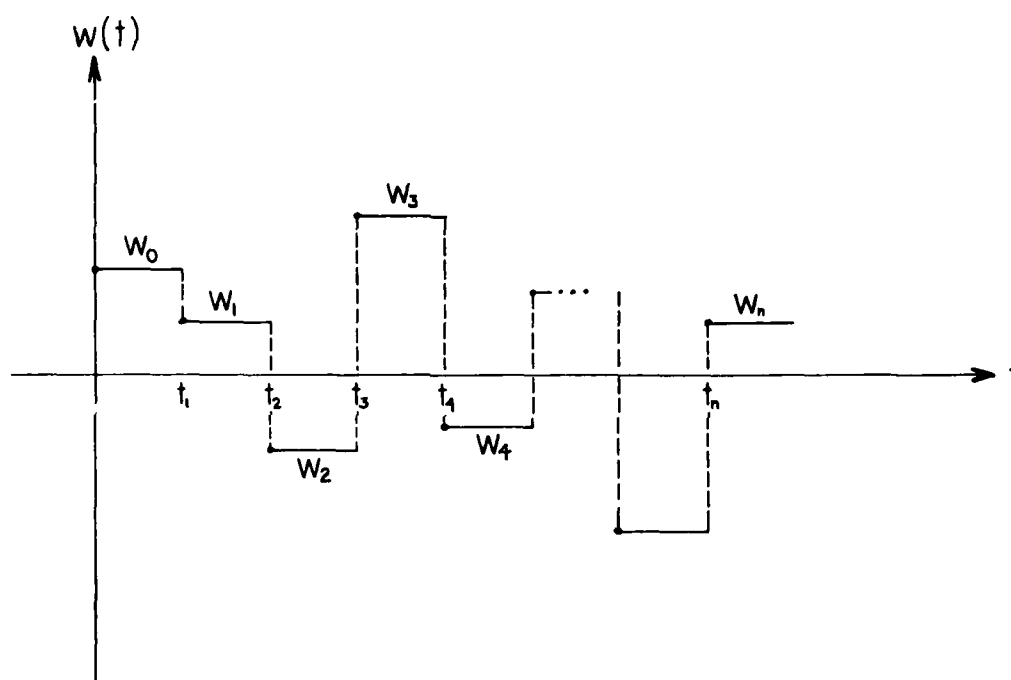


Fig. A.1 Approximation of a Random Process  $w(t)$  by Discrete Random Constants. (Note that  $w(t)$  as shown here is a scalar and represents  $w_f(t)$  or  $w_1(t)$  or  $w_2(t)$  referenced in Eq. 3.7)

Now, at a measurement time point  $t_k$ , the measurement  $y_k$  is related (after linearization) to the state at  $t_k$  by the relation

$$y_k = H_k x_k + \epsilon_k \quad (\text{A.5a})$$

where  $\epsilon_k$  is the measurement noise, with variance  $R_k$ . Substituting Eq. (A.4) in Eq. (A.5a),

$$\begin{aligned} y_k &= \tilde{H}_k \phi(k,0) x_0 + \tilde{H}_k \sum_{i=1}^k \int_{t_{i-1}}^{t_i} \phi(k,\tau) B(\tau) d\tau w_{i-1} + \epsilon_k \\ &= H_k x_0 + \eta_k \end{aligned} \quad (\text{A.5b})$$

where the combined noise term

$$\eta_k = \tilde{H}_k \sum_{i=1}^k \left[ \int_{t_{i-1}}^{t_i} \phi(k,\tau) B(\tau) d\tau \right] w_{i-1} + \epsilon_k \quad (\text{A.6})$$

and  $H_k = \tilde{H}_k \phi(k,0)$ .

In order to simplify the notation, define

$$\psi_k = \left[ \int_{t_0}^{t_1} \phi(k,\tau) B(\tau) d\tau \mid \int_{t_1}^{t_2} \phi(k,\tau) B(\tau) d\tau \mid \dots \mid \int_{t_{k-1}}^{t_k} \phi(k,\tau) B(\tau) d\tau \right] \quad (\text{A.7a})$$

$$U_k^T = [w_0^T \ w_1^T \ \dots \ w_{k-1}^T] \quad (\text{A.7b})$$

so that we can write

$$\eta_k = \tilde{H}_k \psi_k U_k + \epsilon_k \quad (\text{A.8})$$

After processing, say,  $m$  scalar measurements, the equations as in (A.5b) can be placed in the following matrix form as

$$y = H x_0 + \eta \quad (\text{A.9})$$

where

$$y = \begin{bmatrix} y_1 \\ y_2 \\ \cdot \\ \cdot \\ y_m \end{bmatrix}, \quad H = \begin{bmatrix} H_1 \\ H_2 \\ \cdot \\ \cdot \\ H_m \end{bmatrix} \quad \text{and } \eta = \begin{bmatrix} \eta_1 \\ \eta_2 \\ \cdot \\ \cdot \\ \eta_m \end{bmatrix}$$

each  $H_i$ ,  $i = 1, 2, \dots, m$  being a  $1 \times n$  row vector. To compute the least-squares estimate of the epoch state  $x_o$  from Eq. (A.9), given an a priori epoch state  $\bar{x}_o$  and its covariance  $\bar{P}_o$ , from the data equation,

$$\bar{x}_o = x_o + \epsilon_o \quad \text{where} \quad E\{\epsilon_o \epsilon_o^T\} = \bar{P}_o \quad (\text{A.10})$$

the following procedure is used. Augment the measurements in Eq. (A.9) with the a priori information contained in Eq. (A.10) to obtain:

$$\begin{bmatrix} \bar{x}_o \\ y \end{bmatrix} = \begin{bmatrix} I \\ H \end{bmatrix} x_o + \begin{bmatrix} \epsilon_o \\ \eta \end{bmatrix}$$

or

$$z = \lambda x_o + v \quad (\text{A.11})$$

The covariance matrix for the augmented error,  $v$ , can be obtained as

$$\begin{aligned} \tilde{\Gamma} &= E\{vv^T\} \\ &= E\left\{ \begin{bmatrix} \epsilon_o \\ \eta \end{bmatrix} \begin{bmatrix} \epsilon_o^T & \eta^T \end{bmatrix} \right\} = \begin{bmatrix} E(\epsilon_o \epsilon_o^T) & E(\epsilon_o \eta^T) \\ E(\eta \epsilon_o^T) & E(\eta \eta^T) \end{bmatrix} \end{aligned} \quad (\text{A.12})$$

Note that,

$$\begin{aligned} E\{\varepsilon_o \eta^T\} &= E\{\varepsilon_o (\eta_1^T \eta_2^T \dots \eta_m^T)\} \\ &= E\{\varepsilon_o (\varepsilon_1^T \dots \varepsilon_m^T)\} + E\{\varepsilon_o (U_1^T \psi_1^T \tilde{H}_1^T \quad U_2^T \psi_2^T \tilde{H}_2^T \quad \dots \quad U_m^T \psi_m^T \tilde{H}_m^T)\} \end{aligned}$$

Since  $\varepsilon_o$ , the error in the a priori state is uncorrelated with the measurement noise ( $\varepsilon_i$ ,  $i = 1, \dots, m$ ) and with the process noise ( $w_i$ ,  $i = 0, 1, \dots, m-1$ ), it follows that

$$E\{\varepsilon_o \eta^T\} = E\{\eta \varepsilon_o^T\} = 0 \quad (\text{A.13a})$$

The diagonal terms of  $\tilde{\Gamma}$  are

$$E\{\varepsilon_o \varepsilon_o^T\} = \bar{P}_o \quad (\text{A.13b})$$

and  $E\{\eta \eta^T\} = \Gamma$ , where

$$\Gamma = \begin{bmatrix} E(\eta_1 \eta_1^T) & \dots & E(\eta_1 \eta_m^T) \\ \vdots & & \vdots \\ E(\eta_m \eta_1^T) & \dots & E(\eta_m \eta_m^T) \end{bmatrix} \quad (\text{A.13c})$$

Now, the  $(i, j)^{\text{th}}$  element of  $E(\eta \eta^T)$  is:

$$\begin{aligned} E(\eta_i \eta_j^T) &= \tilde{H}_i \psi_i E(U_i U_j^T) \psi_j^T \tilde{H}_j^T + \tilde{H}_i \psi_i E(U_i \varepsilon_j^T) + E(\varepsilon_i U_j^T) \psi_j^T \tilde{H}_j^T + E(\varepsilon_i \varepsilon_j^T) \\ &= \tilde{H}_i \psi_i E(U_i U_j^T) \psi_j^T \tilde{H}_j^T + R_i \delta_{ij} \end{aligned}$$

where, assuming that the process noise  $w_i$ ,  $i = 1, \dots, \ell$  and the observation noise are uncorrelated, it follows that  $E[\varepsilon_i U_j^T] = E[U_i \varepsilon_j^T] = 0$  for all  $i$  and  $j$ . Substituting for  $\psi$  and  $U$ , from Eqs. (A.7a) and

(A.7b),  $\rho_{ij}$  is defined as

$$\begin{aligned} \rho_{ij} &= \tilde{H}_i \psi_i E(U_i U_j^T) \psi_j^T \tilde{H}_j^T \\ &= \tilde{H}_i E \left\{ \left[ \sum_{\ell=1}^i \int_{t_{\ell-1}}^{t_\ell} \Phi(i, \tau) B(\tau) d\tau \cdot w_{\ell-1} \right] \left[ \sum_{m=1}^j w_{m-1}^T \int_{t_{m-1}}^{t_m} B^T(\tau) \Phi^T(j, \tau) d\tau \right] \right\} \tilde{H}_j^T \\ &= \tilde{H}_i \left\{ \sum_{\ell=1}^{\min(i, j)} \int_{t_{\ell-1}}^{t_\ell} \Phi(i, \tau) B(\tau) d\tau \cdot Q_{\ell-1} \int_{t_{\ell-1}}^{t_\ell} B^T(\tau) \Phi^T(j, \tau) d\tau \right\} \tilde{H}_j^T \end{aligned} \quad (\text{A.14})$$

where  $Q_\ell = E\{w_\ell w_\ell^T\}$ . Finally then the elements of  $\Gamma$  are given as

$$\Gamma_{ij} = E\{\eta_i \eta_j^T\} = \rho_{ij} + R_i \delta_{ij} \quad \text{and}$$

$$\Gamma = \begin{bmatrix} \rho_{11} + R_1 & \rho_{12} & \cdots & \rho_{1m} \\ \rho_{21} & \cdot & \cdot & \cdot \\ \cdot & \cdot & \cdot & \cdot \\ \cdot & \cdot & \cdot & \cdot \\ \rho_{m1} & \cdot & \cdot & \rho_{mm} + R_m \end{bmatrix} \quad (\text{A.13c})$$

From Eqs. (A.12) and (A.13), it follows that

$$\tilde{\Gamma} = \begin{bmatrix} \bar{P}_o & 0 \\ 0 & \Gamma \end{bmatrix} \quad (\text{A.15})$$

The least-squares solution corresponding to Eq. (A.9) and (A.10) is given then by the following expression.

$$\begin{aligned} \hat{x}_o &= (\lambda \tilde{\Gamma}^{-1} \lambda)^{-1} \lambda^T \tilde{\Gamma}^{-1} z \\ &= (H^T \Gamma^{-1} H + \bar{P}_o^{-1})^{-1} (H^T \Gamma^{-1} Y + \bar{P}_o^{-1} x_o) \end{aligned} \quad (\text{A.16})$$

It is to be noted that the  $m \times m$  matrix,  $\Gamma$ , is not a diagonal matrix and therefore the computation of  $\hat{x}_0$  by Eq. (A.16) involves inversion of first, an  $m \times m$  matrix and then, an  $n \times n$  matrix where  $m$  is the number of observations processed and  $n$  is the dimension of the state vector.

## Appendix B

### Process Noise Variance Computation for Adaptive Filtering

The main idea involved in arriving at the equations for estimating the process noise covariance ( $Q$ ) is based on the assumption that the filter residuals be consistent with their statistics. In other words, defining the (predicted) residuals as

$$r_{k+l} = y_{k+l} - E\{y_{k+l}/Y^k\}, \quad l > 0 \quad (B.1)$$

where  $y_{k+l}$  is the measurement deviation at time  $t_{k+l}$  defined in Eq. (2.2) and  $E\{y_{k+l}/Y^k\}$  is the expected value of the measurement deviation at time  $t_{k+l}$  based on measurements up to time  $t_k$ , it is required that

$$r_{k+l}^2 = E\{r_{k+l}^2\}, \quad l = 1, 2, \dots, m_q \quad (B.2)$$

$y(\ )$  and hence  $r(\ )$  are assumed to be scalars in this discussion. From Eq. (B.2) one derives the process noise covariance  $Q_k$  required at time  $t_k$  to propagate the state error covariance matrix  $\hat{P}_{k-1}$  to the next time point  $t_{k+1}$  as given in Eq. (3.10). Note that such an adaptive filter will have a time lag ( $t_{m_q}$ ), since  $(k+m_q)$  observations have to be obtained before prediction to time  $t_{k+1}$  can be made. The state-noise compensation matrix  $Q$  for the dynamic model defined in Eq. (3.6) is a  $7 \times 7$  matrix with non-zero values for the first, 6<sup>th</sup> and the 7<sup>th</sup> diagonal elements and with zero for all other elements. Here a  $3 \times 3$  diagonal matrix  $Q'$  is considered with non-zero diagonal elements and consequently an appropriate matrix  $B$  is introduced by pre-multiplying  $Q'$  so that  $Q = BQ'B^T$  and

$$Q' = \begin{bmatrix} q_f \\ q_1 \\ q_2 \end{bmatrix}$$

Using the same notations as in Chapter 2, for the filter residual, we have

$$E\{r_{k+l}^2\} = \tilde{H}_{k+l} \Phi(k+l, k) \hat{P}_k \Phi^T(k+l, k) \tilde{H}_{k+l}^T + \tilde{H}_{k+l} \left[ \sum_{i=1}^{\ell} \Phi(k+l, k+i) B Q' B^T \Phi^T(k+l, k+i) \right] \cdot \tilde{H}_{k+l}^T + \sigma_{k+l}^2, \ell = 1, 2, \dots, m_q \dots \quad (B.3)$$

Imposing the condition

$$r_{k+l}^2 = E\{r_{k+l}^2\}, \ell = 1, 2, \dots, m_q$$

will give rise to the following set of equations:

$$r_{k+l}^2 - \tilde{H}_{k+l} \Phi(k+l, k) \hat{P}_k \Phi^T(k+l, k) \tilde{H}_{k+l}^T - \sigma_{k+l}^2 = \tilde{H}_{k+l} \left[ \sum_{i=1}^{\ell} \Phi(k+l, k+i) G Q' G^T \Phi^T(k+l, k+i) \right] \tilde{H}_{k+l}^T \quad \ell = 1, 2, \dots, m_q \quad (B.4)$$

Each equation corresponding to  $\ell = 1, 2, \dots, m_q$  is a scalar equation. However, the scalar on the right hand side of (B.3) can be written as the product of a row vector and a column vector, so that the above  $m_q$  equations can be put in the following matrix form:

$$\epsilon = A[\text{diag } Q'] \quad (B.5)$$

where  $\epsilon$  is  $m_q \times 1$ ,  $A$  is  $m_q \times 3$  and  $[\text{diag } Q']$  is  $3 \times 1$ . Then the solution to Eq. (B.4) can be computed as

$$[\text{diag } \bar{Q}'] = (A^T A)^* A^T \epsilon \quad (\text{B.6})$$

where  $(P)^*$  is the pseudo-inverse of  $P$ . This leads to the estimator

$$\text{diag } \hat{Q}' = \begin{cases} 0, & \epsilon \leq 0 \rightarrow \text{each element of } \epsilon \leq 0 \\ \text{diag } \bar{Q}', & \text{otherwise} \end{cases} \quad (\text{B.7})$$

subject to the condition that if  $(\hat{q}_{jj}) < 0$ , then set  $(\hat{q}_{jj}) = 0$ , since the diagonals are variances and cannot be negative.

DISTRIBUTION LIST

for

"Estimating the Motion of Maneuvering Targets Using Passive Measurements"

(All addressees receive one copy unless otherwise specified)

Defense Technical Information Center  
Cameron Station  
Alexandria, Virginia 22314 12 copies

Center for Naval Analyses  
2000 North Beauregard Street  
Alexandria, Virginia 22311

Alphatech, Inc.  
260 Hillside Avenue  
Arlington, Massachusetts 02174

Defense Advanced Research  
Projects Agency  
Tactical Technology Office  
1400 Wilson Boulevard  
Arlington, Virginia 22209

Office of Naval Research  
Arlington, Virginia 22217  
Code 431 2 copies  
Code 436

Dr. Fred W. Weidmann  
Tracor, Incorporated  
Tracor Sciences & Systems  
6500 Tracor Lane  
Austin, Texas 78721

Dr. Richard L. Moose  
Virginia Polytechnic Institute  
and State University  
Department of Electrical Engineering  
Blacksburg, Virginia 24061

Dr. Thomas E. Fortmann  
Bolt, Beranek and Newman, Inc.  
50 Moulton Street  
Cambridge, Massachusetts 02138

Massachusetts Institute of Technology  
Laboratory for Information and  
Decision Systems  
Cambridge, Massachusetts 02139

Dr. George Johnson  
IBM/Federal Systems Division  
9500 Godwin Drive  
Manassas, Virginia 22110

Dr. Nasser Ahmid  
Kansas State University  
Department of Electrical Engineering  
Manhattan, Kansas 66506

Naval Postgraduate School  
Monterey, California 92940  
Technical Library  
Dr. H. Titus  
Dr. N. Forrest  
Dr. G. Sackman

Dr. C. Carter  
Naval Underwater Systems Center  
New London Laboratory  
Code 313  
New London, Connecticut 06320

Naval Underwater Systems Center  
Code 352  
Newport, Rhode Island 02840 2 copies

Dr. J. Anton  
Systems Control, Incorporated  
1801 Page Mill Road  
Palo Alto, California 94304

Office of Naval Research Branch Office  
536 South Clark Street  
Chicago, Illinois 60605

Dr. Thomas O. Mottl  
The Analytic Sciences Corporation  
Six Jacob Way  
Reading, Massachusetts 01867

VERAC, Inc.  
4901 Morena Boulevard  
Suite 209  
San Diego, California 92117

Naval Surface Weapons Center  
White Oak Laboratory  
Code U-20  
Silver Spring, Maryland 20910 2 copies

Dr. Yaakov Bar-Shalom  
The University of Connecticut  
Department of Electrical Engineering  
and Computer Science  
Box U-157  
Storrs, Connecticut 06268

Mr. J. Conrad  
Naval Intelligence Support Center  
Code 20  
Suitland, Maryland 20390

Mr. V. T. Gabriel  
General Electric Company  
Sonar Systems Engineering  
Farrell Road Plant  
Building 1, Room D6  
Syracuse, New York 13201 2 copies

Naval Air Development Center  
Warminster, Pennsylvania 18974

Manager, ASW Systems Project Office  
Naval Material Command  
ASW-118  
Washington, D. C. 20360

Naval Research Laboratory  
Washington, D. C. 20375  
Code 2627  
Code 5308  
Code 7932

Naval Sea Systems Command  
Washington, D. C. 20360  
Code 63R-1  
Code 63R-16

Dr. Peter Schultheiss  
Department of Engineering  
and Applied Science  
Yale University  
New Haven, Connecticut 06520

Tracor, Incorporated  
6500 Tracor Lane  
Austin, Texas 78721

**DAT  
FILM**